UNIVERSITÀ DELLA CALABRIA

UNIVERSITA' DELLA CALABRIA

Dipartimento di Fisica

Dottorato di Ricerca in

Scienze e Tecnologie Fisiche Chimiche e dei Materiali

CICLO

XXXV

Chiral Induction in Chromonic Materials

Settore Scientifico Disciplinare Fis/07

Coordinatore: Ch.mo Prof. (Gabriella Cipparrone)

Firma Firma oscurata in base alle linee guida del Garante della privacy

Supervisore/Tutor: Ch.mo Prof. (Maria Penelope De Santo)

Firma Firma oscurata in base alle linee guida del Garante della privacy

Supervisore/Tutor: Ch.mo Prof. (Federica Causin)

Firma [redacted]

Supervisore

Firma [redacted] Firma oscurata in base alle linee guida del Garante della privacy

Dottorando: Dott./ssa (Lorenza Spina)

Firma oscurata in base alle linee guida del Garante della privacy

...To Myself

Sommario

Introduction

This thesis is focused on the study of chromonic liquid crystals.

These are a particular class of lyotropic liquid crystals that is able to self-assemble in water in columnar supramolecular aggregates. Chromonics are less studied than thermotropic liquid crystals that are widely used in optical and electrooptical devices. Examples of chromonics are drugs, food dyes and DNA, then, due to their biocompatible nature they are promising for applications in the biological and medical fields.

The self-assembly of chromonic molecules is driven by van der Waals, hydrophobic and electrostatic interactions. The columnar aggregates align in water to form liquid crystalline phases, in particular a nematic phase (N) with long-range orientational order can be observed. The nematic phase is characterized by an unusually small resistance to twist distortions. Distortions and topological defects can be amplified by confining chromonics inside curved geometries.

The reasons to study these materials are different.

The self aggregation mechanism is not fully understood: similar stacking energies give rise to different phase diagrams and the interaction of chromonics with polymers, that are usually employed in planar liquid crystal cells, depends strongly on the material. It is difficult to generalize the properties of these compounds in contrast to what happens with thermotropic liquid crystals.

Interestingly, apart native cholesteric chromonics, chirality can be induced in these compounds doping them with a suitable chiral aminoacid. Some doped chromonics (DSCG) show cholesteric phase with a large amount of dopants while other are not easily twisted (SSY). Furthermore, the connection between chirality at the molecular scale and the macroscopic chiral structure of liquid crystalline phases is not yet understood, and quantitative prediction of the twist periodicity, remains an unsolved problem.

Finally, an appealing property is the molecules biocompatibility which makes these materials and their mesophases suitable to find application in sensors, food packaging and biological fields.

In recent years researchers demonstrated that chromonics assume a spontaneous torque when they are confined in cylindrical or spherical geometry. Most of the studies are focused on tactoids or cylindrical capillaries with intriguing results. This work thesis, instead, is devoted to the confinement of chromonics in microspheres produced either by emulsions or by the microfluidic approach together with the analysis of thin dried films of the same mesophases.

The emulsions allow to investigate different topologies since it is possible to vary the anchoring conditions at the surface using different oils, to play with the ionic strength, with chiral dopants and to simultaneously investigate microspheres of different radius. The spherical confinement is ideal to comprehend the self assembling mechanism of these fascinating compounds.
This thesis opens new perspectives in this field even if not all the questions found an answer.
This work is organised into the following chapters:

- In Chapter 1, an introduction to thermotropic and chromonic liquid crystals is presented. The various mesophases, symmetry, anchoring and optical properties are described in detail. The concepts of hydrogen bonding and hydrophobic interactions are also recalled.
- In Chapter 2, the liquid crystals textures are described, which are observed by confining materials in planar and curved geometries.
- In Chapter 3, the analysis of experimental data obtained on model chromonic liquid crystals using polarised light microscopy, X-ray diffraction and atomic force microscopy techniques is presented. The effects on topological structures due to the confinement of materials in planar and spherical geometry and the effect of chiral dopants and ions are described.
- In Chapter 4, experimental studies are presented which have been carried out but which require further investigations. In particular, it concerns the study of newly synthesised chromonics and the effect of an electric field on the optical structure of a pure, chiral chromonic in planar and spherical confinement. Finally, a preliminary study on the confinement of liposomes in a chromonic matrix is reported.

Chapter 1 Liquid Crystals

This chapter is an introduction to thermotropic and lyotropic/chromonic liquid crystals (LCs). The mesophases, their symmetry, anchoring properties and optical properties are described in detail. The concepts of hydrogen bonding and hydrophobic interactions are, in addition, recalled.

1.1 History

Identification of liquid crystalline properties occurred in the 19th century. Between 1850 and 1888, researchers from different fields discovered that certain materials behaved strangely at temperatures close to their melting point. It was observed that the optical properties of these materials changed discontinuously with increasing temperature.

In 1850, W. Heinz reported that stearin (triglyceride resulting from the condensation of three stearic acid molecules with glycerol) dissolved from solid to cloudy liquid at 52°C, changed to opaque at 58°C and to transparent liquid at 62.5°C. Others reported the blue colour change when the compounds were cooled. Biologists have observed anisotropic optical behaviour in 'liquid' biological materials, a behaviour that is usually only expected in the crystalline phase.

In 1888, an Austrian botanist named Friedrich Reinitzer, interested in the biological function of cholesterol in plants, was observing the melting behaviour of an organic substance (known as cholesteryl benzoate). He observed that the substance melted into a turbid liquid at 145.5°C and became a clear liquid at 178.5°C (1). He repeated an earlier observation that showed that, on cooling the clear liquid, there was a brief appearance of blue colour at the transition temperature and that a blue-violet colour appeared just before crystallisation. Discussions with Otto Lehmann, a crystallographer, and others led to the identification of a new phase of matter called the liquid crystalline phase.

The term “liquid crystals” refers to materials that possess phases with a molecular order that is intermediate between the one of a crystalline solid and the one of an isotropic fluid. In a crystalline solid, the molecules exhibit a high degree of both positional and orientational order, with very few degrees of translational freedom (Figure 1.1a), in contrast, in a liquid the molecules have no particular order and possess great freedom of movement (Figure 1.1c). The molecules of a LC are in an intermediate position (Figure 1.1b), retaining some translational freedom while tending to assume preferential positions and/or orientations.

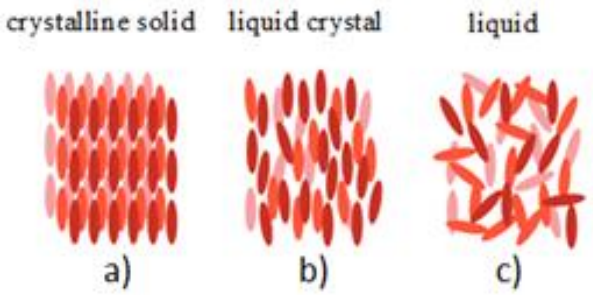

Figure 1.1: molecular order in a) crystalline solid phase, b) liquid crystalline phase and c) liquid phase.

In a LC, the molecules are arranged and/or oriented in a crystal-like way, however, it can flow like a liquid. Due to these singular prerogatives, LCs exhibit peculiar electrical, magnetic and optical properties that make them extremely interesting not only from a molecular point of view but also for technological applications.

1.2 Fundamental aspects of LCs

There are two types of LCs: thermotropic and lyotropic. Thermotropic LCs exhibit a phase transition into the LC phase as temperature is changed, whereas lyotropics exhibit phase transitions as a function of concentration of the mesogen in a solvent (typically water) as well as temperature. One class of lyotropic molecules are chromonics. These are lesser-known materials; in fact, the history of chromonic LCs begins with Sandquist's work in 1915 on solutions of phenanthrene sulphonic acid, in which he describes optical patterns observed under a polarising microscope that reveal the existence of a liquid-crystalline phase. Between the 1920s and 1950s, studies were caried out on the lyotropic mesomorphism of drugs such as salvarsan (a chemotherapeutic agent) and neosalvarsan. In these years, most work focused on phase classification (nematic and columnar hexagonal). In 1971, the first basic observations and phase diagram of the chromonic DSCG were published (2).

The basic units in thermotropic LCs are molecules. A pronounced anisotropy of shape is the main feature of molecules which give rise to a thermotropic mesophase. Examples of molecular geometries associated with thermotropic LCs are rod, disc and banana-shape. Three mesophases can be distinguished based on the arrangement that the molecules spontaneously assume in space. Thermotropics are widely used in low-energy displays and many sensor devices (3).

The lyotropic mesophases, instead, are the result of the interaction between the solvent and the constituent mesogens. A particular feature of lyotropics is the self-assembly of molecules into supramolecular structures, which are the basic units of these mesophases. Another particular

feature is that they are biocompatible materials, therefore the physico-chemical properties of lyotropics are exploited in the biological and medical fields and their study has been relevant to improve some technological aspects of cosmetics, soaps, food and detergents.

Lyotropic mesogens are amphiphilic molecules characterized by the co-presence of hydrophilic and hydrophobic functional groups (Figure 1.2), able to self assemble in micellar structures according to the shape of molecules (4).

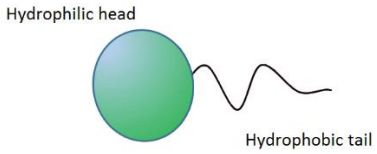

Figure 1.2: Representation of an amphiphilic molecule.

1.3 Hydrophobic and Steric effects

Lyotropic mixtures are mostly composed of water. The interaction of lyotropic molecules with water molecules is fundamental for the formation of a lyotropic mesophase, due to the presence of hydrophobic and steric interactions.

The concepts “hydrophobic” and “hydrophilic” refer to the affinity of a particular molecule for water molecules. Due to the permanent dipole moment of water molecules, the interactions involved are electrostatic in nature. Therefore, polar molecules dissolve easily in water and non-polar substances are difficult to dissolve in water. In these interaction hydrogen bonds play a key role.

The hydrogen bond is a special case of intermolecular interaction involving a hydrogen atom with a highly electronegative element, such as fluorine (F), oxygen (O) and nitrogen (N). Water molecules, due to the presence of hydrogen bonds, pack into a tetrahedral structure (Figure 1.3).

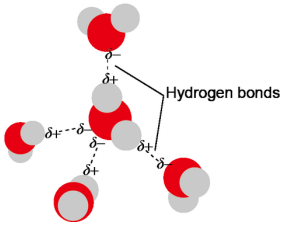

Figure 1.3: Tetrahedral structure of water. The dotted lines are the hydrogen bonds.

When water molecules interact with apolar molecules (such as oil), that are incapable of forming hydrogen bonds, the tetrahedral structure of water breaks down. The presence of the apolar molecules will force the water molecules to organise themselves into a more ordered

configuration that maximises the number of bonds the water molecule can make with neighbouring molecules. This new, more ordered configuration, energetically less favoured, leads to strong attraction between non-polar molecules, known as hydrophobic interaction.

1.4 Liquid crystalline phases

Thermotropics LCs, show different phases: nematic, smectic, and cholesteric phases. Lyotropics LCs show a richer set of phases: micellar isotropic, nematic, cholesteric, lamellar, hexagonal and cubic phase (4). In this paragraph the main characteristics of nematic and cholesteric mesophases are reported since they are observed in both thermotropic and chromonic LCs.

1.4.2 Nematic phases

The nematic mesophase (Figure 1.4) consists of elongated molecules packed without any positional order and characterised only by a common preferential orientation, represented by the unit vector n̂ defined as the "director". The anisotropy of the nematic phase is due to the tendency of the rod-like fluid molecules to align their long axis parallel to the director, as through van der Waals interactions. Molecules are arranged with the major axis predominantly oriented along the director but they are free to rotate on themselves and slide over each other in the direction of the major axis; in fact, the barycenter of the individual molecules are randomly distributed.

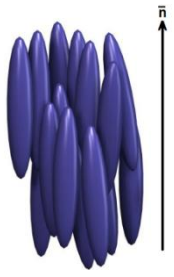

Figure 1.4: Representation of the nematic mesophase.

The nematic mesophase is invariant since - n̂ and n̂ are indistinguishable and it possesses cylindrical symmetry.

1.4.3 Cholesteric phases

The cholesteric mesophase is observed in systems composed of chiral molecules (i.e. molecules that do not have mirror symmetry), or in mixtures of achiral nematics with optically active dopants, which are called induced cholesteric systems. The molecules in the cholesteric phase can be represented as organized in nematic planes, the director n̂, defined in each plane, follows a helical pattern in the volume (Figure 1.5).

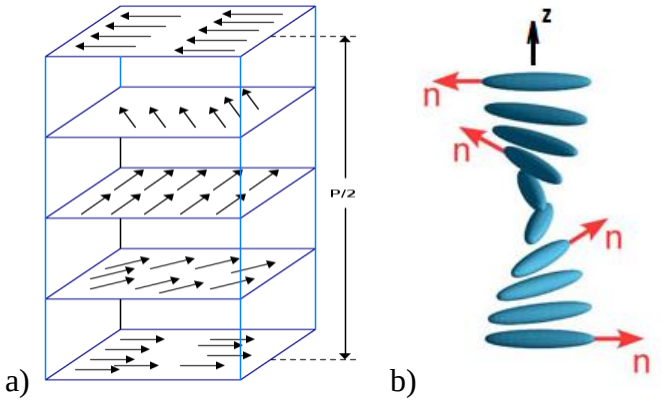

Figure 1.5: Cholesteric mesophase: (a) director rotation in nematic planes, (b) helix pitch.

The distance for which the director makes a complete turn, returning to its initial position, is called the "helix pitch" and is denoted by p. Due to the symmetry between - n̂ and n̂, the spatial periodicity L, is half the pitch $L = \frac{p}{2}$.

The helix pitch may vary depending on the conditions of the external environment. This property is of particular importance since some cholesteric mesophases are able to selectively reflect visible light with a wavelength similar to the pitch length. The rotation of the director around the z-axis can be described by the triad of the n̂ versor in the three directions:

$$n_x = \cos(q_0 + \Phi)$$

$$n_y = \sin(q_0 + \Phi)$$

$$n_z = 0$$

where, the direction of the helix axis z in space and the phase angle ϕ are arbitrary and q_0 is the wave number which is equal to $q_0 = \pm\frac{2\pi}{p}$. Its sign determines if the helicity is right- or left-handed, while, its modulus represents the spatial periodicity, $L = \frac{\pi}{|q_0|}$.

1.5 Chromonic liquid crystals

Chromonics are a subset of lyotropic liquid crystals. Their name is derived from the Greek word "*chroma*" meaning colour, indicating the fact that many chromonics are coloured (5).
Chromonics usually consist of a rigid hydrophobic discotic core, composed of hydrophobic aromatic rings, with hydrophilic groups around them (6).
Examples of chromonic LCs are some drugs (such as disodium chromoglycate often used in anti-asthmatic treatments), dyes (such as Sunset Yellow used in the food industry), DNA nucleotides such as guanine derivatives, DNA itself and cellulose. All these materials are biocompatible. Chromonic molecules are able to self-assemble in supramolecular columnar structures. Aggregation occurs even in dilute solutions and produces columns of increasing length when the solution is concentrated (6). Molecules aggregate due to non-covalent interactions, for example, van der Waals interactions between aromatic nuclei (π-π stacking), hydrophobic and electrostatic interactions. These materials are able to form two mesophases, shown in Figure 1.6: at low concentrations, the N phase, consisting of a nematic matrix of columns; at higher concentrations, the M phase, in which the columns pack into a regular two-dimensional hexagonal lattice.

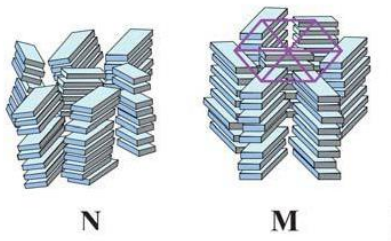

Figure 1.6: N and M mesophases.

1.6 Molecular stacking

As discussed in the previous paragraph, chromonic materials, unlike other lyotropic materials, consist of molecules that are plate-like instead of rod-shaped, are aromatic instead of aliphatic, are rigid instead of flexible, and the hydrophilic solubilizing groups are arranged around the peripheries of the molecules and not at the ends.
The driving force for molecular aggregation appears to be an enthalpically driven face-to-face adhesion of the aromatic rings. Thus, in many respects, chromonic systems are more similar to thermotropic columnar systems than to conventional amphiphiles (6).
The tendency of chromonic molecules to aggregate in columns is present even in dilute solutions. In addition to hydrophobic and hydrophilic effects, there are also π-π interactions

between chromonic molecules. The π-π interactions between the aromatic complexes drive aggregation; however, the flexibility and nature of the chains connecting the complexes, the nature of other functional groups around the complexes, and the electrostatic and dipolar interactions between the complexes define the organization between these molecules. These interactions constrain the aromatic complexes to arrange themselves in very specific orientations relative to each other (7).

According to Hunter and Sanders (8) conventional van der Waals forces, which act effectively from atom center to atom center, are sufficient to explain the stacking of chromonic molecules. For a pair of two- or three-ring systems 3.5 Å apart, the calculated face-to-face bonding is comparable to hydrogen bonding. Since the systems are planar, Van der Waals interactions will be maximal when the molecules are stacked face to face. Therefore, the lowest energy situation is the one with the molecules stacked on top of each other in the eclipsed position. This interaction, however, is modified by electrostatic factors such as Coulomb repulsions between the high electron density regions above and below the plane of the rings.

The phase behavior of chromonic molecules is based on two aspects of their stacking. The stacking angles and the degree of order between stacks. During stacking, chromonic molecules can position themselves on each other, so the stack is perpendicular to the flat chromonic molecule, or they can undergo displacement so the stack is angled.

When stacking occurs with a significant displacement the molecule is said to have undergone "J stacking" (Figure 1.7a) If the angle is large the molecule is considered an "H stacking" structure (Figure 1.7b).

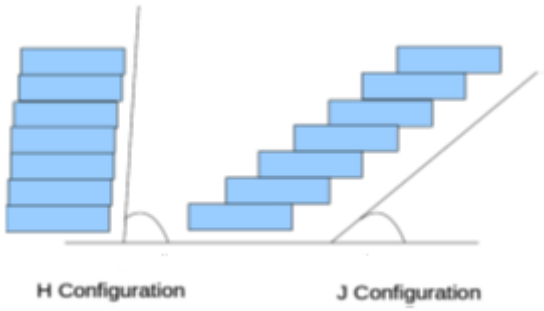

Figure 1.7: Classification of molecular stacking configuration. a) J stacking, b) H stacking.

However, H and J stacking do not completely describe molecular stacking. In stacking, molecules are not only displaced relative to each other, but are also rotated, which gives rise to more complex stack shapes.

1.7 Phase diagrams

The best way to illustrate the behaviour of an amphiphilic material in water is to show the phase diagram, characterised by the concentration of the amphiphile along the horizontal axis and the temperature along the vertical axis (9) (10). An example of a phase diagram for a chromonic liquid crystal is the solution of DSCG in deionised water (Figure 1.8). (11).

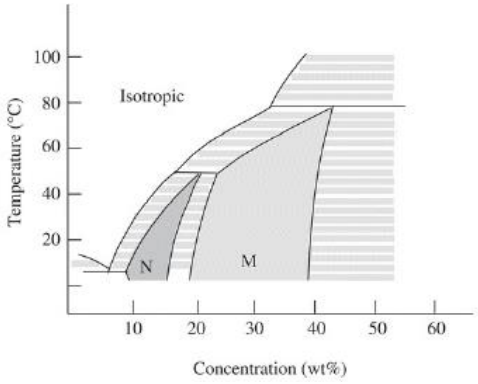

Figure 1.8: DSCG Phase diagram.

For DSCG concentrations between 10 and 15wt%, a nematic (N) phase appears at room temperature. For concentrations of 20wt% or more, a columnar phase (or M-phase) appears. The phase diagram contains large intervals in which the two phases coexist. At room temperature, the N and M phases coexist in the range of 15 to 20wt%. Near the equilibrium temperature, large intervals of coexistence appear between the isotropic (I) and the nematic (N) phase or between the I and M phases. The temperature of the transition from the respective mesophase to the isotropic liquid phase increases uniformly with increasing DSCG concentration.

Chapter 2 Elasticity and textures

The second chapter is devoted to the description of the optical properties of LCs and textures that are observed by confining materials in planar and curved geometries. Due to the combination of these properties, LCs are suitable for interesting technological and scientific applications.

2.1 Symmetry and order parameter

The symmetry of the nematic phase is cylindrical, so there is an axis (the director) along which the phase properties exhibit one set of values, while in all other directions perpendicular to this axis another set of values is exhibited. Figure 1.4.

Due to external factors, the degree of alignment of molecules may change (12). It is therefore necessary to introduce a parameter that quantitatively describes the degree of long-range orientational order. This parameter is called the order parameter and is denoted by S.

Considering a single molecule oriented with respect to the director (Figure 2.1), let the director lie along the z-axis of a Cartesian system, the orientation of the rod-like molecule can be described using the three Eulerian angles θ, Φ and Ψ.

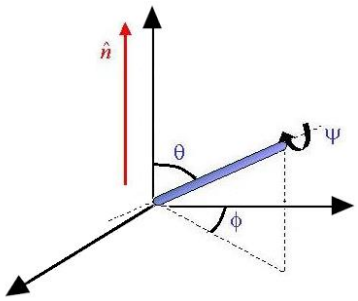

Figure 2.1: Cartesian representation of a molecule with respect to the director.

In liquid crystals no order is allowed for both the Ψ angle (rotation along the molecular axis) and the Φ angle (rotation in the azimuthal plane), but it is allowed for the θ angle, between the director and the long axis of the molecule. In nematics, the most probable angle is θ=0, i.e. the molecular long axis is parallel to the director n̂. One could choose $cos\theta$ as the order parameter, which is the projection of the molecular long axis along the director, but many experiments performed have shown that the heads and tails of molecules are indistinguishable and being randomly distributed in a fluid, the average of $cos\theta$ over all molecules in the volume is zero. Therefore, to describe the degree of order of the system it is more convenient to use the value

of $cos^2\theta$ averaged over all molecules in the fluid. When all molecules are perfectly aligned with n̂, θ =0 and $\langle cos^2\theta \rangle$ =1. In contrast, if the molecules are randomly oriented with respect to the director, all values of θ are equivalent and thus $\langle cos^2\theta \rangle = \frac{1}{3}$.

The scalar order parameter for the nematic phase is defined by Equation:

$$S = \frac{1}{2}(3\langle \cos^2\theta \rangle - 1) \qquad (1)$$

Thus, S=1 indicates a condition of perfect order, while S=0 indicates that the molecules are oriented in a completely random manner and one is therefore in presence of an isotropic, disordered liquid.

2.2 Elasticity

To describe phenomena involving LCs on a larger scale than the molecular one, it is more convenient to consider them as continuous media (1).

Suppose we study a nematic liquid crystal and consider a small spatial region in the sample containing a sufficient number of molecules so that the long-range orientational order is well defined. The macroscopic nematic sample is, therefore, described by many small spatial regions characterised by a local director. The free energy of the liquid crystal is related to the possible distortions of the director. There are three different fundamental spatial distortions of the director, called twist, splay and bend.

In the twist distortion, shown in Figure 2.2b, the director always lies parallel to a given x-y plane, forming with the x-axis an angle ϕ(z) that depends only on the z-coordinate (one-dimensional distortion).

In the splay and bend deformation, shown in Figure 2.2a and 2.2c, the director n̂ always lies parallel to a given x-z plane and varies only as a function of z. This is also a one-dimensional deformation because it depends only on the z-coordinate and is planar because n always remains in the same plane (x-z plane).

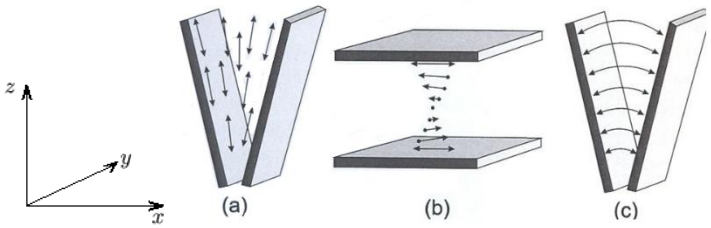

Figure 2.2: (a) splay, (b) twist and (c) bend distortions.

These three fundamental distortions are independent of each other, such that no combination of twist and/or splay can compensate for a bend etc.

The total free energy F_D related to bulk elastic deformations of the director field can thus be calculated by integrating a bulk energy density f_D,

$$F_D = \int f_D dV \tag{2}$$

f_D containing one term each for splay, twist and bend, over the volume of the sample. The following equation is the Oseen- Frank equation that describes the bulk energy density where K_{11}, K_{22} and K_{33} are referred to as Frank's constants:

$$f_D = \frac{1}{2}\{K_{11}\,[\nabla\cdot\,\bar{n}(\bar{r})]^2 + \,K_{22}\,[\bar{n}(\bar{r})\cdot\nabla\times\bar{n}(\bar{r})]^2 + \,K_{33}\,[\bar{n}(\bar{r})\times\nabla\times\bar{n}(\bar{r})]^2\} \tag{3}$$

the three terms are related to the distortions of the director's field:

$[\nabla\cdot\,\bar{n}(\bar{r})]^2$ Term of *splay* (4)

$[\bar{n}(\bar{r})\cdot\nabla\times\bar{n}(\bar{r})]^2$ Term of *twist* (5)

$[n(\bar{r})\times\nabla\times\bar{n}(\bar{r})]^2$ Term of *bend* (6)

As shown in equation (4), the splay term contains the divergence of the director field ($\nabla\cdot\,\bar{n}$), while the terms representing the two rotational distortions twist and bend (equation 5 and equation 6) contain the rotor ($\nabla\times\bar{n}$). Since each term is squared, the elastic constants must be positive, in order to have a finite energy minimum.

If the order parameter (S) is not uniform within the volume considered, a fourth term, denoted as saddle-splay, must be included (12).

2.3 Anchoring energy

Liquid crystal molecules can assume different orientations when confined between two surfaces (1) (13). The term "anchoring" refers to the orientation of the director n̂ respect to the confining surfaces; these surfaces are usually two glass surfaces, covered with a polymeric

material capable of imposing a precise alignment on the liquid crystal molecules. Various types of anchoring can be distinguished (shown in Figure 2.3):

Degenerate planar: the long axis of the molecules is oriented parallel to the substrate, at an arbitrary azimuthal angle;

Uniform planar: in addition to having the molecular long axis oriented parallel to the substrate, there is also a preferred azimuthal angle;

Homeotropic: the molecular long axis is perpendicular to the substrate, there can also be a uniform alignment with an inclined orientation called tilt.

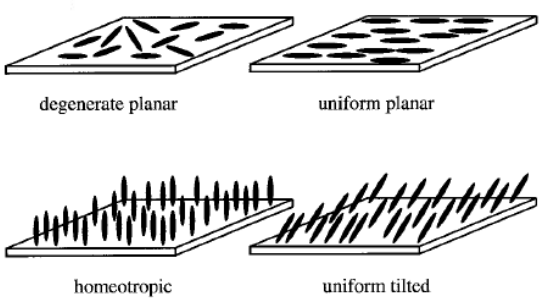

Figure 2.3: Schematic representation of different anchoring conditions: a) degenerate planar; b) uniform planar; c) homeotropic; d) uniform tilt.

To achieve a uniform planar alignment, the confining surfaces can be treated with a polymeric material subjected to the rubbing technique, which consists in creating microgrooves on the polymer by rubbing it with a velvet cloth. This procedure aligns the molecules in the direction of the microgrooves parallel to the confining surface as shown in Figure 2.4a.

To achieve a homeotropic alignment, the substrate can be covered with a material whose molecules are oriented with their long axis orthogonally to it (e.g. a surfactant), so that the liquid crystal molecules also arrange themselves in the same way via van der Waals-type or steric molecular interactions (Figure 2.4b).

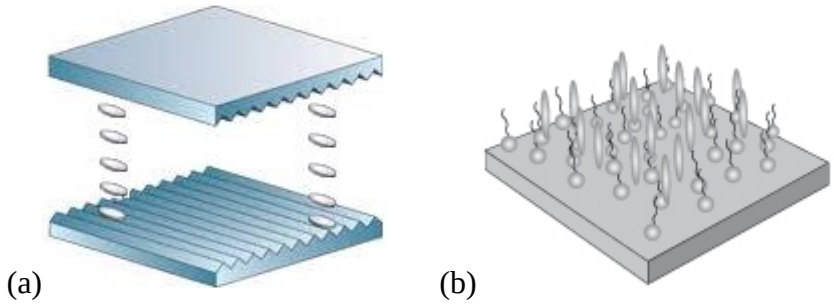

Figure 2.4: Schematic representation of (a) planar alignment along grooves on a rubbing-treated substrate, (b) homeotropic alignment on a substrate treated with a surfactant.

To describe the director deformation imposed by the confining surfaces, it is necessary to introduce a term, the anchor energy F_S. This term is related to the interaction of the molecules

with the surface and is expressed as a function of the director n̂ according to the Rapini-Papoular equation (equation 7):

$$F_S = -\frac{1}{2} W (\bar{n} \cdot \overline{n_0})^2 \qquad (7)$$

W is the anchoring coefficient and $\hat{n}_0$ is the direction of anchoring imposed by the surface. Both W and $\hat{n}_0$ are related to the microscopic interactions between the liquid crystal molecules and the surface.

The elastic energy *E* associated with a liquid crystal confined between two surfaces (equation 8), then, can be divided into two components: one component that depends on the deformations of the liquid crystal in the volume and one that depends on the interactions with the surface.

$$E = \int F_D \left(n_\alpha, \frac{dn_\alpha}{dx_\beta} \right) dV + \int F_S \, dS \qquad (8)$$

2.4 Birefringence

Birefringence is a physical phenomenon that occurs in optically uniaxial media that are able to split light into two rays: ordinary and extraordinary. The two rays emerging from the birefringent medium are linearly polarised but with a direction of vibration perpendicular to each other, independent of the polarisation of the incident light. An example of a birefringent media are LCs.

It is possible to represent the polarisation properties and refraction index through a mathematical surface known as the 'optical indicatrix' (Figure 2.5), which represents the envelope of vectors whose modulus is the index of refraction and whose direction is the direction of vibration of the polarised rays.

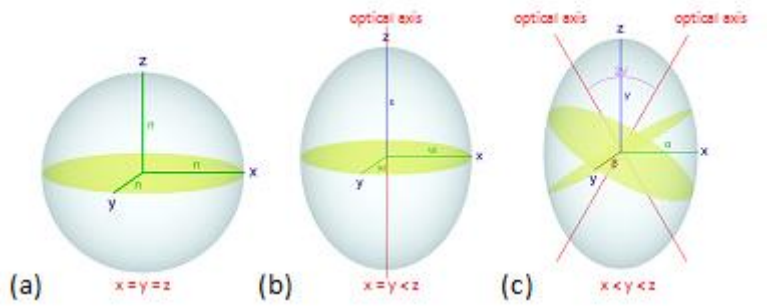

Figure 2.5: representation of optical indicatrix.

To assess the optical properties of a liquid crystal, given a direction of propagation of an electromagnetic wave, it is necessary to consider the cross-section of the optical indicatrix perpendicular to this direction, which is obtained by cutting it by a plane passing through the centre. When the cross-section of the optical indicatrix is circular (Figure 2.5a) the liquid crystal will behave as isotropic material, otherwise the liquid crystal will exhibit birefringence phenomena (Figure 2.5b and 2.5c). The axis along which a birefringent liquid crystal takes on mono-refractive properties is called the 'optical axis'.

Furthermore, only for the ordinary ray is Snell's law valid. Since the refractive index is given by the ratio between the velocity of radiation in vacuum and the velocity of radiation in the medium, the refractive indices are different from each other, n_0 and n_e are the ordinary and extraordinary refractive indices, respectively, and this leads to a phase shift which is given by

$$\delta = \frac{2\pi}{\lambda}(n_e - n_o)d \qquad (9)$$

where λ is the wavelength in vacuum, d is the thickness of birefringent medium and $\Delta n = (n_e - n_o)$ is the birefringence of the medium.

Birefringence can be a positive or negative quantity and this can distinguish a positive uniaxial crystal from a negative one. When $n_e > n_o$, then $\Delta n > 0$ we have a positive uniaxial crystal and the ellipsoid assumes an elongated shape (Figure 2.6a), when $n_e < n_o$ and then $\Delta n < 0$ we have a negative uniaxial crystal and the ellipsoid assumes a flattened shape (Figure 2.6b).

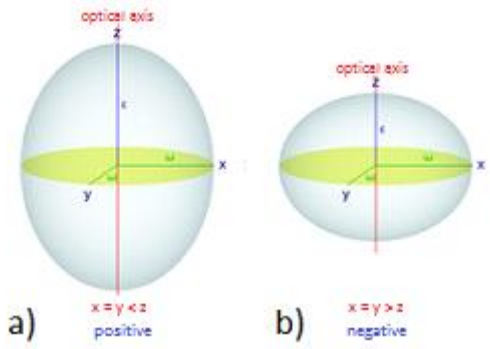

Figure 2.6: Optical indicator representation of (a) positive birefringence, (b) negative birefringence

For cholesteric LCs, the optical anisotropy is negative, thus $n_{oh} > n_{eh}$, where $n_{eh} \equiv n \| h$; and $n_{oh} \equiv n \perp h$ are the extraordinary and ordinary refractive indices, the h-index denotes that the macroscopic optical axis corresponds to the helix axis. If the local nematic refractive indices are given by n_o and n_e, the average refractive indices with respect to the helix axis can be written as:

$$n_{eh} = n_o \qquad (10)$$

$$n_{oh} = \sqrt{(n_e{}^2 + n_o{}^2)} \quad (11)$$

2.5 Optical activity

One of the peculiarities of cholesteric LCs is their ability to selectively reflect light in a certain wavelength range related to the cholesteric helix pitch. This phenomenon can be explained by analogy to the Bragg diffraction of X-rays from crystalline lattices.

As it is known, crystals are periodic structures consisting in a set of discrete parallel planes separated by a constant parameter d. The phenomenon of Bragg diffraction occurs only when the wavelength of the incident radiation is comparable to the distance between the crystalline planes (Figure 2.7).

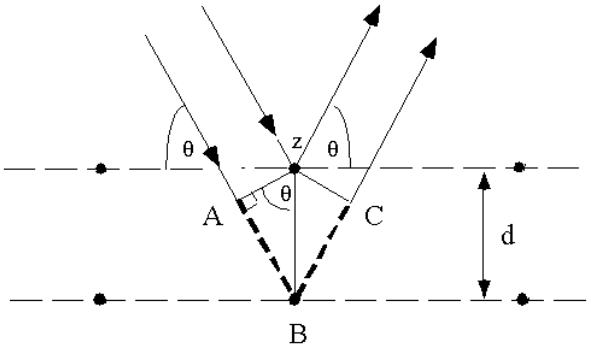

Figure 2.7: Bragg-type diffraction from lattice planes.

This effect only occurs if there is constructive interference between the waves reflected from different crystallographic planes, therefore if the following equation is satisfied:

$$2dsin\vartheta = n\lambda \quad (12)$$

where θ is the angle of incidence of the electromagnetic radiation with wavelength λ, and n is the number of planes involved in the reflection. Similarly, Bragg diffraction of visible light occurs in cholesteric LCs. A beam of light impinging on a cholesteric material is split into its two circularly polarised components, one of which is simply transmitted while the other is totally reflected. The rotation of the circularly polarised reflected component is in accordance with the rotation of the structure's helix. When light passes through a cholesteric liquid crystal, it is selectively reflected if the following relation is satisfied:

$$\mathrm{m}\lambda_b = \mathrm{p}\bar{n}\cos\phi \quad (13)$$

where ϕ is the angle of incidence of the light beam and $\bar{n}$ represents the average refractive index of the medium $\bar{n} = \frac{n_o + n_e}{2}$. In the case of parallel incidence to the helix axis, the maximum reflection occurs for the wavelength $\lambda_b = \mathrm{p}\bar{n}$.

As mentioned above, the liquid crystal possesses birefringence Δn, so we have that an entire wavelength range is reflected by the cholesteric material, this is called photonic band gap: $\Delta\lambda_b = \mathrm{p}\Delta n$ (Figure 2.8).

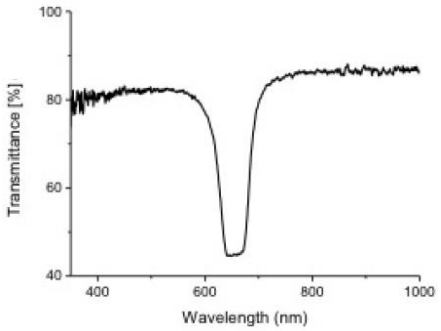

Figure 2.8: Photonic bang gap of a chiral LC.

2.6 Topological defects and textures

When a LC is observed using an optical microscope between crossed polarizers, due to the effect of birefringence, different coloured textures are observed. When LCs is confined between two uncoated glasses, the director is oriented parallel to the substrates (13). If this orientation is not homogeneous textures, known as ***Schlieren***, are observed, which contain black lines (Figure 2.9). Black lines correspond to positions where the nematic director is parallel to the analyser (or polariser). They join in a point known as *singularity*. Singularities are topological defects with a strength s, absolute value of which is obtained by dividing by 4 the number of lines contained in a circumference drawn around the defect. The sign can be obtained by rotating polarizers, if the lines rotate in the same direction as the polarizer a positive sign is assigned to the defect, otherwise if they rotate in the opposite direction is assigned a negative sign.

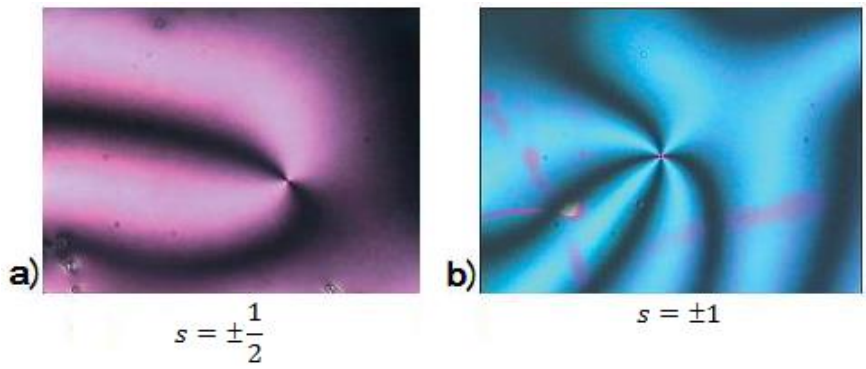

Figure 2.9: Schlieren textures with (a) a defect of strength s=±1/2 and (b) a defect with strength s=±1

The points of singularity never move while the displacement of the lines is continuous, this is due to a continuous variation of the director's field n̂. In a sample, double or quadruple singularities can be observed; there are not only isolated defects, but also lines connecting several defects of opposite sign. In a sample, the sum of all defect forces generally is zero. In general defects of equal strength but opposite sign can attract each other until they annihilate, forming a uniform defect-free area, on the other hand, defects with the same sign but different strength values cannot annihilate but can combine to form a new singularity whose strength is given by the sum of the forces of the individual defects.

Another example of texture is the ***threadlike*** texture, shown in Figure 2.10. The dark lines are line singularities, which connect two $s = \pm\frac{1}{2}$ point defects or form closed rings.

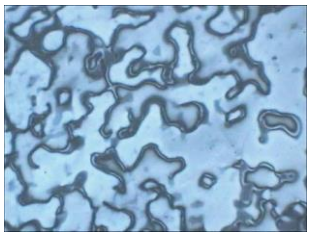

Figure 2.10: Threadlike texture.

A texture that appears similar to the threadlike one is that of the surface inversion walls, which correspond to a 180-degree turn of the director in the plane of the substrate (Figure 2.11a). Two closely spaced dark lines are visible as in Figure 2.11b.

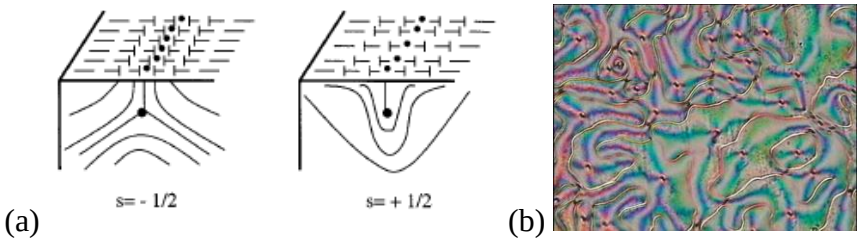

Figure 2.11: a) Possible director configurations in the vicinity of surface disclination lines. B) Nematic texture with surface disclination lines.

In thin samples, where substrates have not been treated, the ***marble*** texture is usually observed (Figure 2.12). Several areas of the sample appear uniform, but may change colour slightly, due to a change in birefringence related to in-plane and out-of-plane director changes.

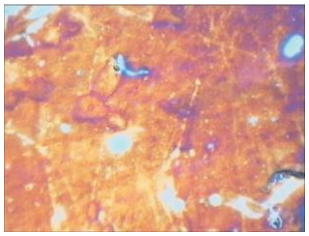

Figure 2.12: Marble texture in a nematic liquid crystal.

For mesogens exhibiting a crystalline-nematic transition, the *marble* structure appears from the heating of crystallites in the nematic phase. In this case, an area with uniform director direction is formed. The preferred direction may vary from one area to another.

In general, from a technological point of view, it is extremely important to create a uniform texture. For this purpose, the nematic sample can be confined between two treated substrates, for example, by rubbing. In this case, a sample is obtained that behaves optically as a uniaxial material, with the optical axis parallel to the substrate. The light transmitted through a well-oriented nematic sample placed between crossed polarisers varies according to the law

$$I \sim sin^2(2\varphi) \qquad (14)$$

where φ is the azimuthal angle.

When the director n̂ is oriented along a direction of polarisation, the sample appears black. The maximum intensity is observed when the optical axis is at 45° between polariser and analyser (Figure 2.13).

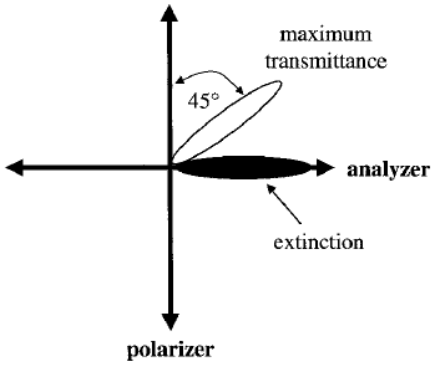

Figure 2.13: Director orientation for a uniform uniaxial planar nematic between crossed polarizers at extinction (black) and maximum transmittance positions (45°).

In presence of homeotropic alignment, the director is oriented perpendicular to the substrates, in which case the direction of light propagation coincides with the optical axis, so there is no birefringence phenomena and the sample appears black when observed between crossed polarisers for all azimuthal angle positions. This is a pseudo-isotropic structure because the sample appears like it is in its isotropic phase. To distinguish the isotropic structure from the pseudo-isotropic a soft pressure on the glasses can be exerted, if the material is nematic a bright flash appears (due to an instantaneous reorientation of the director and the optical axis).

For cholesteric LCs textures observed using polarized light optical microscopy are quite different from the nematic ones. When the chiral liquid crystal is confined between two untreated glass substrates, one of the most commonly observed textures are the so-called *oily streaks* (Figure 2.14).

a) 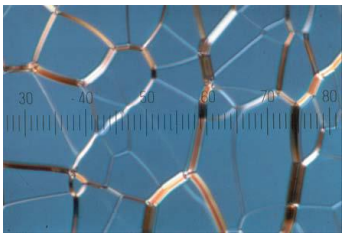 b) 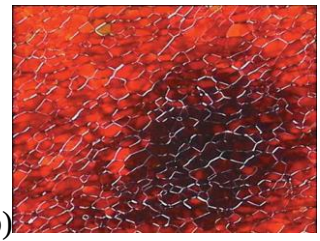

Figure 2.14: a) Oily streaks texture for a cholesteric under planar anchoring conditions with pitch p ≈ 2μm; (b) Oily streaks texture for a cholesteric with pitch p ≈ 450nm.

Since the director is planar to the substrates, this means that the axis of the cholesteric helix is oriented perpendicular to the glass plates. Such a structure can be seen as a network of line defects dispersed in a uniform helical structure.

When the cholesteric helix axis is parallel to the glass plates (the anchoring conditions at the surface are homeotropic), different textures are usually observed: *fan-like* and *fan-shaped* (Figure 2.15a and 2.15b). The first is observed in cholesterics that have a very short pitch, the second, on the other hand, is observed in cholesterics that have a larger pitch. Further increasing

the pitch can give rise to the so-called cholesteric polygonal pattern (fingerprint texture), an example of which is shown in Figure 2.15c. A variety of defects, such as edge dislocations and pinches (Figure 2.15d) may exist in polygonal textures.

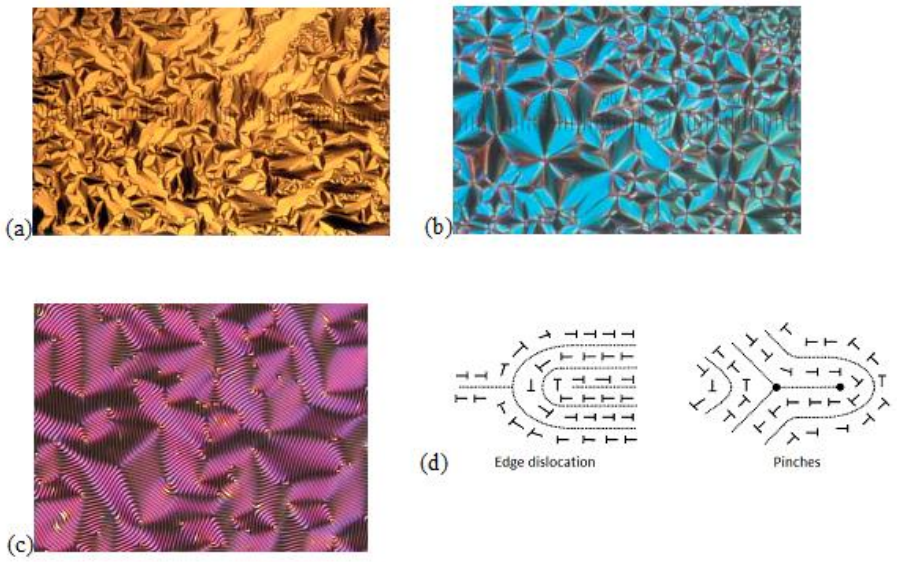

Figure 2.15: (a) Fan-like texture; (b) Fan-shaped texture; (c) Polygonal cholesteric texture (fingerprint) of a sample with wide pitch, d) Common defects found in cholesterics.

2.7 Thermotropic liquid crystals in spherical confinement

Recently, much attention has been focused on the study of the confinement of LCs in curved geometries. When a liquid crystalline volume is confined in a spherical geometry, the anchoring conditions at the interface impose topological constraints on the director field that inevitably cause topological defects to form (12). These defects are interesting to observe not only from a scientific point of view but can also be useful for technological applications (in the fields of sensor technology, photonics and security).

The confinement of thermotropic liquid crystals in microspheres is easily obtained by dispersing them in an immiscible fluid (water or glycerol). Due to immiscibility, an interface is formed between the liquid crystal and the surrounding fluid. Since there is an energy cost associated with each interface to form it, liquid crystal droplets tend to minimise surface free energy by assuming a perfectly spherical shape. Inside the microsphere, the nematic director field depends on three factors: the anchoring of the liquid crystal at the interface, the elastic properties of the liquid crystal and the size of the sphere. Typically for thermotropic materials, K_{11} and K_{22} often have the same value, while K_{33} is approximately twice as high.

In a liquid crystal microsphere, the balance between volume and surface energy is complex.

The volume elastic energy F_V scales linearly with the radius of the drop KR, whereas the surface energy F_S is proportional to WR^2 where W is the intensity of the anchoring energy. From this, it is evident that as the radius R of the liquid-crystalline droplet increases, the interface contribution predominates over the volume contribution and, therefore, the influence of topological constraints imposed by the interface vanishes for small droplet sizes.

A characteristic length called anchoring length, defined as the ratio of elastic energy to anchoring energy K/W, can be identified (Figure 2.16).

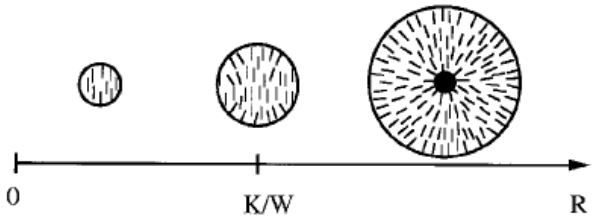

Figure 2.16: Schematization of a nematic liquid crystal drop with a homeotropic surface anchor with varying size

This means that for drops smaller than a critical radius, it will be energetically favourable to change the anchoring to the surface and thus relax the elastic deformation leading to a uniform orientation of the director. This happens for droplets with a radius of the order of a micron. If the droplets are larger than this value, topological defects will appear (14).

Let us consider the situations of strong anchoring, in which the angle of inclination of the molecules on the drop surface is fixed at a constant value. The most common anchoring angles are θ=0 and $\theta=\frac{\pi}{2}$, which correspond to planar and homeotropic anchoring, respectively. For these two types of anchoring, the *Poincaré- Hopf* theorem limits the possible configurations of the director to those containing a total topological charge s =+2 on the surface of the drop. This configuration is recalling the 'hairy ball theorem', according to which, there is no continuous non-zero vector field tangent to a sphere. In Figure 2.17 the singularities, the surface defects, are represented at the poles of the sphere and are called *boojums*. Volume defect points are known as *hedgehogs*.

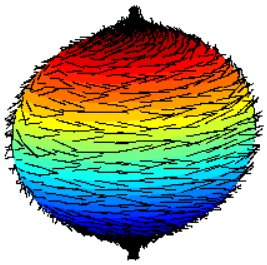

Figure 2.17: Graphic visualization of the hairball theorem.

Under strong anchoring conditions at the drop surface, the equilibrium configuration of the liquid crystal is determined by minimising the elastic distortions due to spherical confinement. Different topologies are observed and can be classified as in the following (14).

For planar anchoring with $K_{11} < K_{33}$, the bipolar configuration is typically observed (Figure 2.18a). In this configuration there are two boojums at the poles with strength s=+1. Bipolar configuration has splay distortions near each defect and bend distortions in the rest of the drop. Adding a twist to this configuration, a twisted bipolar configuration is obtained (Figure 2.18b). The resulting structure still has the two boojums at the poles, but the surface director field now creates an angle α, relative to the axis connecting the point defects. The bipolar twisted configuration forms when $K_{11} \geq K_{22} + 0.431 K_{33}$.

When $K_{11} < K_{22} + 0.431\ K_{33}$ and $K_1 > K_{33}$, the director organises itself into a series of concentric circles, forming a structure that has a defect line along the diameter of the drop (Figure 2.18c), this structure is unstable.

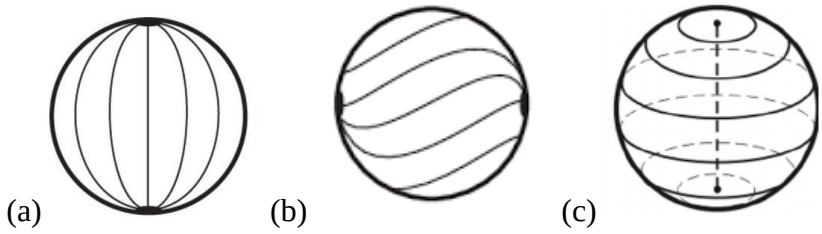

Figure 2.18: Director's field schematization for a spherical droplet in planar anchoring conditions: a) bipolar configuration, b) twisted bipolar configuration, c) defect line along the diameter of the drop.

In the case of homeotropic anchoring, the frequently observed configuration for nematics, which favours splay to bend distortion, is the radial drop (Figure 2.19a). A pure splay is obtained with a localised *hedgehog* in the centre of the drop. A variant of this structure results from the presence of twist distortions to form a twisted radial drop (Figure 2.19b).

For nematics that favour bend to splay distortion, the director is organised around a ring defect located on the surface of the drop along one of the two equatorial lines (Figure 2.19c). In this case the director has cylindrical symmetry, and there is a defect line perpendicular to the director's preferred orientation (on the drop's equator).

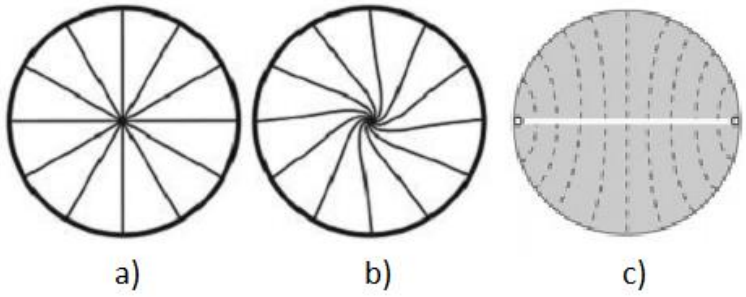

Figure 2.19: Director's field schematization for a spherical droplet in homeotropic anchoring conditions: a) radial drop, b) twisted radial drop, c) ring defect located on the surface of the drop along one of the two equatorial lines.

For cholesterics phases more complex configurations are formed. Two parameters control the configuration of the director within a cholesteric drop: the anchoring conditions at the interface and the twisting power qR, where R is the radius of the drop and $q = \frac{1}{p}$.

For planar anchoring and low twisting power (qR<1), the resulting drop configuration is bipolar twisted (Figure 2.20a). For planar anchoring and high twisting power (qR>1), the most frequently observed configuration is the Frank-Pryce structure, which consists of a central hedgehog with a defect line s=+2 with length R (Figure 2.20e). This line can be explained considering the liquid crystal as a set of nematic planes. The line is the result of the concentric stacking of these nematic layers inside the drop, with each layer slightly rotated respect to the other. Since the total topological charge must be +2 in each layer, the defect line can be seen as a linear stacking of defect points s=+2 in each cholesteric layer. By varying the droplet size with respect to the cholesteric pitch, the configuration of the drop progressively changes from a twisted bipolar to the Frank- Pryce structure (Figure 2.20).

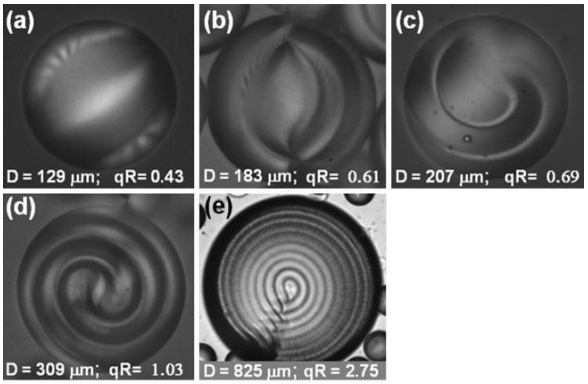

Figure 2.20: Cholesteric liquid crystal droplets with planar anchoring conditions and different twisting power, qR, ordered ascendingly (a-e).

In the case of homeotropic alignment and large qR, the Frank-Pryce structure is prevalent since the conditions at the surface are incapable of varying the packing of the layers.

Homeotropic anchoring at the droplet boundary gives rise to many different structures depending on the relative helicity parameter $N_0 = \frac{2D}{p}$ (D is the droplet diameter) (15) (16) (17).

The dependence of the orientational structures in cholesteric drops with homeotropic surface anchoring on the helicity parameter was investigated by experiments and simulations (15). A sequence of structures was identified comparing the director configurations and topological defects simulated textures with polarised light optical microscopy images. With N_0=1.1 the radial structure is observed, the point defect is located in the centre of the drop and the director distribution is not twisted.

In drops with $N_0 > 1.1$, the twisted radial structure is observed, which still contains only one point defect, but it is sufficiently shifted towards the edge of the drop.

At $N_0 = 1.8$ this defect is almost at the edge of the droplet and does not shift with a further increase in droplet size. At the same time, the high overall twist of the director field compensates for the twisting power of the CLC (see Figure 2.21), which is visualised by the extinction lines of the radial structure.

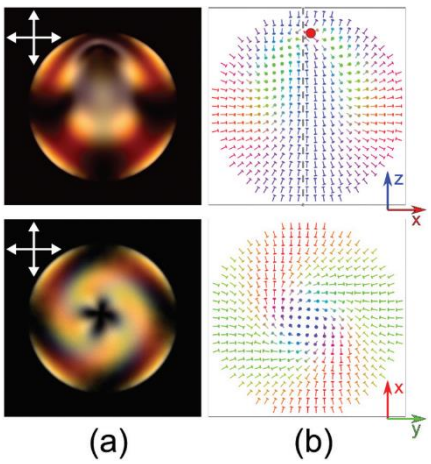

Figure 2.21: Optical textures and director distributions of a drop having a twisted radial structure: (a) simulated cross-polarized images; (b) corresponding director distributions in the central cross-section. The symmetry axis is oriented parallel (top row) and perpendicular (bottom row) to the viewing plane. The thick red line indicates the circular linear defect near the surface.

With $2.9 \leq N_0 \leq 5.8$ the Toron structure is observed. This structure presents the formation of an equatorial circular defect line near the drop surface (Figure 2.22).

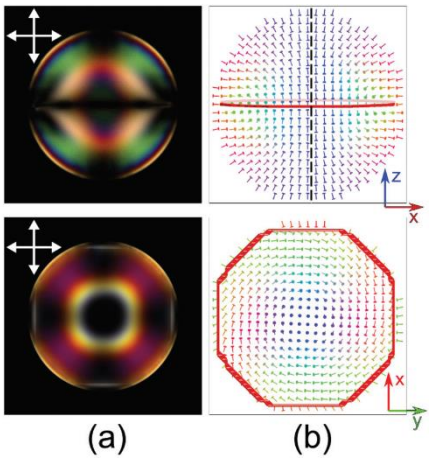

Figure 2.22: Optical textures and director distributions of a droplet having the Toron-like structure: (a) simulated cross-polarized images; (b) corresponding director distributions in the central cross-section. The symmetry axis is oriented parallel (top row) and perpendicular (bottom row) to the viewing plane. The thick red line indicates the circular linear defect near the surface.

A further increase in droplet diameter leads to an intermediate L_0 layer-like structure with a bipolar distribution of helical axes. (Figure 2.23).

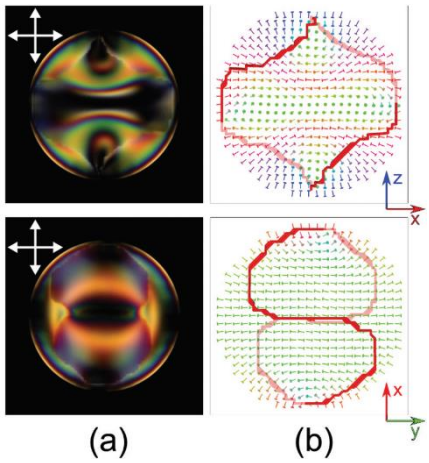

Figure 2.23: Optical textures and director distributions of a droplet having the intermediate (L0) structure: (a) simulated cross-polarized images; (b) corresponding director distributions in the central cross-section. The line of the distorted defect primarily lies in the plane of the film (top row) and perpendicular to it (bottom row). The thick red line indicates the twisted loop defect near the surface.

The central part of this texture has a narrow band along the x-axis, with the director oriented along the observation axis. The circular defect of this texture is sufficiently deformed and intersects the equatorial axis at the four points. The number of twists N in this structure does not vary with the size of the drop. Therefore, we will identify it as an intermediate layer-like structure and denote it as L_0 to indicate both its fixed geometry and its layered nature. A further increase in droplet diameter stabilises the layer-like structures (L) with a regular line of double-twist defects near the surface (Figure 2.24).

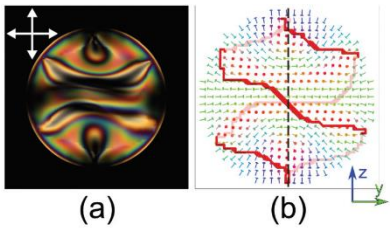

Figure 2.24: Optical textures and director distributions of a droplet having the layer-like (L) structure: (a) simulated cross-polarized images; (b) corresponding director distributions in the central cross-section. The bipolar axis lies in the plane of the film. The polarizer is aligned perpendicularly to the bipolar axis. The thick red line indicates the twisted loop defect near the surface.

The stability of the two types of layer-like structures, L_0 and L, is explained by the bistability of the layer-like structure in the case of smaller diameters. The balance between elastic and defect energies results in two minima of energy (L_0 and L) between N_0 = 5.2 and 5.8. These minima are separated by an energy barrier, which makes the transformation of L_0 into the regular structure L by further torsion unfavourable. It is worth nothing that in some intervals the different textures can be observed simultaneously (Figure 2.25).

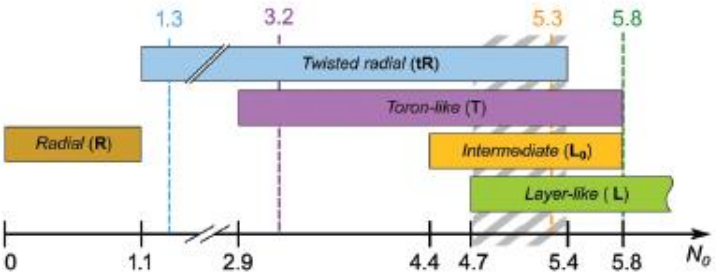

Figure 2.25: Diagram of the droplet state observed experimentally at various droplet sizes expressed by the relative helicity parameter N_0. The range of coexistence of the four structures is shown with grey hatch.

2.8 Chromonics in spherical confinement

The micro-droplets of thermotropic liquid crystals, and the different configurations that the director assumes, have been largely studied, and since the volume elastic properties and anchoring phenomena at the interface are quite easily understood and controlled, they find application in the field of displays, biosensors and microlasers.

Compared to thermotropic liquid crystals, lyotropic liquid crystal droplets are less studied because it is difficult to confine them in a matrix preventing both coalescence and water evaporation.

Furthermore, in chromonics K_{11} and K_{33} have the same order of magnitude, while K_{22} is lower by one order of magnitude. This explain why, when they are confined in curved geometries,

show a large reflection symmetry breaking, i.e. the strong splay and bend deformations of the director are relaxed trough twist deformation.

In 2013, Joonwoo Jeong and his co-workers carried out detailed studies on the chromonic liquid crystal Sunset Yellow confined in microspheres with planar anchoring conditions at the interface (18). The microdroplets were stabilised in a hexadecane matrix containing a non-ionic surfactant: sorbitan monooleate (Span 80) (18). The director, in the nematic phase, adopted a distorted bipolar configuration with a strong twist revealed by optical microscopy in polarised light. Figure 2.26a shows the typical bipolar configuration found in a thermotropic LC with two boojums located at opposite poles of the drop, represented by the black dots, while the yellow rods represent the director configuration. In chromonic LCs, on the other hand, the microspheres show a distorted chiral bipolar configuration in which the director rotates in a helicoidal manner with the axis of the helix perpendicular to the boojums (Figure 2.26b).

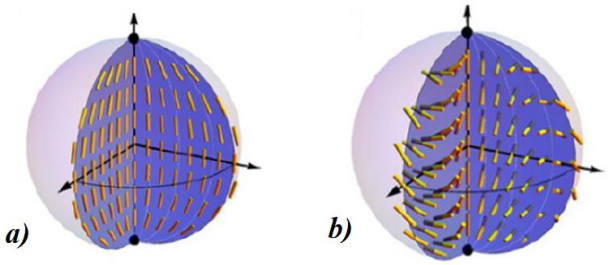

Figure 2.26: Schematic diagrams of: a) bipolar configuration, b) twisted bipolar configuration.

Considering the homogeneous and isotropic nature of the oil matrix and observing the boojums, the authors hypothesised that the anchoring is degenerate and uniformly planar at the interface between liquid crystal and oil.

Recently, an extensive study has been performed on a type of chiral lyotropic liquid crystal that exhibit in water a natural cholesteric phase: cellulose nanocrystals (CNCs). In 2016, Yungfen Li and co-workers reported on the configurations the director takes when a solution of cellulose nanocrystals is confined in microdroplets (19). Unlike in thermotropic chiral mesogens, the confinement of the CNC liquid crystal shows a phase separation between the core and the rest of the droplet. In particular: the core of the drop is in isotropic phase, while, the rest of the drop is in chiral phase, exhibiting a concentric packing of the outer layers consisting of CNC molecules. To describe this behaviour it is important to introduce another term in Oseen-Frank theory of the elastic energy that it is usually neglected for thermotropic LCs: the saddle-splay term, which is an elastic energy related to the distortion of the director field. The saddle-splay term, denoted K_{24}, refers to a deformation of the director field such that **n**(r) is normal to a

saddle surface. Such surfaces have a negative Gaussian curvature, i.e. two principal curvatures of opposite sign, a saddle curve upwards along the crotch but downwards through the crotch. The corresponding energy density is a pure divergence term (equation 15):

$$f_{24} = -\frac{K_{24}}{2}\nabla \cdot (n\nabla \cdot n + n \times \nabla \times n) \qquad (15)$$

Its volume integral, required to calculate the corresponding energy, can be converted into a surface integral via the Gauss' theorem, provided that K_{24} is constant within the integration volume (equation 16)

$$F_{24} = \int f_{24}\, dV = -\frac{K_{24}}{2}\int dS \cdot (n\nabla \cdot n + n \times \nabla \times n) \qquad (16)$$

When considering strongly confined LC samples, such as droplets, the total free energy is:

$$E = F_D + F_{24} + \int F_S\, dS = \int f_D dV - \frac{K_{24}}{2}\int dS \cdot (n\nabla \cdot n + n \times \nabla \times n) + \int F_S\, dS \qquad (17)$$

F_{24} is the only contribution that has a negative sign; a saddle-splay deformation of the boundary interface actually decreases the energy if $K_{24} > 0$.

When considering samples with a large size, the saddle-splay term is ignored because it does not influence the bulk energy away from the boundaries. Furthermore, when the sample boundaries are flat, the contribution of F_{24} disappears totally. In contrast, on small samples with strongly curved boundaries, the contribution of F_{24} can play an important role.

If K_{24} varies within the sample volume (the order parameter S is non-uniform), Gauss's theorem cannot be applied and the saddle-splay contribution must be treated as an elastic bulk energy.

When the boundaries are strongly curved, the boundary conditions impose elastic distortions within the LC, increasing the free energy. Unlike the elastic bulk constants of splay, twist and bend, since the saddle-splay energy density contains no squared terms, the saddle-splay constant K_{24} can take on negative and positive signs.

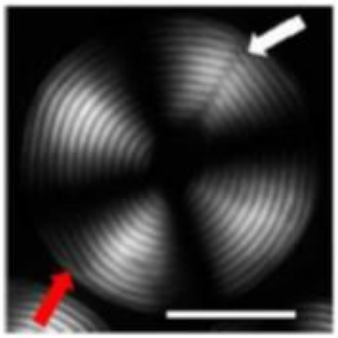

Figure 2.27: Polarised light microscope image of a CNC cholesteric microdroplet. The scale bar is 50 μm. The white arrow indicates the defect running perpendicular to the cholesteric layers. The red arrow indicates an edge dislocation parallel to the cholesteric layers.

The optical microscope image in polarised light (Figure 2.27) shows the characteristic structures of the cholesteric phase, a Maltese cross and a shell with alternating light and dark concentric rings corresponding to the surfaces at constant refractive index. The concentric spherical packing of the cholesteric layers begins at the interface between the microsphere and the matrix, and gradually propagates towards the centre of the drop. The centre appears as black highlighting the presence of an isotropic core. As deduced from the topology, in the spherical confinement of the cholesteric phase, the equilibrium state must be accompanied by a minimum number of defects; the disclination is indicated with a white arrow and the presence of an occasional dislocation with a red line.

A very important difference between chromonic and thermotropic chiral liquid crystals is the size of the isotropic core, which is much larger in chromonics. To understand the mechanism that leads to the creation of such a large isotropic core in CNC droplets, one must consider the balance between elastic, condensation and surface energies. The free energy associated with the formation of an isotropic core with radius r_i, in a microsphere whose radius is larger than the cholesteric helical pitch, is given by the following formula (19):

$$F = 8\pi\,(K_{11} - K_{24})\,(R - r_i) + 4\pi\sigma_{chi}r_i^2 + \frac{4}{3}\pi(f_i - f_{ch})r_i^3 \qquad (18)$$

The first term is related to the distortion of the cholesteric layers, the second is related to the energy at the cholesteric-isotropic interface, and the third is the difference in free energy between the isotropic and cholesteric phases. As explained above, the constants K_{11} and K_{24} are the splay and saddle splay of the cholesteric phase, respectively, σ_{chi} is the tension at the interface between the chiral and isotropic phases, and f_i and f_{ch} are the free energy density of the isotropic and chiral phases. Since the terms (K_{11}-K_{24}), σ_{chi} and (f_i-f_{ch}) are all greater than zero, the only term that favours the existence of an isotropic core is -8π(K_{11}-K_{24}) r_i, for which

the elastic energy is reduced when the curved chiral layers are replaced in the centre of the drop with an isotropic spherical region. This implies that a fraction of CNC is transferred from the core into the cholesteric shell. The fraction transferred in the volume is very small and no significant change in the measured pitch is observed in the shell. To obtain an order of magnitude estimate of the inner core, the difference in free energy density is approximated by the chemical potentials of the isotropic μ_i phase and the cholesteric μ_{ch} phase and related to parameters such as the volume of the individual CNC, V_{CNC}, the exact distribution of the shape and size of the CNC, the Boltzmann constant, the temperature and the average excluded volume of a CNC.

Minimising the energy in the previous equation with respect to r_i, it is found that:

$$r_i^* = \frac{\sqrt{2\Delta f(K_1 - K_{24}) + \sigma_{chi}^2} - \sigma_{chi}}{\Delta f} \tag{19}$$

where $\Delta f = f_i - f_{ch} \sim \frac{\mu_i - \mu_{ch}}{v_{CNC}}$ does not depend on the size of the droplet. To gain an idea of the size of the core, we consider the tension at the interface σ_{chi} between the isotropic and cholesteric phase formed by an aqueous suspension of CNC core of the order of $10^{-7} – 10^{-6}$ Jm^{-2} as determined experimentally (20). The value of Δf is approximately 20 Jm^{-3}.

For K= 10pN, a typical value for chromonic liquid crystals, the equation predicts a radius r_i of the order of 1μm, which is close to the experimentally measured value. This radius is two or three orders of magnitude larger than the one recorded for a thermotropic liquid crystal, usually between 2nm and 50nm. The reason for this is that the quantity Δf is about five times larger than the Δf in the cholesteric phase of the CNCs (21). There is no literature available on the confinement of non-native chiral cholesterics in microdroplets.

2.9 Liquid crystals in an electric field

LCs are dielectrical anisotropic media, that is, the dielectric constant of the material depends on the direction in which it is measured. The dielectric tensor of nematic liquid crystals, using a reference frame with Z axis parallel to the director, can be expressed as:

$$\begin{bmatrix} \varepsilon_\perp & 0 & 0 \\ 0 & \varepsilon_\perp & 0 \\ 0 & 0 & \varepsilon_\parallel \end{bmatrix} \tag{20}$$

where $\varepsilon_\perp$ and $\varepsilon_\parallel$, denote the dielectric constants measured perpendicularly and parallel to the director, respectively. Dielectric anisotropy is defined by $\Delta\varepsilon = \varepsilon_\parallel - \varepsilon_\perp$, where $\Delta\varepsilon$ can be either

positive or negative, depending on the molecule dipole moment. If the dipole moment is aligned with the long axis of the molecule, in the presence of an electric field the molecule will be oriented in the same direction as the electric field, so $\Delta\varepsilon$ will be positive. In contrast, if the dipole moment is perpendicular to the molecular axis, there will be an alignment of the molecules perpendicular to the applied field, with $\Delta\varepsilon$ being negative (1).

Considering a planar cell, containing a nematic liquid crystal with positive dielectric anisotropy, if an electric field is applied normally to the surfaces, the LC nematic director will distort (Figure 2.28).

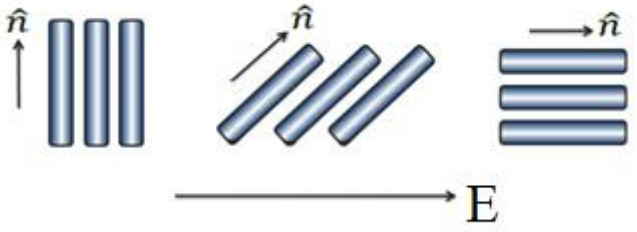

Figure 2.28: Example of director distortion $\hat{n}$.

When a critical intensity E_H is reached, the liquid crystal exhibits a continuous transition, called the Fréedericksz transition, due to the realignment of the director along the field direction. This critical intensity is given by the approximate equation:

$$E_H \cong \frac{4}{d}\sqrt{\frac{4\pi K}{|\Delta\varepsilon|}} \qquad (21)$$

where d is the cell thickness and K represents the elastic constants (K_{11}~K_{33}).

Cholesteric LCs also reorient in the presence of an electric field. The effect of the electric field depends on the surface treatment of the substrates confining the chiral mixture, the cholesteric helix pitch, the ratio between cell thickness and helix pitch, and the frequency and intensity of the applied field.

Suppose we have a CLC placed between two glasses covered with a conducting material and treated to provide planar alignment, with the thickness between the two glasses larger than the helix pitch. In the absence of an electric field, we have a planar structure, with the helices parallel to each other and arranged orthogonally to the glass slide (Figure 2.29a). When a moderate electric field is applied, there is an increase in the pitch of the cholesteric helix, until the structure begins to deform, and the cholesteric material is arranged in a focal conic structure (Figure 2.29b). The creation of poly-domains occurs, giving rise to a mosaic texture that returns to its initial state when the field is switched off.

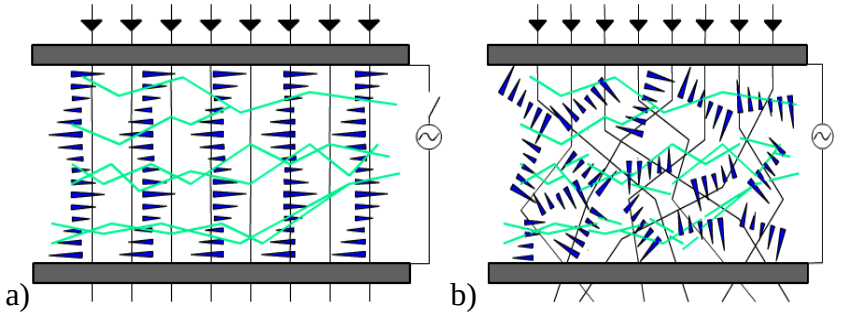

Figure 2.29: (a) Structure of cholesteric mixture in the absence of electric field; (b) Structure of cholesteric mixture in the presence of moderate electric field.

If the electric field is increased further, the cholesteric liquid crystal is arranged in a homeotropic structure.

In 1982 R. Bartolino and his collaborators studied the effects of the electric field on the structure of cholesteric LCs, finding a well-defined sequence of deformations in samples in which the thickness is larger than the pitch of the helix (22).

In the graph, shown in Figure 2.30, Λ represents the wavelength of the reflection peak when the electric field is applied and Λ_0 represents the wavelength of the reflection peak at zero field. On the horizontal axis is shown E/E_H where E is the applied field and E_H represents the threshold value of the first observed strain.

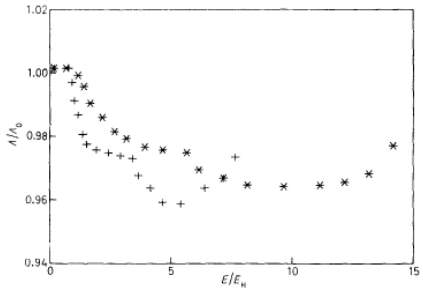

Figure 2.30: Wavelength of the normalized reflection peak Λ / Λ_0 versus the applied normalized field E/E_H.

Three threshold values of the electric field were identified for which different deformations occur. For low fields, the first deformation observed is a texture exhibiting ripples, followed by a focal conical structure, while for high fields, there is a different deformation not studied in detail due to difficulties with hydrodynamic motions.

Chapter 3 Model chromonics

This chapter is devoted to the analysis of experimental data obtained on model chromonic liquid crystals using polarized light optical microscopy, x-ray diffraction and atomic force microscopy techniques. The effects on texture due to confinement of materials in planar and spherical geometry, and the effect of chiral dopants are described.

3.1 Materials

Chromonics

Disodium chromoglycate and Sunset Yellow, both purchased from Sigma Aldrich, are used as model chromonic materials.

Specifically, disodium chromoglycate, whose molecular structure is shown in Figure 3.1 is an anti-asthmatic drug. The brute formula is $C_{23}H_{14}O_{11}Na_2$ and the molecular weight is 512.33 g/mol. The compound, an odourless, white, hydrated crystalline powder, is the disodium salt of dibasic acid: 1, 3-bis(2-carboxychromon-5-yloxy)-2-hydroxypropane (23). Its crystals are an interstitial solid solution, with water as the interstitial component.

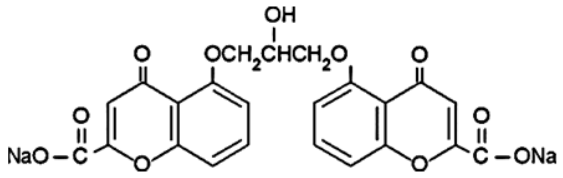

Figure 3.1: Molecular structure of DSCG

The unit cell expands to accommodate up to about nine water molecules before collapsing to form liquid crystalline hydrates. DSCG crystals are unique in their degree of reversible water absorption without lattice collapse.

In this work, DSCG was used at a concentration of 13wt% in water because, as can be seen from the phase diagram shown in Figure 3.2, at this concentration it is in nematic phase at room temperature (6), this phase is less viscous than the hexagonal phase and therefore easier to align.

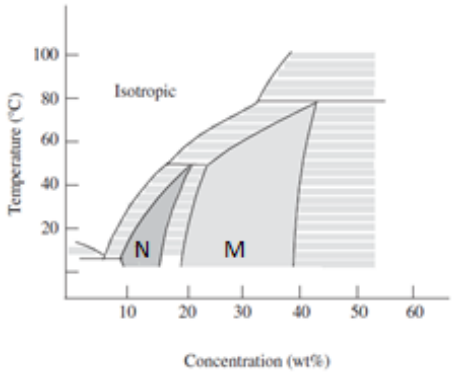

Figure 3.2: DSCG phase diagram

For a concentration range (12.5-18) wt% the twist constant (K_{22}) is more than 10 times smaller than the splay (K_{11}) and bend (K_{33}) constants, while K_{11} and K_{33} are comparable to each other. It was observed that of the three elastic constants, (K_{11}) has the strongest temperature dependence, described by an exponential function of T (Figure 3.3).

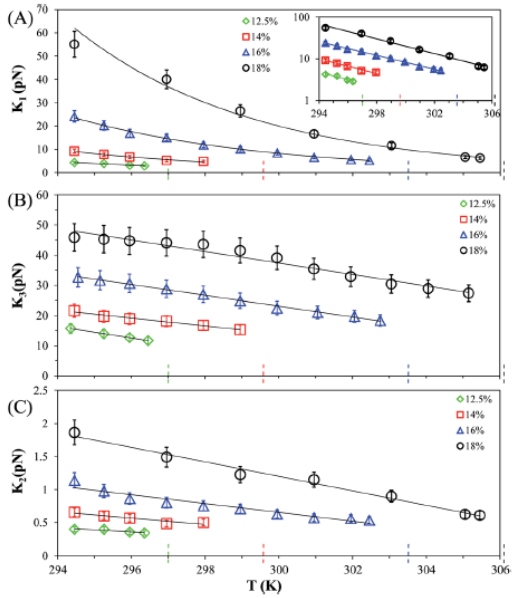

Figure 3.3: Temperature and concentration dependences of elastic constants of a) splay K11, b) bend K33 and c) twist K22 distortions in the nematic DSCG phase. Ref (24).

The analysis performed on DSCG, a material widely studied in the literature in both nematic and chiral phases, was a guideline for the subsequent analysis on Sunset Yellow. Sunset Yellow, namely the disodium salt of 6 – hydroxy – 5 - [(4-sulfophenyl)azo] – 2 - naphthalene sulfonic acid, whose molecular structure is shown in Figure 3.4 is a food dye. The brute formula is $C_{16}H_{10}N_2Na_2O_7S_2$ and the molecular weight is 452.37 g/mol.

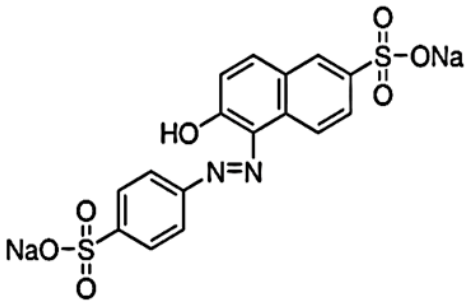

Figure 3.4: Molecular structure of SSY

SSY can exist in two tautomeric forms (25): an NH hydrazone form where the hydrogen resides on the distant nitrogen of the azo bond, and an OH azo-tautomer form, where the hydroxide proton resides on the oxygen in ortho to the azo bond.

Edwards et al (26) showed that the NH hydrazonic form prevails. The azo form can make cis-trans isomers; this change in isomers occurs when the molecule interacts with light in the 480-500nm wavelength range. A 30wt% concentration of Sunset Yellow in water was used, since, as it can be seen from the phase diagram shown in Figure 3.5 (26), the nematic phase (N) appears at a concentration of about 30-40wt% by weight, and the hexagonal phase (C) at about 40-45wt% by weight.

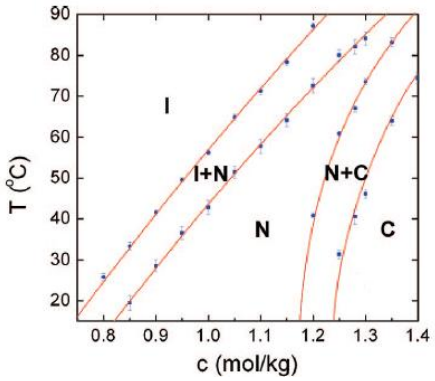

Figure 3.5: SSY phase diagram

The modulus of elastic constants was also found for SSY, and similarly to DSCG, the twist constant (K22) is much smaller than the splay (K11) and bend (K33) constants, while K11 and K33 are comparable to each other. To induce chirality in chromonics, three different aminoacids were tested: L-Alanine, L-Lysine, Trans-4-hydroxy-L-proline. As reported in literature, it is easy to induce a chiral phase in DSCG doping it with chiral aminoacids (24) (27) (28) (29).

Chiral aminoacids

L-Alanine [(S)-2-aminopropanoic acid], shown in Figure 3.6, purchased from Sigma Aldrich, is a non-polar amino acid that occurs as a white-yellow crystalline powder and is a water-soluble left-handed dopant. This aminoacid has a twisting power of 0.75 μm^{-1} $wt\%^{-1}$ (28). The molecular weight is 89.09 g/mol.

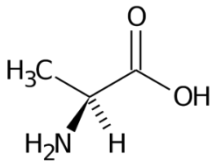

Figura 3.6: Molecular structure of L-Alanine

L-Lysine [(2S)-2,6-diaminohexanoic acid hydrochloride], purchased from Sigma Aldrich, is a polar amino acid that occurs as a white crystalline powder (Figure 3.7). L-Lysine is a left-handed dopant that is easily soluble in water. This aminoacid has a twisting power of 0.8 $\mu m^{-1} wt\%^{-1}$ (29). The molecular weight is 182.65 g/mol.

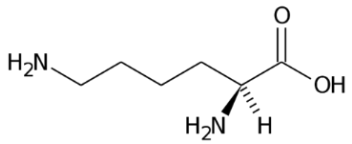

Figura 3.7: Molecular structure of L-Lysine

Trans-4-Hydroxy-L-proline [(2S,4R)-4-hydroxypyrrolidine-2-carboxylate], (Trans-Hyp) purchased from Steinheim, Germany, is a cyclic amino acid (Figure 3.8) and occurs as a white crystalline powder at room temperature. It is easily soluble in water and is a left-handed chiral dopant. This aminoacid has a twisting power of 2.5 μm^{-1} $wt\%^{-1}$ (28). The molecular weight is 131.13 g/mol.

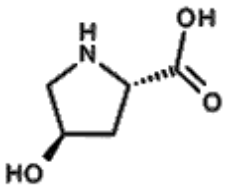

Figura 3.8: Molecular structure of trans-4- hydroxy-L-proline

Immiscible matrices

Both paraffin oil and polydimethylsiloxane (PDMS) have been used in emulsions as an immiscible matrix. Paraffin oil (Sigma-Aldrich) is obtained in the petroleum distillation

process. It is a colourless, odourless oil and is not soluble in water. Polydimethylsiloxane (Sylgard, Sigma-Aldrich) is a liquid polymer that appears oily and transparent and has a high viscosity.

PDMS was used both pure, as an oil in which to disperse the liquid crystal, and in thin film form. In this latter case, a solution consisting of 1 part crosslinker and 9 parts PDMS was prepared. PDMS brute formula is $(C_2H_6OSi)n$, the structure of the repeating unit is shown in Figure 3.9.

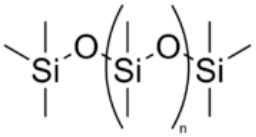

Figura 3.9: repetitive unit of PDMS

Fluorescent dye

The dye used was Oxazine725, [3,7-bis(diethylamino)phenoxazin-5-ium perchlorate; Oxazine 1- Exciton], which appears as a green powder. This dye in water absorbs visible light at 650nm and emits fluorescent light at 725nm, the chemical formula is $C_{20}H_{26}N_3O.ClO_4$, the molecular weight is 423.90; the structure is shown in Figure 3.10.

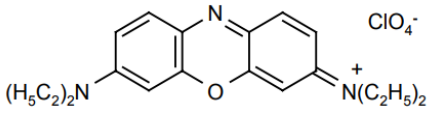

Figura 3.10: Molecular structure of Oxazine725

3.2 Planar confinement

To analyze DSCG and SSY in planar geometry, standard optical cells were prepared. Laboratory glass slides were cut obtaining pieces of size 2.5cm x 2cm and 2.5cm x 3cm, these were washed with soap and water to remove oily impurities and dust deposits. To complete the washing, they were immersed in a NaOH 5wt% aqueous solution and placed in an ultrasonic bath for 6 min at 30°C. Finally, they were rinsed with distilled water (to remove residual traces of NaOH) and dried with a jet of hot air.

A thin layer of polymer solution was deposited by spin-coating on one side of the glass slides. Finally, to remove any trace of solvent, the polymer-coated glasses were placed in an oven. In some cases to orient the liquid crystal molecules, the polymer layer was treated with the rubbing technique.

Cells assembly consists in placing the small glass slide on the big one, with the two polymer layers in front of each other. Two strips of mylar were inserted between two glass slides to create a uniform thickness within the cell (10μm and 25μm), then, a drop of 5μl of liquid crystal mixture was infiltrated.

The cells were observed using a polarized light microscope, specifically, a Leica DMRX (Germany) was used in this work. The images collected were studied using the ImageJ program and the results were processed with OriginPro.

A Bruker D8 Discover reflectometer with a copper anode was used for X-ray diffractometry measurements eather in Bragg Brentano and Asymmetric geometry. The peaks obtained were measured using the OriginPro data analysis program in order to estimate their width and position. While for AFM measurements, a Bruker Multimode 8 equipped with a Nanoscope V controller in tapping mode was used, the images were acquired in air using a cantilever with a resonance frequency of 150 kHz and were analysed with the WSxM program.

3.2.1 Disodium chromoglycate

We tried several polymers to align DSCG and we observed, as already reported in literature that DSCG can be easily aligned in planar configuration using, for example, polymethilmetacrylate (PMMA). On the other hand, homeotropic alignment is more difficult to achieve. This could be related to the presence within the molecule of a very flexible bond that limits interactions with the substrate which, therefore, fails to impose a homeotropic anchoring direction. A few works are reported in literature on that subject in which the homeotropic alignment is obtained by low surface energy materials like PDMS; graphene and CYTOP (30) (2).

3.2.2 Chiral disodium chromoglycate

Chirality was induced in DSCG and textures were studied using PMMA for planar alignment and CYTOP for homeotropic alignment.

The experiments were conducted on a mixture of DSCG 13wt% in wt. and chiral dopant L-Alanine 10wt% in wt. In planar alignment conditions the oily streaks texture (Figure 3.11a), which is typical of thermotropic cholesteric liquid crystals, is observed. For homeotropic alignment the fingerprint texture (Figure 3.11b), is observed. Such a texture is extremely

interesting for applications and can be used to measure the cholesteric helical pitch. The fingerprint texture is stable over time, and a pitch of 12±0.5 μm can be observed.

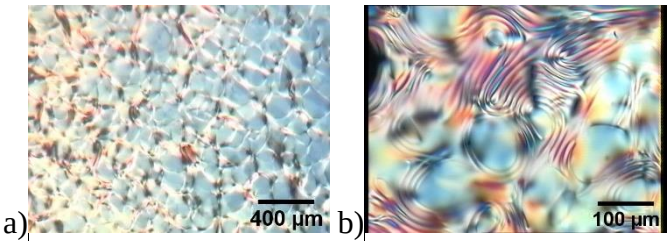

Figure 3.11: a) oily streaks texture of a 13wt% DSCG mixture in 10wt% L-Alanine in planar alignment conditions, b) fingerprint texture of a 13wt% DSCG mixture in 10wt% L-Alanine in homeotropic confinement.

Similar fingerprint texture was also observed doping DSCG with Trans-Hyp, while no chirality induction was observed for L-Lysine.

3.2.3 Sunset Yellow

A mixture of Sunset Yellow 30wt% in wt. in water was prepared and its textures are observed in planar and homeotropic confinement. Sunset Yellow, differently from DSCG prefers to align in homeotropic configuration. Sometimes the final homeotropic texture is reached after a metastable state in which stripes develop inside the cells. The presence of stripes-like textures is not new in the case of Sunset Yellow; in fact, it has already been observed using a hydrophobic fluoropolymer as an aligning surface or in capillaries (27) (31).

J. Jeong et al proposed the model shown in Figure 3.12 based on their experimental observations (30).

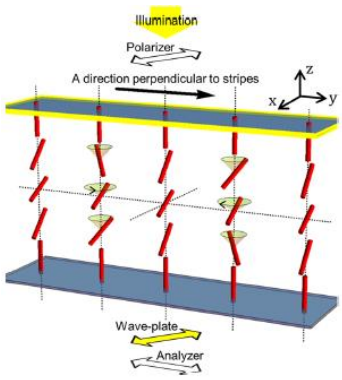

Figure 3.12: Model proposed for the stripes obtained in SSY for homeotropic anchoring conditions.

According to their model, stripes arise from the interplay among the surface energies, the self-assembly properties of materials and the anisotropy of elastic constants. In fact, the elastic constant of twist is at least an order of magnitude lower than that of splay and bend. Finally, the thickness of the cell plays a role in the size of the stripes.

The homeotropic alignment obtained on these surfaces may be related to noncovalent interactions between LCLC molecules and the alignment layers, such as hydrophobic

interactions, π-π stacking, or van der Waals interactions. In all articles, the stripes are transient and disappear in favour of a homeotropic alignment with different times depending on the treatment used. Periodicities of tens of microns are obtained.

We were able to obtain planar alignment only using rubbed Cytop (Asahi Glass), an highly hydrophobic fluoropolymer. Hence, for Sunset Yellow, the best confining surfaces that provide a uniform alignment are PMMA that provides a homeotropic alignment and rubbed Cytop that provides a perfect planar alignment (Figure 3.13a-b). The other substrates used, however, provide more complex and unstable textures as in the case of PDMS.

a) 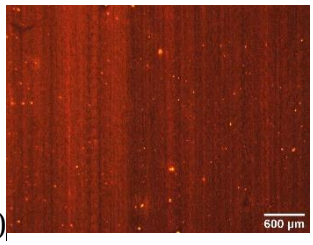

b) 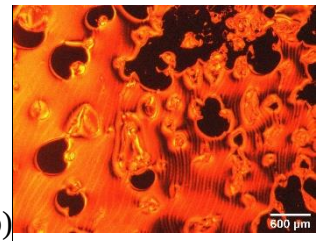

Figure 3.13: a) perfect planar alignment in cell with Cytop rubbed glasses, b) stripes observed in cell with rubbed PDMS coated glasses.

3.2.4 Chiral Sunset Yellow

Several attempts have been done to induce chirality in SunsetYellow. In literature there are no data on this subject. Two L-aminoacids were used and the alignment in different anchoring conditions was studied.

- *L-Lysine*

A mixture of 30wt% Sunset Yellow in 10wt% L-Lysine was placed in a cell between rubbed PMMA coated glasses and using a thickness of 10 µm. Since L-Lysine is highly soluble in Sunset Yellow, then, it was possible to prepare mixtures of SSY 30wt% with different concentrations (10, 20 and 30wt% L-Lysine) in an attempt to increase the twisting effect and consequently to lower the helical pitch. Initially, the chiral chromonic showed a planar alignment (Figure 3.14a), after 6 days, the observed area became homeotropic (Figure 3.14b).

a) 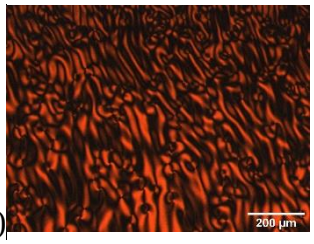 b) 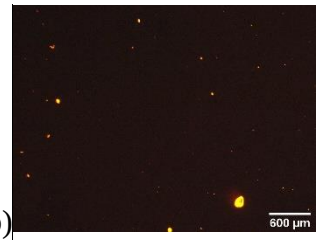

Figure 3.14: (a) Planar alignment for a Sunset mixture structure in cell with 10µm thickness, (b) homeotropic alignment observed after few days.

Using a cell thickness of 25 µm, the chromonic showed a homeotropic alignment that remained stable on time (Figure 3.15).

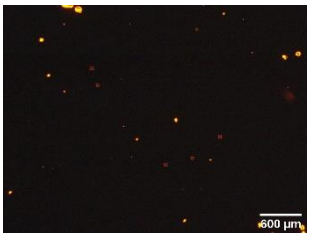

Figure 3.15: Homeotropic structure of the mixture in a cell with a 25µm thickness.

The same behaviour for the two cell thicknesses was observed for mixtures containing 20wt% L-Lysine. The mixture of 30wt% Sunset Yellow in 30wt% L-Lysine, instead, appeared to be isotropic. This may be because the high concentration of L-Lysine shifted the phase diagram of Sunset Yellow.

A final mixture of 40wt% Sunset Yellow in 30wt% L-Lysine was confined in a cell with planar anchoring and with 10 µm cell thickness. The mixture had a planar alignment with stripes formation evolving into homeotropic texture. Unfortunately, after few hours the formation of small, irregularly shaped aggregates not referable to known structures was observed. One can assume the formation of crystallites due to segregation of the two materials. On the other hand, using a cell thickness of 25 µm, the texture showed a dense pattern, not easy to identify, which remained stable over time.

In conclusion, with L-Lysine, it was not possible to observe the typical textures of the cholesteric phase even increasing the thickness of the cell: in both cases (SSY 30wt% and SSY 30wt% doped with L-Lysine) thread-like textures, typical of the nematic phase, prevail (Figure 3.16).

a) 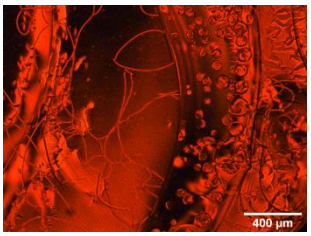 b) 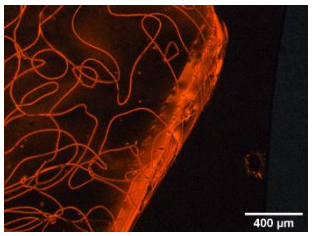

Figure 3.16: POM images of wedge cell with 380μm thickness: a) SSY 30wt% and b) SSY 30wt% doped with L-Lisine 10wt%

- *L-Alanine*

The mixture of Sunset Yellow 30wt% and L-Alanine 10wt% confined in a cell with rubbed PMMA-coated glasses and with a 10 μm thickness, initially forms stripes with a pitch of 21.5±0.5 μm (Figure 3.17a) that, in time, evolve into homeotropic alignment (Figure 3.17b).

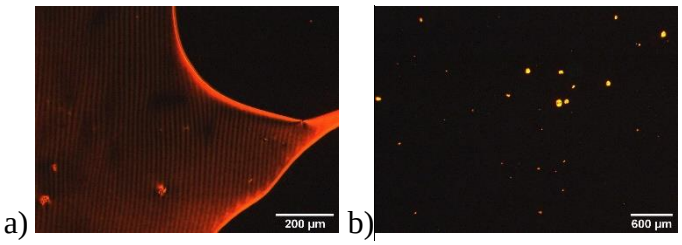

Figure 3.17: 30wt% Sunset Yellow with 10wt% L-Alanine confined in a cell with rubbed PMMA-coated glass and with 10 μm thickness observed: a) immediately after creating the cell; b) after few minutes.

The addition of the chiral dopant does not appear to induce chiral structures in the mixture for L-Alanine either.

- *Trans-4-hydroxy-L-proline*

Confining the mixture of 30wt% Sunset Yellow and 26wt% Trans-Hyp in a thick cell (200 microns) with PDMS-coated glasses, the presence of a fingerprint texture with a pitch of 46 μm is observed (Figure 3.18).

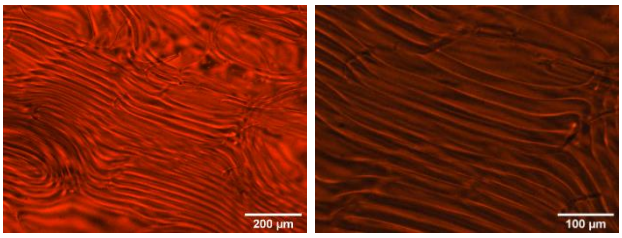

Figure 3.18: 30wt% Sunset Yellow and 26 wt% Trans-Hyp between two PDMS covered glasses.

Differently from the other two aminoacids, Trans-Hyp induces chirality in Sunset Yellow and it is the first time this phenomenon is observed in this particular chromonic in planar geometry.

3.3 Chromonics confined in micrometric droplets.

The confinement of chromonics in spherical geometries is obtained preparing emulsions. Emulsions were prepared by adding a small amount of a water-based chromonic solution in an oily matrix. In particular, polydimethylsiloxane (PDMS) and paraffin oil were used. By

mechanical agitation, a large number of microspheres were obtained. To observe the microspheres by microscopy techniques, an optical cell was prepared by placing a coverslip on a laboratory glass. Two mylar stripes of 190 μm and a drop of emulsion were placed between the two glasses. The cell was sealed using adhesive tape or glue.

3.3.1 L-Alanine doped DSCG

As previously discussed in Section 2.7, the configuration of the nematic director inside microspheres depends on several factors including the size of the microspheres themselves, the anchoring conditions at the interface and the elastic constants of the liquid crystal studied (14). PDMS was chosen as the confining medium, resulting in a stable mixture with microspheres with a well-defined contour.

- Optical textures

When pure DSCG is confined in microspheres (32), different textures are observed as a function of their size. In particular, bipolar textures are observed in large droplets, while small droplets exhibit the typical Maltese cross (Figure 3.19).

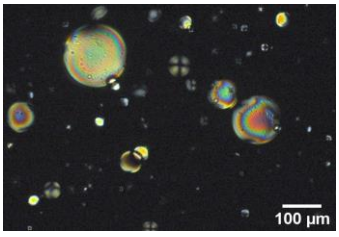

Figure 3.19: DSCG confined in microspheres

Maltese cross is related to the orientation of the liquid crystal molecules with respect to the polarizer and analyzer. The arms of the cross are visible because the light is not transmitted; in fact, along these two directions, the liquid crystal molecules are either perpendicular to the polarizer or to the analyser. In all other directions, that is, for all angles at which the molecules are not perpendicular to either the polarizer or the analyzer, the light is transmitted.

To induce chirality, DSCG was dissolved in 10wt% L-Alanine water solution. An emulsion was prepared by dispersing the liquid crystalline solution of chiral DSCG in PDMS. The resulting microspheres exhibited a well-defined chiral texture with concentric circles, the Frank-Pryce texture, which propagates from the borders to the central core as already observed for native chiral chromonics. In addition, the presence of radial disclination (a defect line along the radius) was clearly visible, in the same way as it is in thermotropic liquid crystals. The

possibility of obtaining this kind of texture in chiral chromonic liquid crystal microspheres was not obvious, because we are in the presence of a three-component system composed mainly of water, whose temporal stability is a delicate thermodynamical equilibrium. Nevertheless, the chiral texture is evident and the pitch is homogeneous, for example, in Figure 3.20, the diameter of the microsphere is about 89 μm with a pitch of 10.7±0.5 μm. This is the first reported observation of a Frank-Pryce texture in a chiral induced chromonic.

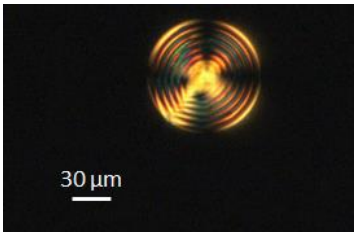

Figure 3.20: Microsphere of DSCG doped with L-Alanine

The core observed in this figure, reminds the one observed in chiral microspheres of cellulose nanocrystals (CNC) (33). In CNCs, the core is isotropic and shows up as a black spot in the center of the microsphere when observed between crossed polarizers. In the observed case, however, the core is bright (34).

Since in thermotropic liquid crystals confocal images provide more information about the shape and layered structure of the cholesteric microspheres, using the same approach, the solution was doped with Oxazine725. Unfortunately, the dye molecules were uniformly dispersed in the chromonic microsphere and do not provide additional information.

In principle, the dye used for confocal analysis should not interfere with the system under investigation, but in this case an improvement in the quality of Frank- Pryce textures was noted; this texture was observed in several microspheres of different diameters. The presence of Oxazine 725, in these concentrations (about 0.1 wt%), did not cause changes in the pitch of the cholesteric structure. The improved texture definition could be related to the fact that the molecule is charged and that the counter-ions can screen the charges present on the columnar aggregates of DSCG, reducing the electrostatic double-layer interactions by stabilizing the texture.

Figure 3.21a showed a 164 μm diameter microsphere with a well-defined Frank-Pryce texture, and the presence of a radial disclination line; the birefringent core had an oval shape and the observed pitch is 10.4 ± 0.5 μm.

In some cases, a double disclination line was observed (Figure 3.21b) and, for larger spheres, an increase in the size of the central core was observed (Figure 3.21c).

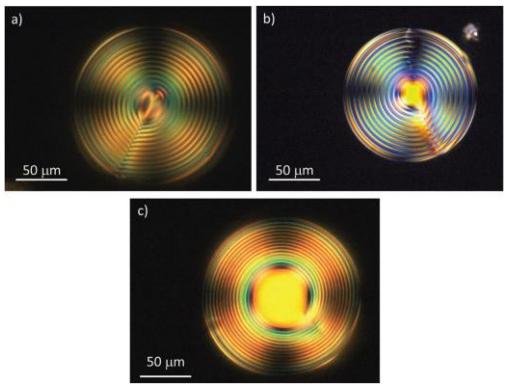

Figure 3.21: Microspheres of DSCG doped with L-Alanine and Oxazine725 in a PDMS matrix exhibiting different features: a) single disclination line, b) double disclination lines, and c) large central core.

The graph in Figure 3.22 compares the pitch versus diameter measurements on the microspheres shown for both the sample containing Oxazine 725 and the sample containing DSCG alone with L-Alanine. With the presence of the dye, the data are for the most part confined to a narrow range of values without showing abrupt changes, in contrast to what is observed in the samples without the dye.

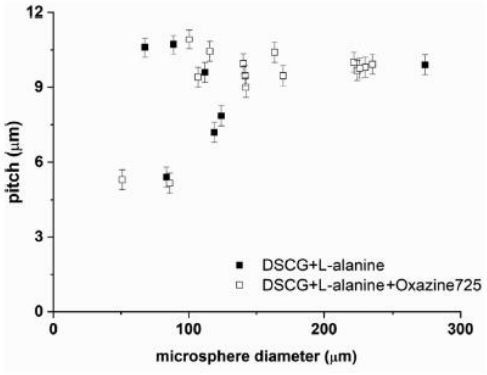

Figure 3.22: Cholesteric pitch as a function of microsphere diameter: DSCG+L-Alanine filled square and DSCG+L-Alanine+Oxazine hollow squares.

There is no substantial dependence of pitch on microsphere diameter, apart from small values observed for smaller diameters (smaller than 50 µm) that can be attributed to the balance between boundary conditions and twisting power (14).

We can assume that only L-Alanine is ejected from the core to pass into the zone where the concentric circle structures are observed. Thus, it may occur that only DSCG in nematic phase remains in the internal region, since a loss of chiral order is observed.

Unfortunately, even if the quality of Frank-Pryce texture is impressive, for a system that is mainly composed of water, it degrades in time. Texture deterioration in microspheres of DSCG

containing L-Alanine and Oxazine 725 was observed in a time interval of about 24 hours (Figure 3.23).

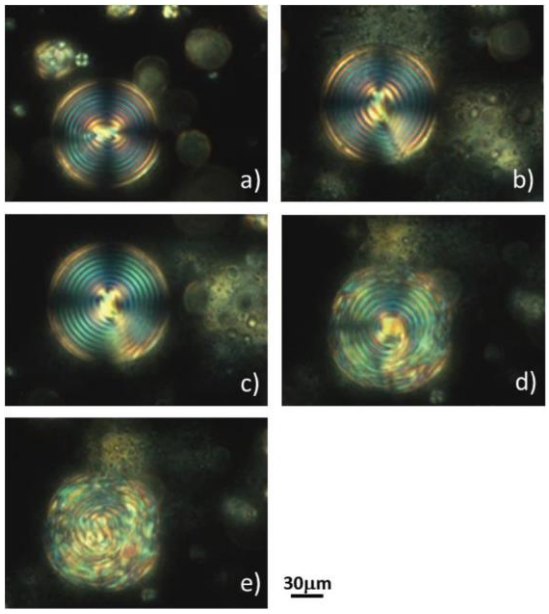

Figure 3.23: Microsphere degradation in about 24 h.

A microsphere with a diameter of about 122 µm is observed in a radial conformation (Figure 3.23a), in which concentric structures with a pitch of 9.6±0.5 µm have formed. After a few minutes, a defect begins to form along the radius of the microsphere (Figure 3.23b) until the texture deforms (Figure 3.23c).

It is deduced that the main cause of degradation is evaporation of water, that causes a transition to a different phase. The cholesteric structure begins to unfold from the surface of the microsphere, the disorder gradually increases toward the center of the microsphere until the Frank-Pryce structure is lost and the microsphere is in the nematic phase. Probably, during optical observation, the sample is heated and molecular diffusion occurs, which causes rearrangement of the chromonic phase. PDMS is excellent as an oil matrix because of its viscosity and the boundary conditions given on the surface but, unfortunately, it is permeable to water vapour (35) (36).

- *Ions effect on textures*

The effect that two different molar concentrations of potassium chloride (KCl), 0.01 M and 0.1M, have on the texture of chiral DSCG was also studied.

The lowest molarity solution (0.01 M) seems to disadvantage the formation of ordered structures made of concentric rings. In the case in which the structure forms (Figure 3.24a), the measured pitch is 9.0 ± 0.5 µm. In the smaller microspheres, the typical Maltese cross of

nematic droplets is observed. In contrast, the 0.1 M KCl solution seems to favor the formation of the chiral structure. The pitch of the microsphere in Figure 3.24b is 9.8 ± 0.5 μm.

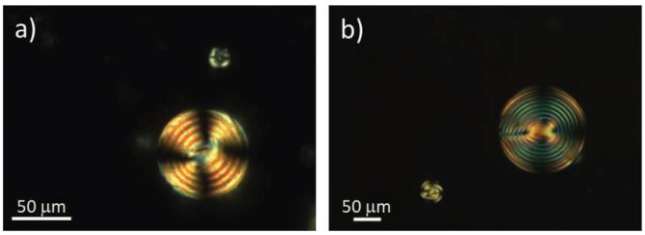

Figure 3.24: Chiral chromonic microspheres containing a) 0.01 M KCl solution and b) 0.1 M KCl solution.

In contrast to what has been reported in the literature for KCl, the pitch does not vary significantly in either case. The 0.1 M KCl samples show optically well-defined Frank-Pryce textures, suggesting that the electrostatic interaction between the salts and DSCG plays an important role in stabilizing the system.

In a 1984 paper, Lee and Labes report a study on the variation of the twisting power of a mixture of DSCG and different amino acids. Among their reported results, they present the effects that potassium chloride has on the pitch of a DSCG 13wt% solution doped with L-Alanine 12wt%. As it is shown in the table in Figure 3.25 (29), the addition of a given salt concentration leads to the change in measured pitch when the mixture is confined between two flat surfaces.

KCl Effect on the Pitch of 13 wt % DSCG/12 wt % *l*-alanine/H_2O

KCl Concentration mole liter^{-1}	Pitch (μm) at 20 °C	$T_{Ch \rightarrow I}$ (°K)
0	6	314.3
1×10^{-1}	12	306.1
1×10^{-2}	25	305.0
1×10^{-3}	30	301.5
1×10^{-4}	35	300.5
1×10^{-5}	30	301.7

Figure 3.25: Pitch variation with changing KCl concentration in an L-Alanine-doped DSCG sample (29).

In contrast, with microsphere confinement, no appreciable change on the pitch is observed after the addition of KCl in both 0.1M and 0.01M concentrations. In all cases, the measured pitch is about 10 μm which is a larger value than that reported in the table in Figure 3.25 for the DSCG containing L-Alanine alone. The helix pitch seems to be strongly influenced by small concentrations of salt and poorly affected by gradually increasing concentrations.

The data collected and summarized in the graph Figure 3.26, show that the pitch is contained for all samples in the range from 5 to 11 μm.

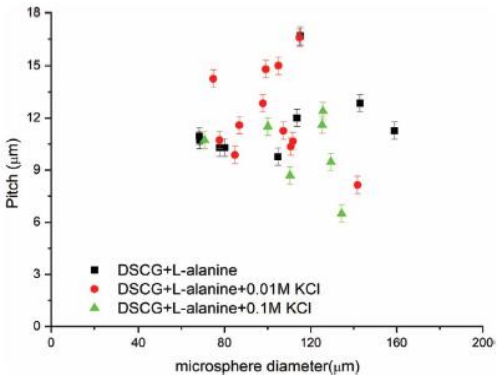

Figure 3.26: Cholesteric pitch as a function of microspheres diameter for DSCG+L-Alanine, DSCG+L-alanine+0.1 M KCl and DSCG+L-Alanine+0.01 M KCl

The addition of salt influences the structure in the same way as the addition of Oxazine725 does, and this can be understood by considering the effects of salt already observed on the phase behaviour, structure and rheology of LCs. In fact, in ref (37) authors showed the results of a research on the effect that the presence of salts has on the nematic phase of DSCG. In particular, they showed that the addition of sodium or potassium salts shifts the isotropic/nematic phase boundary by more than 10°C by stabilizing the nematic phase at the expense of the isotropic phase. The explanation for this is that some salts, particularly those with Na^+ and K^+ cations, promote the growth of rodlike DSCG aggregates. The nematic phase is reached when the rods reach a critical length and a certain volume fraction.

- *X-ray and AFM measurements*

To better understand the role of the chiral dopant in the supramolecular self-assembly mechanism, chromonic thin films were deposited on polymeric substrates.

The PDMS substrate was prepared by mixing PDMS with the hardener in the proportion of 9:1; once mixed, the solution was degassed under vacuum in order to eliminate air bubbles. The preparation was deposited uniformly on a slide using a spin coater and left to dry at a temperature of 110°C for about one hour. The substrate was, then, treated using a plasma cleaner. The action of the plasma on the PDMS causes bond breaking, resulting in increased wettability and change in surface energy.

Once the substrate was ready, 50μl of the liquid crystalline solution was deposited on the surface of PDMS. Samples were, then, placed in an air-tight humidity-controlled container and left to dry at a temperature of 4°C for one week. X-ray diffractometry and atomic force microscopy measurements were, then, carried out.

A sample of the DSCG nematic phase was prepared. As the nematic DSCG phase slowly dries, it transforms into the hexagonal phase, and the ordered structure is preserved when the sample is measured (Figure 3.27).

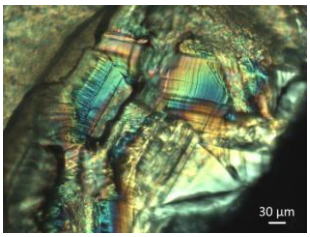

Figure 3.27: 13wt% dehydrated DSCG film on PDMS.

As reported in the literature, the powder itself is highly hygroscopic. In ref (23) the authors report on a systematic study of DSCG powder at different humidity conditions and compared the results with the crystallographic data of DSCG single crystal.

The single crystal structure is similar to a parallelepiped (Figure 3.28), in particular, the unit cell has the following dimensions 11.5Å x 15.8Å x 3.92Å and the central part is supposed to have a certain degree of flexibility.

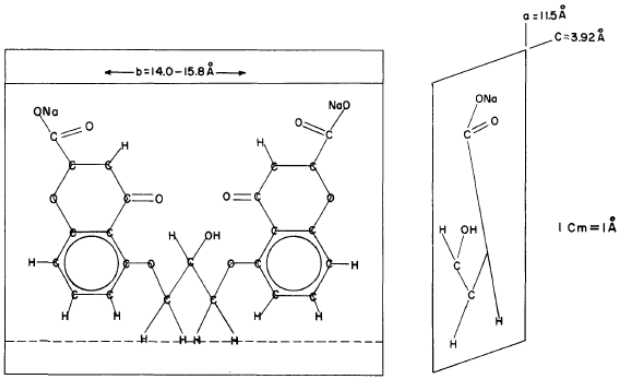

Figure 3.28: Crystal structure of DSCG (23).

In order to measure the distance between molecules, Bragg's law described in Section 2.5 is used, where λ=1.5418Å is the wavelength of the X-ray source ($CuK_{\alpha 1}$ and $CuK_{\alpha 2}$). X-ray measurements were acquired from 1° to 15°, whereas, measurement at high angles was not performed in all samples due to poor signal-to-noise ratio.

The hexagonal phase was found for the pure, low-angle DSCG sample as shown in Figure 3.29.

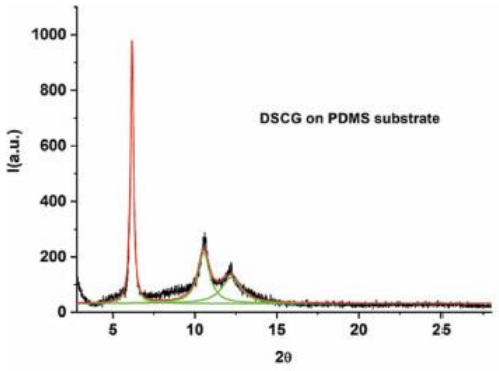

Figure 3.29: XRD spectra of DSCG thin film on a PDMS substrate

X-ray analysis shows the three typical peaks of the hexagonal phase, indicating good packing of the molecules, also confirmed by the peak width. The molecules are oriented with the b side of the molecule (Figure 3.29) perpendicular to the surface.

In Figure 3.30, the pure DSCG sample is compared with the cholesteric mixtures of DSCG doped with L-Alanine and DSCG doped with Oxazine and L-Alanine. The hexagonal arrangement is hindered and supra-molecular structures appear, related to the b-parameter of the single-crystalline cell. In addition, at high angles, reflections of the L-Alanine single crystal appear (38). The presence of L-Alanine, therefore, perturbed the order of DSCG and led to the formation of supramolecular structures due to the coupling between two molecules. These measurements confirm what was observed during the microsphere texture degradation in time due to water evaporation, the chiral aminoacid is expelled from the nematic phase.

The addition of Oxazine resulted in a situation similar to the case of L-Alanine alone, since the amount of dye added to the mixture is about one part per thousand.

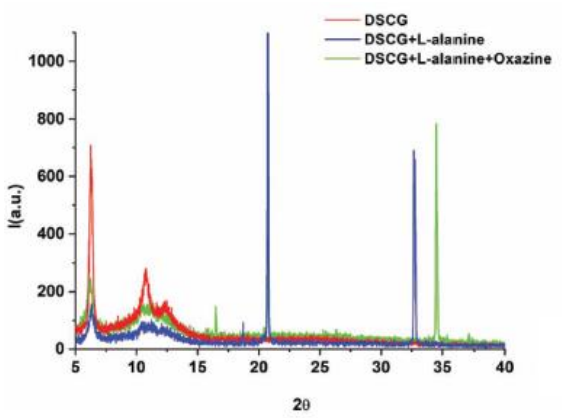

Figure 3.30: XRD spectra comparison between DSCG, DSCG+L-Alanine, and DSCG+L-Alanine+Oxazine samples.

Salt addition causes a change in the X-ray spectrum. The KCl-doped samples show two other reflections related to the molecular crystallographic axis, denoted as a in ref (23). The cylinders are on the surface, so the molecular stacking distance was not observed (c axis).

With the presence of 0.01M KCl, the formation of a fourth peak is observed (Figure 3.31), which in the literature (39) is attributed to the width of the molecule within the assembled layers. The appearance of this peak could be attributed to structure misalignment and increased disorder.

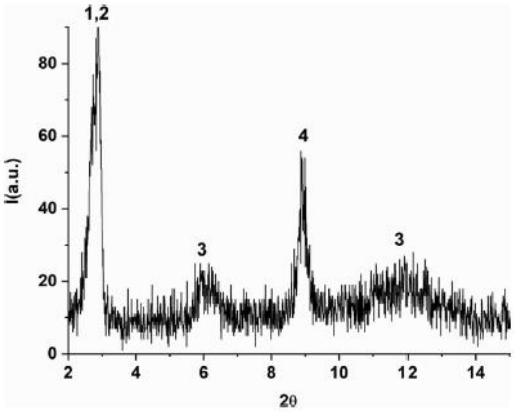

Figure 3.31: XRD spectrum for samples containing 0.1 m KCl: 1,2 peaks of supramolecular order; 3 peaks of hexagonal order, 4 peak of order relative to the a-axis.

Since XRD probes the sample volume, an AFM investigation is performed to probe the air-thin film interface. AFM measurements were acquired in tapping mode using a lever with a resonance frequency of 150kHz (Bruker, TAP150).

The surface of the sample of pure DSCG on plasma-treated PDMS is uniform but has a high roughness of 130±30 nm. Streaks are identified on the surface that are oriented along precise directions (Figure 3.32a), confirming the transmission electron microscope observation reported in Ref. (28) showing a structure related to a thin film of DSCG very similar to that observed in Figure 3.32b. Further confirmation is found in the article by Kostko et al. (37) in which the authors report a cryo-TEM analysis of a 10wt% sample of DSCG in its nematic phase. Figure 3.32c shows the presence of parallel rods. The start and end points of the rods are not visible so that the order appears to be orientational and not positional.

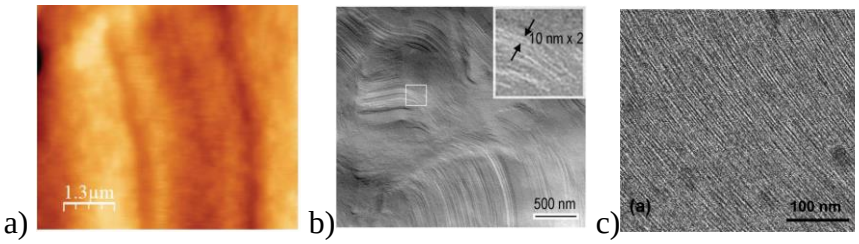

Figure 3.32: a) AFM image of pure DSCG, b) transmission electron microscope image of 15wt% DSCG in water, c) cryo-TEM data for a 10wt% DSCG solution. (37).

The measurements made in this work are not able to clearly show the presence of the thin rods because the radius of the AFM tip is comparable to their size.

The addition of L-Alanine results in a change in surface topography (Figure 3.33). Ordered filaments collected in bundle-like structures, which turn and break abruptly, are observed over areas of several tens of microns. Also in this case, the surface appears uniform with a surface roughness of 152 ± 36 nm.

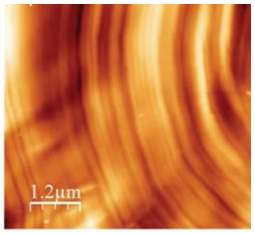

Figure 3.33: Topography of DSCG+L-Alanine on PDMS.

The sample containing L-Alanine and Oxazine 725 shows (Figure 3.34) the same characteristics as the previous sample because the percentage of Oxazine in solution is about 0.1wt%.

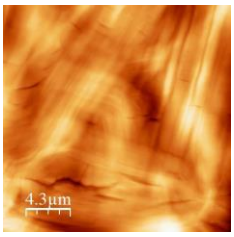

Figure 3.34: Topography of DSCG+L-Alanine+Oxazine on PDMS.

The addition of KCl salt, in a concentration of 0.01M, increases the disorder in the surface topography. It is observed that in some areas there is the presence of the ordered structures observed earlier surrounded by large areas without any particular feature. The surface roughness is 161±34 nm ((Figure 3.35a).

By increasing the salt concentration (0.1M), the surface appears completely disordered, exhibiting granular structures of about 200 nm and elongated structures of about 400 nm. This is emphasized by the increase in roughness, which now is 221±54 nm ((Figure 3.35b).

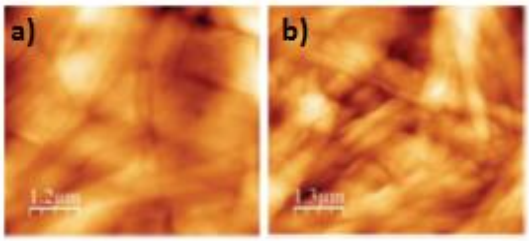

Figure 3.35: AFM images of: a) DSCG-L-Alanine+0.01M KCl, b) DSCG+L-Alanine+0.1M KCl

To explain such a sharp change in topography, reference can be made to the article by Kostko et al (37) in which the authors investigate the effects that the presence of 350 mM of different types of salt have on the structure of a DSCG sample. In particular, Figure 3.36 shows that by

adding sodium chloride to a solution of DSCG, a similar pattern of arrangement of the rods shown in Figure 3.32c is visible. The rods remain mostly parallel but agglomerates are observed in some areas. The morphology of the sample takes on a more disordered appearance.

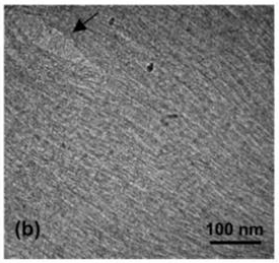

Figure 3.36: Cryo-TEM image for DSCG 10wt%+ NaCl 350mM (37).

In Kosko paper, a mechanism is proposed to explain this phenomenon that is based on the assumption that cations from the added salt integrate into the DSCG structure and participate in the self-assembly of the aggregates. Counterions bind to the aggregates by adsorption onto the aggregate or intercalation within the aggregate. The authors hypothesize that the presence of additional sodium ions within DSCG rods promotes aggregate growth. It is possible that the role of these cations is related to the formation of salt bridges. Thus, cations may serve not only as bridges between adjacent molecules in the sample plane but also between molecules that are above and below the plane. The total effect that occurs is an increase in the size and number density of DSCG rods in solution. Even in the case of using a potassium salt, this mechanism could explain the observed variation in topography.

3.3.2 Trans-4-Hydroxy-L-proline doped DSCG

Based on the experiments performed in the paragraphs previously discussed, the effect of an aminoacid with higher twisting power than L-Alanine, Trans-4-Hydroxy-L-proline was evaluated (32).

To prepare the chiral mixture, DSCG was dissolved in 26wt% Trans-Hyp in ultrapure water. The material was, then, confined in spherical geometry and, also in this case, the Frank-Price optical texture is obtained (Figures 3.37a and 3.37b)

Due to the high chiral twisting power of Trans-Hyp compared with that of L-Alanine, the pitch is significantly decreased. These findings open new perspectives on the possibility to use these materials in biocompatible optical device. It is also interesting to note that the birefringent core is not observed in the microsphere containing Trans-Hyp, whose imaged area is completely covered by concentric rings. In this case, the Frank-Pryce chromonic structure is indistinguishable from that observed in chiral nematic thermotropic liquid crystals.

a) 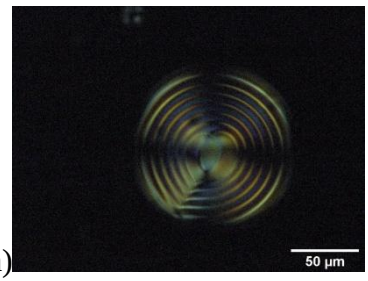 b) 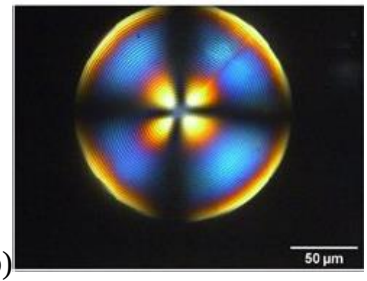

Figure 3.37: Microsphere containing: (a) DSCG + L-Alanine;(b) DSCG + Trans-Hyp.

The measured average half-pitch is 1.65 ± 0.10 μm, in agreement with what is reported in the literature (28), and significantly shorter than that measured on L-Alanine-doped microspheres, which was 5.20 ± 0.20 μm.

Also this case (40) we found that Oxazine 725 improves the texture quality (Figure 3.38a Figure 3.38b). In this case, a slightly lower average half-pitch, 1.50 ± 0.10 μm, was measured with respect to the one observed for DSCG doped with Trans-Hyp alone (Figure 3.37b).

a) 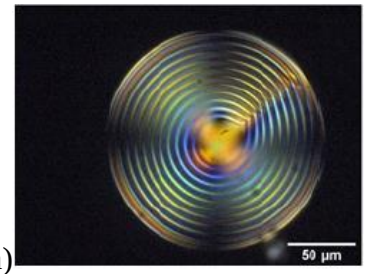 b) 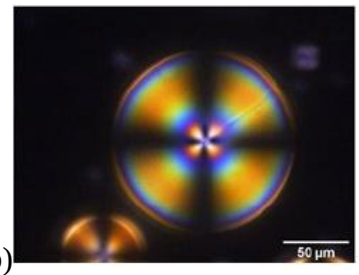

Figure 3.38: Microsphere containing: (a) Oxazine doped DSCG + L-Alanine; and (b) Oxazine-doped DSCG + Trans-Hyp.

Figure 3.39 highlights the distribution of microspheres considering the chirality parameter 2D/p (28) (41) (42), where D is the sphere diameter and p is the pitch. This parameter is widely used in chiral thermotropic liquid crystals to classify the textures observed in microspheres and, in this case, highlights the pitch variations as a function of sphere geometry (15).

From the histograms shown in Figures 3.39a and 3.39c, it can be seen that compared with chromonics prepared by doping DSCG with L-Alanine, those prepared with Trans-Hyp show more microspheres with well-defined Frank-Pryce textures.

Figures 3.39c and 3.39d show, in the case of DSCG containing L-Alanine, that the number of microspheres with well-defined textures increases when the material is doped with Oxazine 725. The same is observed with regard to Trans-Hyp doped chromonic, in fact it is clearly visible from the histogram shown in Figure 3.39b, which is shifted toward higher values of the chirality parameter than the histogram observed in Figure 3.39a.

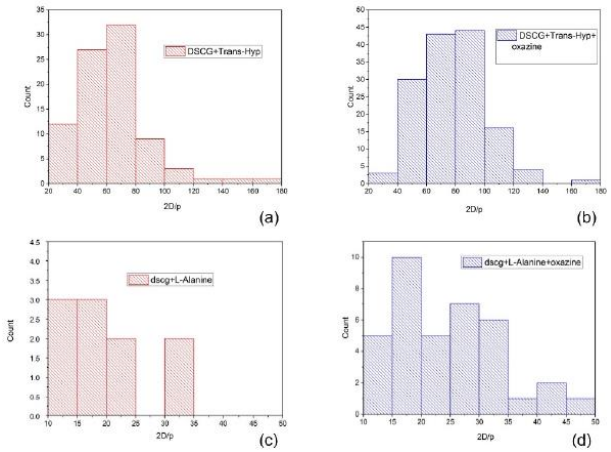

Figure 3.39: Chirality parameter distribution for: (a) DSCG + Trans-Hyp, (b) Oxazine-doped DSCG +Trans-Hyp, (c) DSCG + L-Alanine and (d) Oxazine-doped DSCG + L-Alanine.

In addition, the number of spheres analyzed is significantly higher for the Oxazine 725-doped sample than for the undoped sample, confirming that the small molecules of ionic dye contribute in inducing the ordered structure.

If the microspheres are stored at room temperature, the Frank-Pryce structure, deteriorates after about 2 weeks; the degradation time depends on the temperature and humidity of the environment. This process is not reversible. If stored in a refrigerator at 4°C, the structure is maintained for two weeks.

- *X-ray and AFM measurement*

Also in this case thin films of DSCG and Trans-Hyp were analysed though X-ray diffractometry and atomic force microscopy.

Using AFM, it is observed that on a large scale (3 x 3 μm^2) the surface appears homogeneous with a roughness of about 20 ± 4 nm, whereas on smaller scales (Figure 3.40a), the surface shows the presence of terraces with a height of 2.7 ± 0.4 nm (Figure 3.40b), and the average roughness decreases to 2.8 ± 1.1 nm.

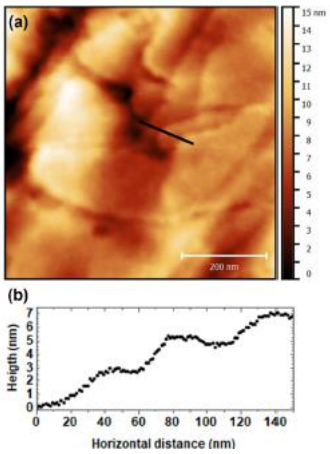

Figure 3.40: (a) AFM topography of DSCG doped with Trans-Hyp; (b) line profile of the terraces

As known in literature (40), DSCG is able to organize into layered structures, this tendency is confirmed when doping it with Trans-Hyp, that seems not to affect chromonic self-assembly. By X-ray measurements, it is observed that at low angles a peak corresponding to 27 Å is hardly visible (Figure 3.41), while at high angles, narrow peaks related to Trans-Hyp are clearly visible. This confirms the phase separation and suggests that the chiral dopant is not intercalated in the DSCG columns (43). What happens at the molecular level is consistent with what has been observed for low helical twisting power dopants. The chiral dopant does not affect the molecular stacking of DSCG, but it attaches to the outside of the cylinders, favoring their twisting, which is also favored by spherical confinement.

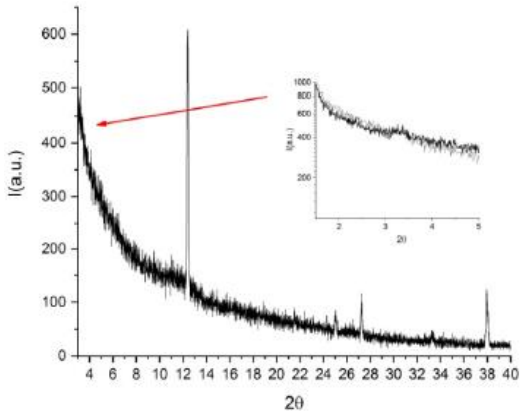

Figure 3.41: X-ray diffractogram of DSCG doped with Trans-Hyp.

During film drying, the 2D order of DSCG is partially lost, unlike pure DSCG, which retained a 2D hexagonal phase (40).

- *Free standing film*

The possibility to encapsulate chiral chromonic microspheres in a polymeric film preserving their optical texture was, then, evaluated. Free standing flexible films in which microspheres were incorporated were obtained by preparing two emulsions, one with the chromonic doped with L-Alanine and another one with the chromonic doped with Trans-Hyp and, for the immiscible matrix, adding the hardener to PDMS in a 9:1 proportion.

Emulsions were deposited in small circular containers about 1.5 cm in diameter and allowed to dry for 3 days at room temperature. The two transparent and flexible films Figure 3.42a and 3.42b were removed from the containers and observed with polarized light microscope. Figure 3.42c and 3.42d shows that, due to the rubbery matrix, the microspheres in both cases appeared opaque. This is the first successful attempt to encapsulate chromonic liquid crystals in a free standing film without modifying their optical features.

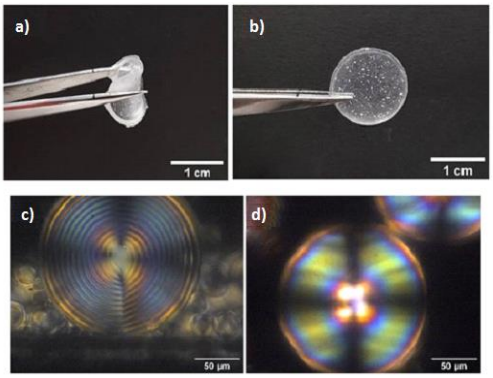

Figure 3.42: a) folded flexible film, b) unfolded flexible film, c) POM images of Oxazine-doped DSCG+L-Alanine, d) POM images of Oxazine-doped DSCG+Trans-Hyp

Comparing the data of the two films (Figure 3.43), the half-pitch observed in the microspheres containing L-Alanine-doped DSCG had an average value of 5.83 ± 0.05 μm, while a half-pitch of 1.74 ± 0.05 μm was measured in the sample with Trans-Hyp. These values are comparable to those measured in the emulsions.

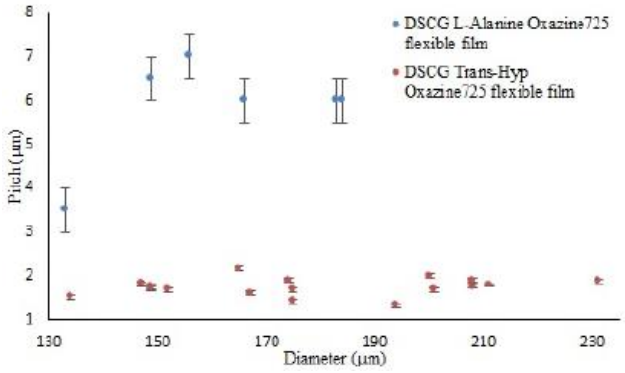

Figure 3.43: Half-pitch as function of microspheres diameter for Oxazine doped DSCG+L-Alanine and Oxazine doped DSCG+Trans-Hyp encapsulated in flexible films.

Using Trans-Hyp as the chiral dopant, the half-pitch obtained is still too large to exploit it in technological applications, nevertheless, it represents an important step forward especially in the field of sensors and optical devices.

3.3.3 Application

The applications in optics for chromonic liquid crystals in planar geometries have been extensively reported in literature (44). In the form of dried thin films, chromonics can be exploited as linear polarizers, optical compensators, retarders, alignment layers and color filters.

In general, all the applications demand a homogeneous and stable alignment on anisotropic surfaces, a condition that is difficult to achieve (45). Currently, a good alignment of chromonics, both planar and homeotropic, on large areas cannot be obtained without the presence of defects and stability issues.

Chromonics have been proposed for applications as biosensors. In 2005, Shiyanovskii et al. presented a sensor composed of a chromonic liquid crystal sandwiched between two rubbed polyimide coated glasses that was observed between crossed polarizers (46), demonstrating that the distortions of the nematic chromonic director around a spherical particle with a planar surface orientation and the consequent light transmittance through the distorted region was a steep function of the particle's size. For their experiments, they used a chromonic nematic liquid crystal containing antigen-coated latex beads and an antibody. The specific recognition of the antigen by the antibody resulted in the agglomeration of the latex beads in the large particles. The presence of these agglomerates caused a director distortion around them that could be easily detected using polarized light microscopy.

Recently, the use of chromonic thin films as humidity sensors was proposed (47). Glushchenko and co-workers demonstrated that the sensing properties related to the self-assembling properties of solid chromonic films as a function of the humidity of the surrounding air. In the dry films, the stacking distance in the molecular aggregates depended on the water content of the ambient atmosphere that modified the weak non-covalent hydrophobic and hydrophilic interactions between the molecular groups. Applying an electric field, a variation of the humidity and, consequently, the stacking distance, caused a dramatic change in the electric current passing through the aggregate that could be easily detected.

The application of chiral chromonics in spherical geometries has not yet been investigated. However, it could also be foreseen in the field of sensors, for example, as time temperature

indicators (TTIs). A TTI is a device or smart label that accumulates the time–temperature history of a material. This type of devices is extremely important, as an example, for the monitoring of the food cold chain to ensure food safety and freshness. There are two types of TTIs, namely, diffusion-based and chemical reaction-activated (48). Diffusion-based TTIs are composed of a temperature phase-change dye and a porous material. When the dye melts due to high temperatures, it permeates the porous materials.

Chemical reaction-activated TTIs are based on a color change induced by the reactions of a chemical component activated above a specific temperature. Unfortunately, both types of TTIs have their respective critical disadvantages due to construction constraints, scarce sensitivity or chemical substance leakage issues.

Chromonic liquid crystals have the potential to be applied as TTIs that lay on the director distortions arising from the aligned chromonic phases reflected in colorful optical textures that are temperature dependent. As an example, chiral chromonic microspheres were successfully trapped in a polymeric free-standing film (32). Storage at 4 C allowed the textures to be maintained for at least 10 days, after which their degradation process began. The degradation was irreversible and it was impossible to recover the initial condition. The texture could be preserved for longer if the film was kept at -20° C, and this could be used to detect temperature variations. The fact that these materials were perfectly biocompatible was ideal since there was no safety issue when they came into in contact with food or medicines.

3.3.4 L-Lysine doped Sunset Yellow

The behaviour of SSY in spherical geometry was studied, using as immiscible matrices both paraffin oil and PDMS.

PDMS, as shown by planar cell experiments, was used to have a homeotropic anchoring at the interface, while paraffin oil was used to have a planar anchoring (Figure 3.14a and 3.14b). To induce chirality in SSY microspheres, L-Lysine and Trans-Hyp were used as chiral dopants (49).

As for DSCG, controlled amounts of salts (KCl and $MgCl_2$) were added to the SSY solution to exploit the effects of ions on the supramolecular arrangement.

- *Optical textures*

Pure SSY microspheres produced in paraffin oil show textures similar to the ones observed in nematic thermotropic liquid crystals with planar anchoring conditions at the interface. Textures depend on the size of microspheres:

- for diameters less than 50 μm, a Maltese cross is observed (Figure 3.44a),
- large microspheres show a bipolar twisted structure (14) (18) (Figure 3.44b), confirming what has been reported in the literature (12) (14) where microspheres with planar condition at the interface show a radial configuration for a radius smaller than the critical radius ($R_C \approx K/W$) and a bipolar configuration for a radius larger than the critical radius R_C.

In the present case, an anchoring energy of $W \approx 10^{-6}$ J/m^2 is estimated considering an elastic constant of K≈10pN (24) and an average radius of 50 μm. Jeong et al reported similar results for SSY (18). They dispersed the nematic SSY solution in hexadecane with a non-ionic surfactant obtaining microspheres with bipolar twisted configuration of the nematic director.
When L-Lysine (Figure 3.44c) and salts (Figure 3.44d-e) are added to nematic SSY, the predominant structure observed is a bipolar twisted configuration, while microspheres showing a Maltese cross disappear.

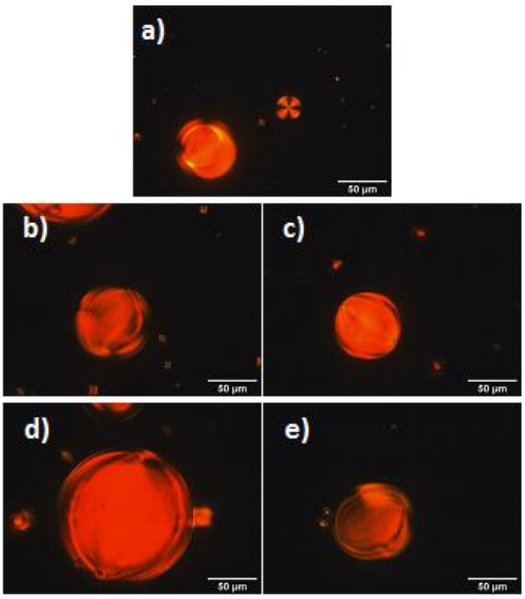

Figure 3.44: POM images of microspheres containing pure nematic SSY showing: (a) a Maltese cross and (b) a twisted bipolar texture. c) SSY doped with L-Lysine 10 wt%,, d) SSY doped with Lysine 10 wt%+0.1 M KCl and e) SSY doped with L-Lysine 10 wt% +0.1 M MgCl2, in paraffin oil.

Adding salts, it is observed that, the presence of a monovalent salt (KCl) does not produce any particular change in the bipolar twisted structure of the larger microspheres, instead, SSY microspheres doped with L-Lysine and divalent salt ($MgCl_2$) show a greater variety of

configurations (Figure 3.45a and 3.45b). This phenomenon is due to the different interaction mechanism of divalent ions with supramolecular cylinders.

In this context, Kostko et al (37) suggest that monovalent ions participate in pure SSY cylinder growth by intercalating between molecules, instead, divalent ions form bridges between molecules in the external part of the cylinder, increasing the overall length of supramolecular aggregates more efficiently.

The morphology of the microspheres depends strongly on the helicity parameter, 2D/p (15), a small variation results in a change in the droplet textures, this could be related to changes in elastic constants, pitch, defect strength and diameter of the microspheres.

Using Trans-Hyp as a chiral dopant, microspheres with more complex textures are observed (Figure 3.45c 3.45d), however, the results reported for microspheres in paraffin oil are still insufficient to demonstrate the twisting power ability of chiral dopants.

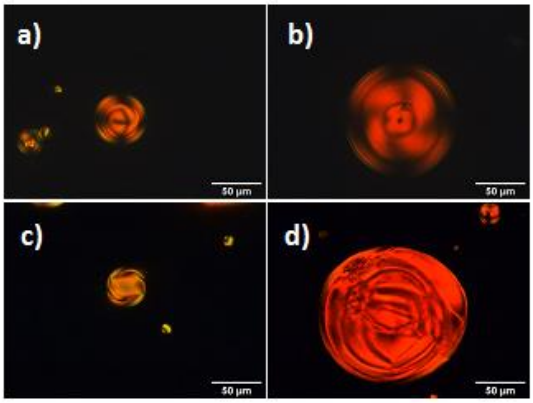

Figure 3.45: POM images of microspheres containing SSY doped with L-Lysine 10wt% and 0.1 M MgCl2 (a,b) and SSY doped with Trans-Hyp 26wt% (c,d) in paraffin oil. (all percentages are in weight)

Better observations of the twisting power effects are reported when PDMS is used as confinement matrix. Different textures were observed depending on the size of the microspheres, or the addition of salt or chiral dopants. It is the first time that such a variety of textures, typical of thermotropic chiral liquid crystals in homeotropic geometry, has been observed in chromonics.

Pure nematic SSY microspheres with a diameter of less than 50 µm show a radial twist texture with the Maltese cross (Figure 3.46a). If the diameter of the microspheres increases, a localised distortion can be observed on the inner part of the sphere (Figure 3.46b).

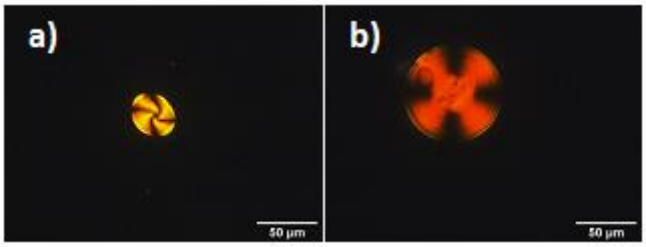

Figure 3.46: POM images of microspheres containing nematic SSY immersed in PDMS and showing (a) a Maltese cross and (b) a texture with a distortion concentrated in the central part.

No rearrangement over time was observed for the microspheres, so the texture may be thought to be more similar to the intermediate layer-like texture as reported in (15). These textures remain stable for a few days.

When L-Lysine is used as dopant, the intermediate layer-like structure is found also in the smallest spheres. There are very few smaller microspheres with distorted Maltese cross, and the same orientation prevails among them. Toron-like structure is also observed (Figure 3.47a, 3.47b). (15) (16) (17) (50). Intermediate structures were also observed (Figure 3.47c).

The observed distortions confirm the growth of reflection symmetry breaking of the mixture because these structures are typical of cholesteric behavior.

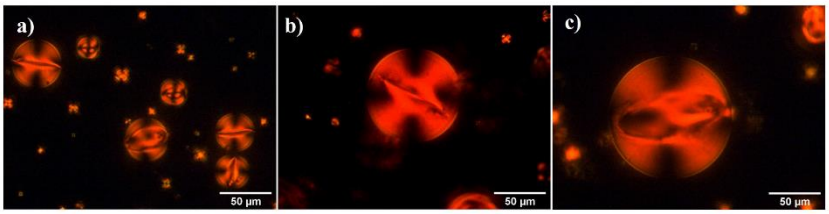

Figure 3.47: a) POM images of microspheres containing SSY doped with L-Lysine 10 wt% in PDMS showing (b) Toron-like texture and c) Intermediate Layer-like structure.

As observed for microspheres prepared using paraffin oil, the addition of monovalent ions (KCl 0.1 M) to the SSY-Lysine mixture does not affect the textures (Figure 3.48).

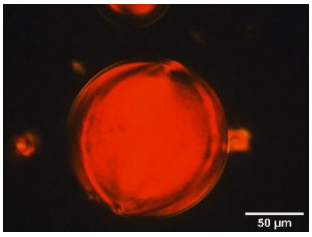

Figure 3.48: POM images of SSY doped with L-Lysine 10 wt% and 0.1 M KCl.

In contrast, the presence of $MgCl_2$ seems to confine the defect to the central region of the microspheres (Figure 3.49). This confirms that divalent ions, as previously observed for planar interfacial anchoring, influence the length of the columns, their flexibility and the interaction forces between them (51).

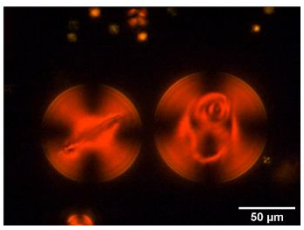

Figure 3.49: POM images of microspheres containing SSY doped with L-Lysine 10 wt% and MgCl2 0.1 M showing both Toron-like and intermediate layer-like textures.

Also when Trans-Hyp is used as chiral dopant, different optical textures are observed: radial twisted, Toron-like and, for microspheres with large diameters, layer-like texture (Figure 3.50a). Small changes in the parameters involved can shift the state of the microsphere from a Toron-like state to an intermediate layer-like state before reaching the layer-like state (16). In contrast to pure nematic SSY microspheres, Trans-Hyp-doped SSY microspheres undergo an internal reconfiguration after 24 hours, resulting in the "Frank Pryce" texture, not previously observed for this chromonic molecule. For microspheres as the ones shown in Figure 3.50b, the induced cholesteric half-pitch is 7 μm.

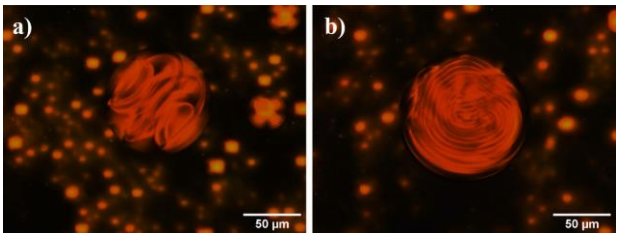

Figure 3.50: POM images of microspheres containing SSY doped with Trans-Hyp 26 wt% in PDMS showing (a) Layer-like texture and (b) Frank-Pryce like texture.

In conclusion, in small microspheres for both oil matrices, a radial configuration characterized by a Maltese cross (twisted in the case of homeotropic boundary conditions) was found. In large microspheres the structure changes depending on the boundary conditions.

Under homeotropic anchoring conditions, a polymorphism was observed for microspheres of LCLCs that had been previously reported only for cholesteric TLC, using L-Lysine as the chiral dopant the Toron-like and intermediate layer-like structures were prevalent, whereas using Trans-Hyp as the chiral dopant the layer-like structure was prevalent. In the last case, an increase in the chirality of the SSY mixture was found to give rise to a Frank-Pryce texture (not observed in the literature).

- *X-rays and AFM measurements*

Thin films prepared with mixtures of pure SSY and chiral SSY were analyzed by X-ray diffractometry and atomic force microscopy. X-ray diffraction patterns are shown in Figures 3.51.

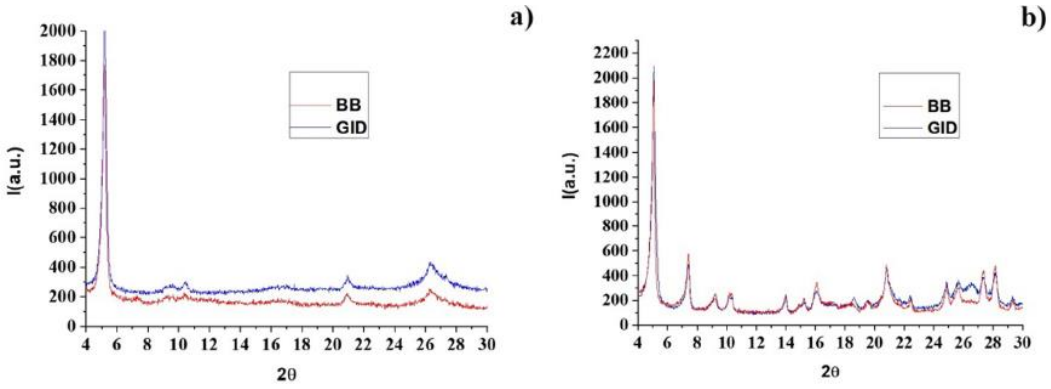

Figure 3.51: X ray diffraction of pure (a) and doped with L-Lysine 10 wt% (b) SSY: Bragg-Brentano (BB) and grazing incidence measurements (GID).

The diffraction pattern for pure SSY (Figure 3.51a) shows peaks relative to the hexagonal or 2D mesophase (26). No differences are observed in the symmetric and asymmetric geometries, confirming that the sample is powder-like. In fact, in the Brentano Bragg geometry, both low-angle (5°) and high-angle (26°) peaks, related to the intercolumnar distance (17.7 Å) and stacking distance (3.43 Å), respectively, are visible in the X-ray pattern, suggesting that the cylinders do not have a preferred orientation, but are perpendicular or planar on the PDMS surface.

This behavior is to be expected since the basic unit of this compound is a dimer, that is, two L-shaped molecules 180° apart. This type of molecule usually gives rise to intrinsically disordered crystal structures. The intercolumnar peak is lower than the average value measured in the nematic phase, but it is not very far from the value of 19 Å obtained in the hexagonal phase (52). However, a strong peak is visible around 21° equal to 4.23 Å that could be due to a different arrangement of the inclination of the molecules in the 2D/3D stack and thus not to the presence of impurities in SSY.

In fact, as also reported by Jeong et al (53), the presence of impurities should not change the stacking distance. Unfortunately, no further information can be obtained from this powder-like diffraction pattern.

In contrast, when observing the diffraction pattern for Lysine-doped SSY (Figure 3.51b), there are "crystalline" features. It appears that L-Lysine is incorporated into the SSY aggregates, by ordering the structure, compared with the previous case, the diffraction pattern shows well-defined and increased peaks and different features are found in the high-angle region.

As shown previously, SSY and L-Lysine are miscible at different molar ratios, but for an SSY-Lysine molar ratio of 2:5 the mixture is isotropic, this indicates that the addition of L-Lysine shifts the phase diagram of SSY to higher concentrations, therefore, the effect of L-Lysine on the liquid crystalline phase of SSY is to shorten the cylinders or increase the flexibility of long cylinders (54) (55). It is known that SSY, as a sulfonate dye, is rarely crystallized without the presence of adjuvants, which can help the crystallization process (56). In this case, L-Lysine acts as an adjuvant in the formation of a crystalline film. The same behaviour is observed for the mixture SSY containing L-Lysine and 0.1 M KCl.

A completely different X-ray pattern for SSY doped with L-Lysine and $MgCl_2$ is shown in Figure 3.52. This pattern shows that the long order peak is suppressed in favor of the short order peaks. Probably the intercalation of L-Lysine reduces the size of the cylinders in water, but the supramolecular organization and ordered domains are globally maintained, whereas the presence of $MgCl_2$ destroys the organization of the domains causing a misalignment of one cylinder with respect to the other.

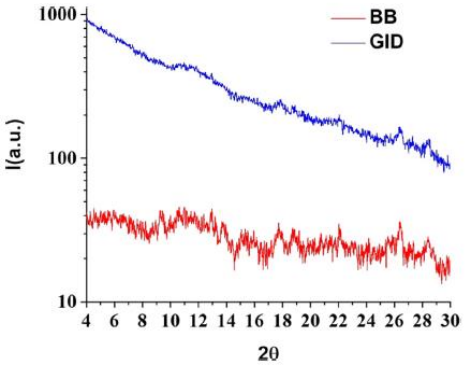

Figure 3.52: X ray diffraction of SSY doped with L-Lysine 10 wt% and 0.1 M MgCl2.

The effect of the chiral dopant Trans-Hyp was analyzed. From the X-ray pattern shown in Figure 3.53a, it can be deduced that Trans-Hyp does not mix with SSY.

Both the XRD pattern and POM observations (Figure 3.53b) indicate the formation of separate crystals of Trans-Hyp in the thin film. For low diffraction angles, the 2D/3D residual order of SSY is found (highlighted by the blue circle in Figure 3.53a); the small red lines indicate the Trans-Hyp peaks (43). The large remaining peak at 26°, of 3.43 Å, is related to the stacking distance between molecules; its width indicates, as in previous cases, the presence of small cylinders.

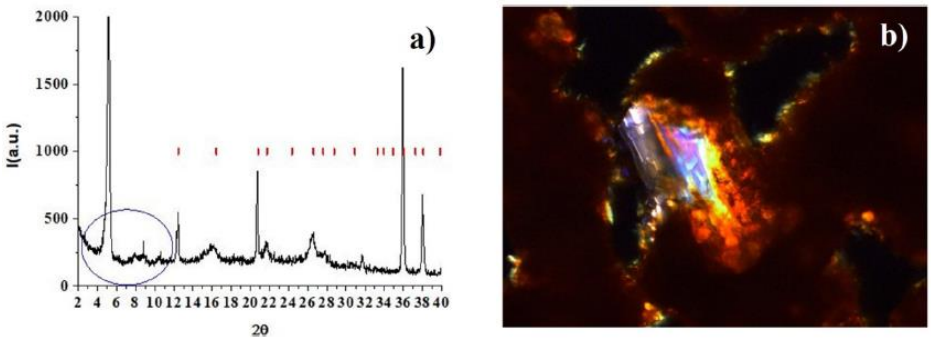

Figure 3.53: a) X ray diffraction of SSY doped with Trans-Hyp, b) POM measurement.

It is clear from the XRD measurements that L-Lysine and Trans-Hyp interact with SSY differently, L-Lysine intercalates in the stacking of SSY, while Trans-Hyp is bound to the outer cylindrical structure. The second interaction mechanism seems more efficient to induce chirality in the system and has a lower energy cost (57).

To obtain information on molecular packing, the thin films were studied by atomic force microscopy. The pure nematic SSY film has a homogeneous surface with a roughness of about 16 ± 5 nm over areas of 2 x 2 μm^2. When the surface was imaged on smaller scales (Figure 3.54a), it shows the presence of terraces with a height of 1.8 ± 0.2 nm. Terraces are also present on the thin film of SSY and L-Lysine with 0.1 M KCl (Figure 3.54b), with a height of 1.2 ± 0.3 nm, and on the thin film of SSY and Trans-Hyp, with a height of 1.8 ± 0.3 nm (Figure 3.54d). In these analyzed cases, the surface appears homogeneous and almost flat.

As for the mixture of SSY doped with L-Lysine and $MgCl_2$, a different morphology is observed; in fact, the film shows a non-homogeneous surface, characterized by grains whose size is on the order of tens of nanometers (Figure 3.54c). The average roughness over 600 x 600 nm^2 is about 11 ± 4 nm.

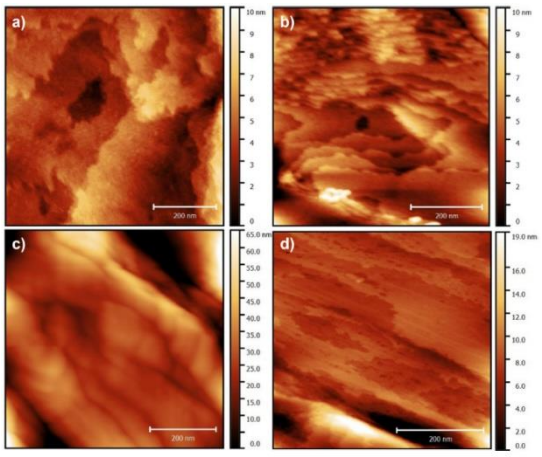

Figure 3.54: AFM topography of (a) a thin layer of pure SSY (b) SSY doped with L-Lysine, (c) SSY doped with L-Lysine and MgCl2 0.1 M and (d) SSY doped with Trans-Hyp.

From these results, it can be deduced that SSY tends to organize into thin layers packed on top of each other, and the supramolecular organization is maintained even when Trans-Hyp or L-Lysine is added to the solution, so the addition of these dopants has little effect on the aggregation mechanisms of SSY. Morphology, on the other hand, is strongly affected by the presence of divalent cations on the nanometer and micrometer scales, suggesting the formation of bridges between molecules on the outside of different aggregates.

Combining AFM, XRD and POM techniques, it was shown that L-Lysine intercalates between cylinders and weakly twists the mesophases. The morphology confirms a similar packing of the layered structure.

Monovalent ions do not affect the structure, instead the addition of divalent salts leads to a disordered structure that shows no layered features, but the induced chirality is slightly enhanced. It can be hypothesized that divalent ions are located on the surface of the cylinders and this causes misalignment of the cylinders through the formation of bonding bridges between them.

The most interesting result is that the Trans-Hyp, unlike L-Lysine, interacts with the outer surfaces of the cylinders, resulting in a chiral configuration, when the system dries in thin film, the chiral dopant is ejected from the mesophase, this is also evidenced by the POM image 3.53b.

In conclusion, it is shown that it is possible to induce chirality for SSY chromonic liquid crystal by using chiral dopants such as L-Lysine and Tran-Hyp, while in planar confinement only Trans-Hyp is able to induce chirality. This can be due to the large symmetry breaking induced by the spherical confinement.

3.4 Microfluidic production of SSY microdroplets.

Through the emulsification procedure, it is not possible to achieve a fine control of microspheres' size, which plays a fundamental role in their final optical texture. This is important for applications in which the production of precise size distributions of micro-structures with peculiar optical features is the pre-requisite for a correct functionality of the device. The size control can be achieved by using a microfluidic approach.

Recent progresses in liquid crystal microfluidics have demonstrated how hydrodynamics, in combination with surface interactions, geometric confinement, and flow modulation can be harnessed to generate topological structures with potential for novel applications. Previous works (58) (59) have shown that interesting phenomena are observed by precisely tuning the

flow of nematic LCs inside microfluidic channels as a function of the confinement conditions in microchannels themselves and their wettability properties. On the other hand, studies on microfluidic generation of droplets embodying a chromonic liquid crystal and an isotropic component are still rare. Only few works report on the production through microfluidics of chromonic cholesteric droplets of cellulose nanocrystals (CNCs) (60) (61) and pure SSY (62). In the last case the authors exploited a microfluidic system that did not make use of electromechanical injection, a crucial point for systems in which viscosity may increase, as, for example, in the case of chromonic materials doped with chiral moieties.

For the purposes of this research work, in collaboration with dr. Valentina Arima and dr. Alessandra Zizzari of the CNR-Nanotec (Institute of Nanotechnology) in Lecce a protocol was developed to produce chromonic microdroplets.

Microdroplets were produced by a microfluidic flow focusing device (Figure 3.55) using a non-ionic surfactant (Span80) dissolved in the paraffin oil phase. The continuous phase (paraffin oil) and the dispersed phase (SSY aqueous solution) were injected with programmable syringe pumps in the outer and inner channels respectively. The droplets were generated at the focusing zone and then collected for the SSY microspheres analysis.

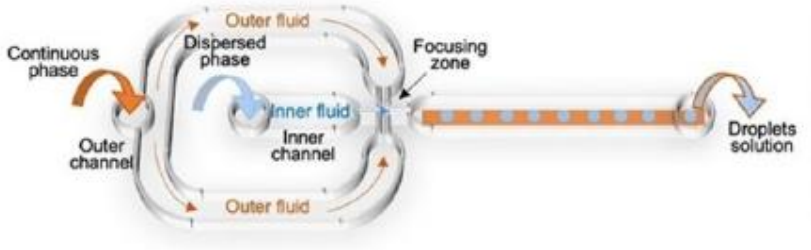

Figure 3.55: Flow Focusing device sketch.

The dispersed (aqueous) phase was injected in the inner microchannel and then squeezed by continuous (oil) phase flow injected by the outer microchannel. In this geometry, the symmetric shear generated by the continuous phase on the dispersed phase allows a highly controlled and stable generation of droplets (63). Using the SSY concentration at 30 wt% and Trans-Hyp at 26 wt%, adding to the paraffin matrix an 8 wt% of the surfactant Span80, using the flow rates of the two fluids set on µL/h for the aqueous phase (SSY) and µL/min for the oily phase (Paraffin oil + 8 wt% Span80), it was possible to produce microdroplets whose diameters range between 10 and about 50 microns.

Systematic polarized optical microscopy measurements were carried out on the different microdroplets. Droplets were imaged at first without polarizers to correctly estimate their

diameter and then between crossed polarizers. The observed textures were identified rotating the microscope plate and rotating the analyzer.

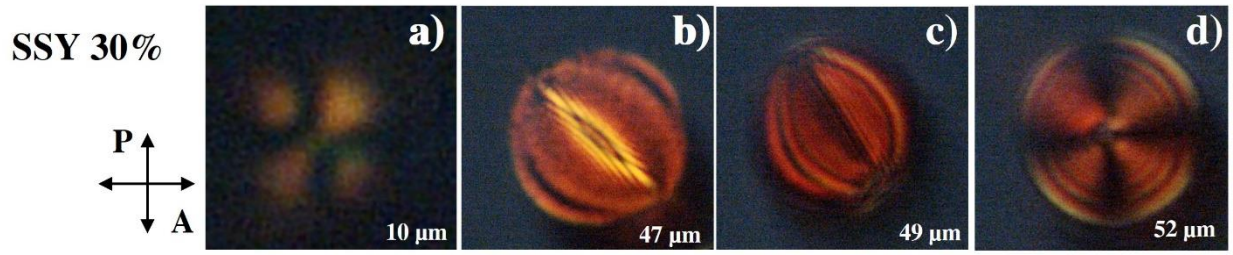

Figure 3.56: POM images between crossed polarizers of microspheres of pure nematic phase SSY at 30 wt% Droplet diameters are estimated on the bright field image (±2 µm).

Figure 3.56 shows the diameter dependent topologies observed in microdroplets of pure nematic phase SSY. In general, small droplets (10-20µm) show a bipolar configuration (BS) (Figure 3.56a). This is the typical texture configuration observed in chromonics microspheres with planar boundary condition in which the director is parallel to the interface and it forms two boojums at the poles. For droplet diameters ranging between 30-50µm (Figure 3.56b-c), we observe a better-defined bipolar structure. In few cases a "concentric drop" texture is observed. In this configuration, the director field is organized in concentric circles with a disclination line that passes through the center of the drop. It is interesting to notice that the surfactant added to allow the production of stable microfluidic droplets, does not affect the optical properties and textures, thus confirming its purely interfacial role in the droplet formation.

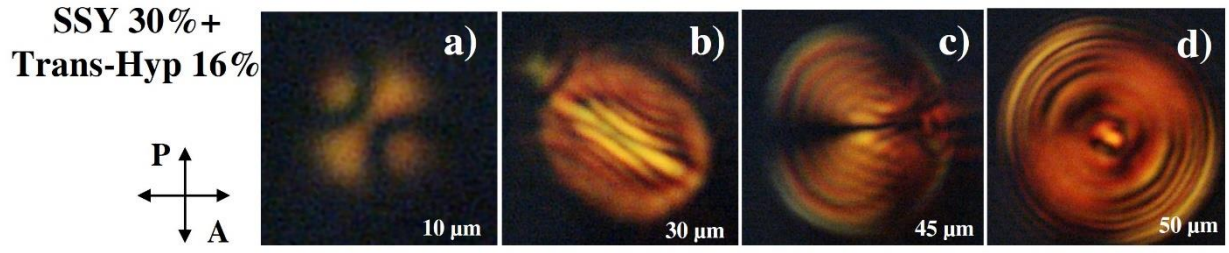

Figure 3.57: POM images between crossed polarizers of microspheres of SSY at 30 wt% + 16 wt% of Trans-Hyp. Droplet diameters are estimated on the Bright field image (±2 µm)

Figure 3.57 shows a collection of SSY microspheres doped with the Trans-Hyp at 16wt%.. Small droplets (10-20µm diameter) show bipolar configuration, as for the pure nematic phase (Figure 3.57a). The addition of the chiral dopant is reflected in the optical texture observed in the microdroplets. In fact, for a droplet diameter larger than 45 µm, the radial spherical

structure (RSS) develops: see (Figure 3.57b-c). In RSS, the director profile is characterized by a splay-bend distortion inside the droplet that generates a disclination line, similar to the so-called Frank-Pryce structure observed in thermotropic liquid crystals. Increasing the droplet diameter, diametrical spherical structure (DSS) is mostly observed (Figure 3.57d). DSS is the most symmetric structure in cholesteric droplets with planar anchoring. It is characterized by a center ring defect and the director field forms curved cholesteric layers with the layer normal in the radial direction.

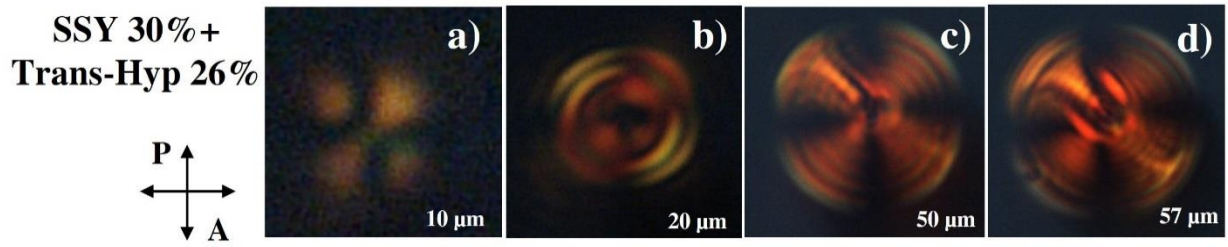

Figure 3.58 POM images between crossed polarizers of microspheres of SSY at 30 wt%+26 wt%. Trans-Hyp, collected according to their dimensions. Droplet diameters are estimated from the bright field image (±2 µm).

Figure 3.58 shows the POM images of SSY microspheres doped with 26wt% of Trans-Hyp at different droplet diameters. As observed for the other doped solution, small droplets with diameter of about 10 microns (Figure 3.58a) show a bipolar configuration, while most interesting topologies are observed for droplets with increasing diameters. For diameters around 20 µm, the texture starts to become distorted in radial concentric rings (Figure 3.58b). This effect is more evident in Figure 3.58c in which a clear Frank-Pryce texture is formed. In Figure 3.58d we can distinguish the so-called Lyre structure, that resembles the shape of the Lyre instrument. This last structure was numerically predicted by Sec et al. (64), in a detailed theoretical study on the geometrical frustration of chiral ordering in cholesteric thermotropic LC droplets. The Lyre structure, of bipolar type, has only two surface defects positioned diametrically along one of the axis parallel to the observation plane. In this highly symmetric structure, the deformation of cholesteric layers is span over the whole volume of the droplet. To the best of our knowledge, this is the first experimental observation of the Lyre structure in a chromonic droplet.

In table 2, we collected schematically the director configurations observed inside the droplets associated to the microdroplet diameter, for each chromonic solution studied in this work. Small droplets (diameters 10÷20 µm) show bipolar configuration for both pure and chiral doped solutions. The distortion increases both with microsphere's diameter and the concentration of the chiral agent. Even if the material used is a chromonic mesogen and not a

common TLCs, the trend observed for the optical textures is in line with the reported data in literature on the diameter/topology dependence in TLCs and Chiral TLCs.

	SSY 30wt%	***SSY 30wt%+16wt% Trans-Hyp***	***SSY 30wt%+26wt% Trans-Hyp***
Bipolar Structure BS Concentric rings *	***10-50μm * 50μm***	***10-20μm***	***~10μm***
RSS		***>45μm***	***20μm***
DSS		***50μm***	***50-60***
Frank-Pryce Lyre			***50μm 57μm***

*Table 2: LCLCs microdroplet optical textures reported for each droplet dimension and each investigated liquid crystal solution. The * indicates a particular optical texture observed for few droplets of about 50μm diameter of pure SSY. The percentage of SSY and Tran-Hyp indicated in the figure are in weight (wt%).*

In conclusion, for the first time, it was possible to produce microspheres containing Sunset Yellow chromonic liquid crystal by microfluidics.

By exploiting and characterizing the interplay of interfacial phenomena, surface effects, and geometric confinement, it was possible to define a protocol to produce SSY microspheres of controlled size and topology. Doping the chromonic material with chiral amino acids allowed the study and production of structures and topologies typically observed in cholesteric TLC microdroplets. Frank-Pryce structure and Lyre structure have been observed in chiral SSY microdroplets. This is a first step toward the goal of obtaining chromonic microspheres with tunable homogeneous optical properties, such as reflection selectivity, which would open new perspectives for the use of these biocompatible materials as sensors and optical devices. Since few works on microfluidic production of chromonic microspheres are reported in the literature, this is a relevant achievement.

Chapter 4 Work in Progress

This chapter is devoted to preliminary experimental studies. In particular, they regard the study of the nematic and chiral phases of a newly synthesized chromonic and the effect of an electric field on the optical texture of a pure and chiral model chromonic in planar and spherical confinement. Finally, a preliminary study on the confinement of liposomes in a chromonic matrix is reported.

4.1 Newly synthesized chromonic

In this paragraph are reported the investigations on a newly synthetized chromonic in which chirality has been induced. The material has been studied in both planar and spherical geometry.

Some metal complexes have been shown to form liquid crystalline phases (65) (66) (67). Due to their numerous oxidation states and coordination geometries, such kind of complexes offer new opportunities to design original mesophases.

The Ag(I) complex, synthesized at the Chemistry Department of University of Calabria, shows liquid crystalline phases in water. The chemical formula of the complex is $C_{26}H_{31}AgN_4O_8$ and the molecular weight is 635.42, its structure is shown in Figure 4.1a.

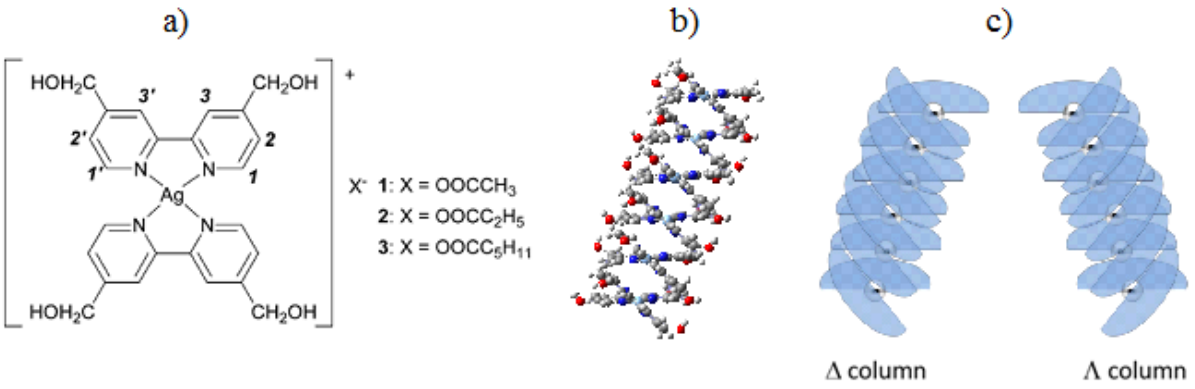

Figure 4.1: a) molecular structure of the Ag(I) complex, b) column of six AgC molecules, c) proposed model stack of chiral columns in the lyomesophase,.

The Ag(I) complex has the ability to organize into columnar structures, as evidenced in the crystalline solid state by single crystal X-ray analysis (68).

The presence of water molecules and the acetate anion interacting via hydrogen bonds with hydroxyl groups at the periphery of the metal containing cation generates the formation of cationic repetitive units despite electrostatic repulsion.

The phase diagram in Figure 4.2 shows that at room temperature the aqueous solution of Ag(I) exhibits a liquid crystalline phase between 15wt% and 60wt% concentration: from 15wt% to 50wt%, the complex has a nematic region (N) that transits directly to the isotropic phase when the temperature is increased. At higher concentrations the complex organizes into a hexagonal (M) phase. At a concentration of 50wt%, increasing the temperature, the M phase transits to the N phase. Above the 60wt% concentration, the hexagonal phase remains stable until it becomes isotropic at 120°C.

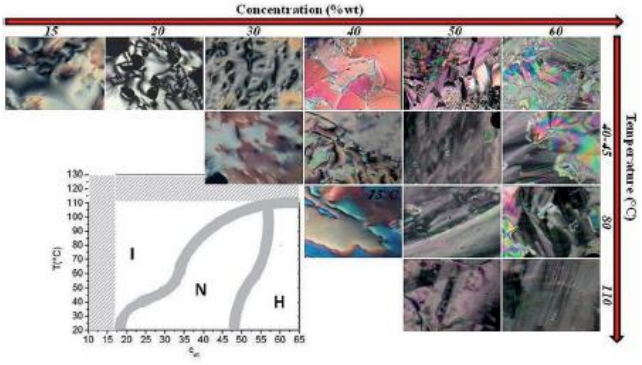

Figure 4.2: phase diagram of Ag(I) complex

The non-amphiphilic nature of these new metal-based complexes, their ability to self-assemble into ordered aggregates in water and the presence of nematic and hexagonal phases at different concentrations, confirm their chromonic nature. The Ag complex is chiral and molecules tend to self assemble in chiral columns (Figure 4.1 b, c).

The Ag(I) complex in its nematic phase, 20wt% wt. in water, was sandwiched between two glasses coated with Cytop, an highly hydrophobic polymer. The Ag(I) complex tends initially to align into a near-perfect planar structure with some characteristic defects (Schlieren structure), which rapidly disappear in favor of well-ordered cylinders covering the entire cell and whose periodicity is correlated with its thickness. After 3 hours, the supramolecular aggregates reorient throughout the entire cell, reaching a homeotropic alignment (68). Stripes can be produced again in the cell by heating the sample to the isotropic phase and cooling it slowly or by pressing the cell with tweezers.

When the Ag(I) complex is confined in an emulsion, using a PDMS matrix, the structures observed are very similar to those reported for cholesteric thermotropic liquid crystals and for SSY doped with L-Lysine. For small microspheres, the typical radial Maltese cross structure is observed (Figure 4.3a), while for larger droplets, more complex structures are observed: Toron-like (Figures 4.3b) and intermediate layer-like (Figures 4.3c) textures, which are characteristic of a cholesteric mesophase.

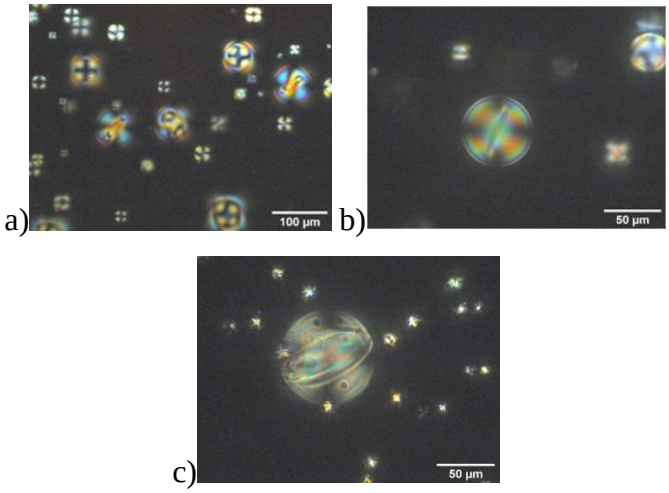

Figure 4.3: Microspheres of Ag(I) complex in its nematic phase showing (a) a Maltese cross, (b)an equatorial defect that, (c) grows after 2 days from emulsion preparation.

When doping the Ag(I) complex with the chiral Trans-Hyp, Toron-like (Figure 4.4a) and intermediate-layer like (Figure 4.4b) textures are observed.

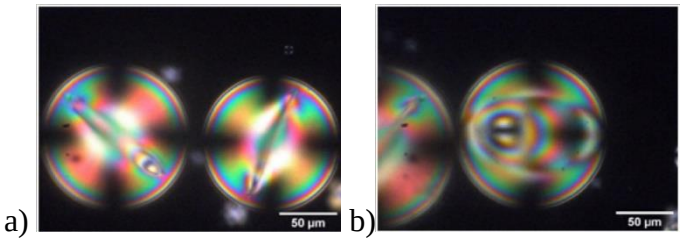

Figure 4.4: Microspheres of Ag(I) 20wt% doped with Trans-Hyp 26 wt% in a PDMS matrix showing (a) Toron-like texture and (b) intermediate layer-like texture.

However, after about 5 days from the first observation, layer-like texture (Figure 4.5a) and a texture reminiscent of Frank-Pryce one (Figure 4.5b) with a periodicity of 8 µm are also observed, and after 11 days, the latter two textures become better defined (Figure 4.5c). In particular, the Frank-Pryce texture shows a variable half pitch, in Figure 4.5d a half pitch of 6.90 µm is observed, while in Figure 4.5e a half pitch of 12 µm is observed. This evolution in textures may be due to the slow water evaporation from the emulsion, that allows the director to reorient and give rise to cholesteric structures.

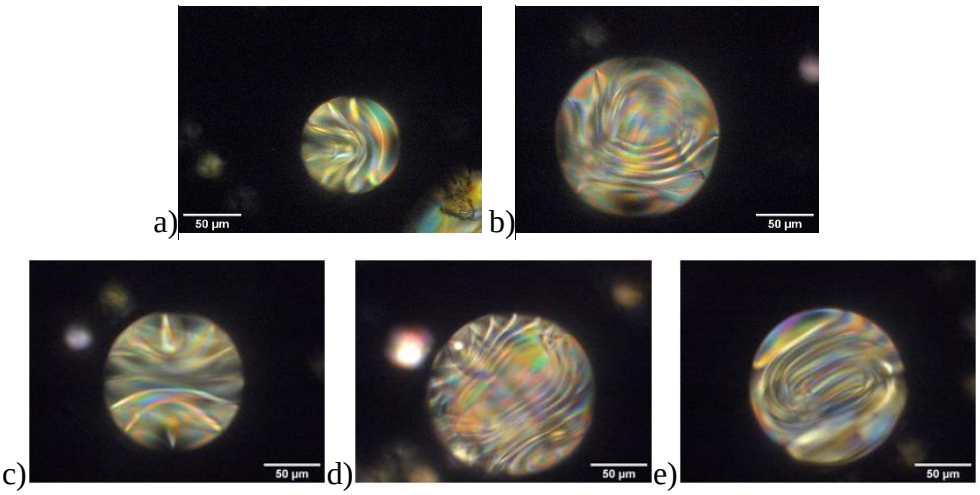

Figure 4.5: Microspheres of Ag(I) 20% doped with Trans-Hyp 26 wt% in a PDMS matrix: a) layer-like textures observed after 5 days, b) Frank-Pryce like texture observed after 5 days, c) layer-like texture observed after 11 days, d,e) Frank-Pryce like texture observed after 11 days.

The undoped nematic Ag(I) complex, unlike the undoped SSY, shows textures that point to the presence of a native chirality (15). Enhanced chiral effects are observed doping the Ag(I) complex mesophase with the chiral Trans-Hyp. The behaviour of this chromonic is similar to that of SSY even if the two molecules are very different. This similarity can help to gain further information on chromonics in general.

In order to understand the role of Trans-Hyp in the formation of the chiral phase, thin films were prepared. As first step, the thin films of undoped Ag(I) and Trans-Hyp doped Ag(I) were observed under polarized light optical microscopy. For the undoped complex, crystalline domains were observed (Figure 4.6a), while for the doped complex, large crystallites were observed (Figure 4.6b).

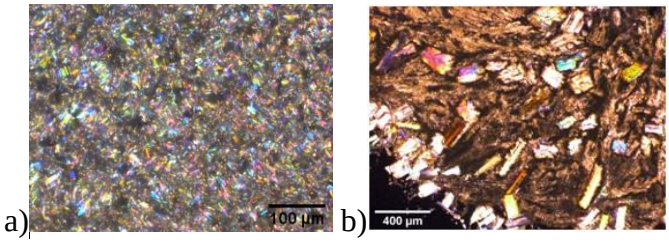

Figure 4.6: POM images of a thin film of: a) undoped Ag(I) complex and b) Ag(I) complex doped with Trans-Hyp

The Ag(I) 20wt% complex doped with Trans-Hyp 26wt% was monitored during the drying procedure and the typical fingerprint of the cholesteric phase was observed: the average half step is (11.5 ± 2.9) µm, thus confirming the results observed in the curved geometry (Figure 4.7).

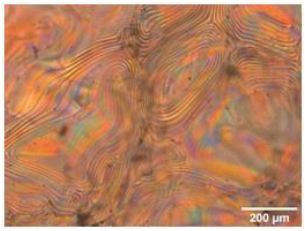

Figure 4.7: fingerprint textures observed on a thin film of Ag(I) complex doped with Trans-Hyp during drying procedure.

At this point, other techniques as X-rays diffraction and atomic force microscopy are needed to investigate the chiral arrangement of supramolecular aggregates.

4.2 Electric field effect on chromonic textures

In literature it is very rare to find papers concerning the application of electric fields to chromonics. This is an important topic in view of possible application of chromonics in electro-optics but it is also a delicate issue when concerning water based systems.

In ref. (69) Dan Qu and Eyal Zussman explored how the helical axis orientation and pitch of pure lyotropic cellulose nanocrystals CNC are affected by an electric field when suspended in water. In ref. (70) G.Y.Li et al. applied an electric field on the model chromonic SSY to study its electro-optical properties, including threshold voltage and relaxation times, at different temperatures and concentrations of SSY.

In this research work, the effect of electric field on the textures of undoped DSCG 13wt% and doped DSCG 13wt% with alanine 10wt% and with Trans-Hyp 26wt% was studied. These mixtures were prepared using deionized water to avoid the presence of ions in solution, which could interfere with the measurement. The effect of the electric field was evaluated by confining the mixtures in planar geometry as well as in the spherical one.

In planar geometry, cells were prepared using clear glasses covered with ITO and applying a voltage perpendicular to the cell glasses using a voltage generator. Between the two glass slides, two strips of mylar to create a uniform thickness inside the cell (190 µm) and a drop of about 10µl of liquid crystal mixture were inserted. Copper tape was used to connect the cell to the generator (Figure 4.8).

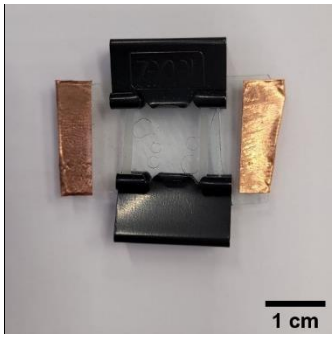

Figure 4.8: optical cell

A square wave of 1 KHz with a variable amplitude between 1 and 10Vpp was applied to the cell. Textures were monitored by POM observations.

4.2.1 Planar geometry

The effect of the electric field on texture was initially observed in an undoped 13wt% DSCG mixture.

Initially the mixture shows a degenerate planar texture (Figure 4.9a). After applying 3Vpp a change in texture is observed with the presence of bubbles. At 6Vpp bubbles disappear, and the sample takes on a blue coloration (Figure 4.9b-4.9f). At 7Vpp the sample turns black (Figure 4.9h), since the electric field reorients the cylinders in homeotropic configuration.

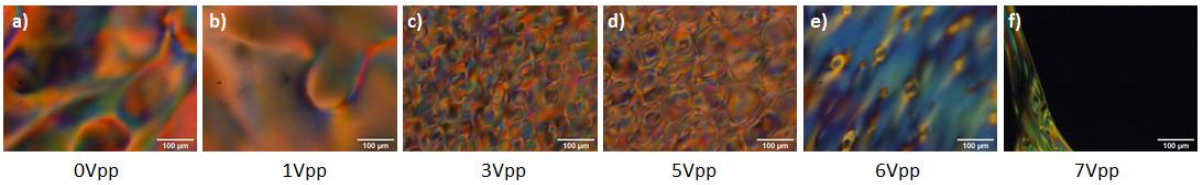

Figure 4.9: texture of the DSCG sample with a) no field applied, b-e) bubbles created by increasing the voltage from 1 to 6 Vpp, f) at 7Vpp sample turns black.

If the voltage is reversed there is the formation of a small area with planar texture that gradually expands (Figure 4.10).

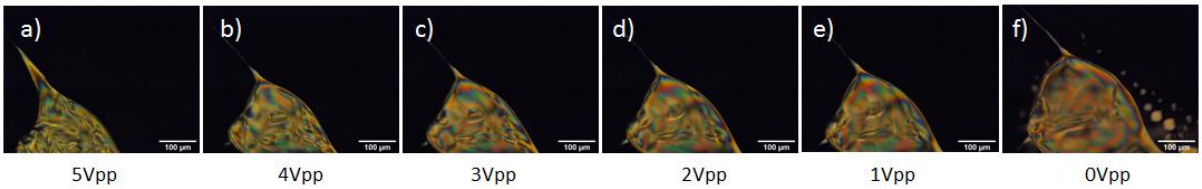

Figure 4.10: DSCG sample texture change lowering the voltage amplitude.

After two hours, the sample rearranges in microspheres that present a distorted bipolar texture (Figure 4.11).

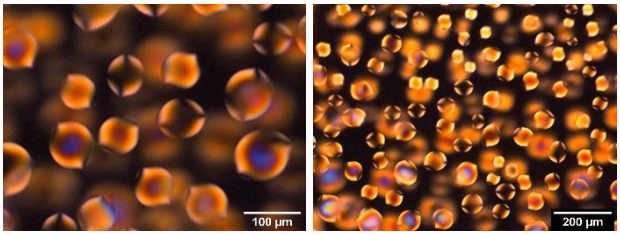

Figure 4.11: DSCG sample textures 2 hours after switching off the electric field.

The same type of test is repeated for the chiral mixture of DSCG 13wt% doped with L-Alanine 10wt%. Initially, the sample shows a chiral texture, with a pitch (p) of about 25 µm (Figure 4.12a). After applying the field, a slight decrease in p is observed. At 2Vpp the measured pitch is about 22 µm (Figure 4.12b). Increasing the signal amplitude, there is an increase in p, reaching a value of 30 µm at 4Vpp (Figure 4.12c), while there is again a decrease in p until a value of 15 µm at 5Vpp. For voltages higher than 5Vpp the sample becomes black (Figure 4.12d).

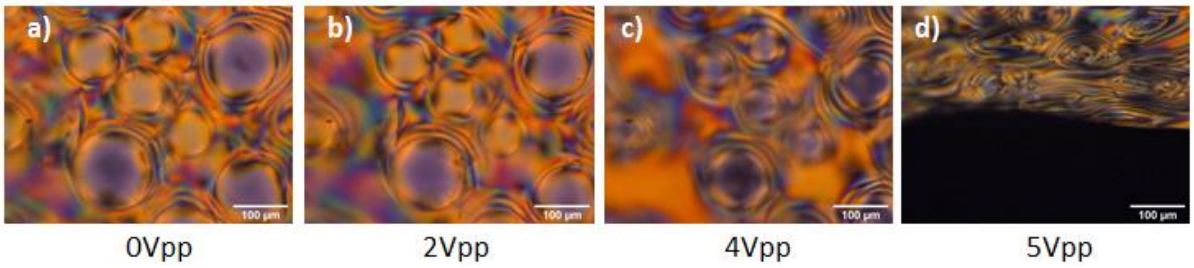

Figure 4.12: texture of the L-Alanine doped DSCG sample with: a) no field applied, b) 2Vpp c) 4Vpp and d)5Vpp

When the applied voltage is reversed, the formation of a small area that presents a chiral texture that gradually expands is observed (Figure 4.13). Decreasing the voltage the pitch decreases, at 4Vpp it is about 20 µm, and at 0Vpp the pitch is 17µm showing a significant hysteresis.

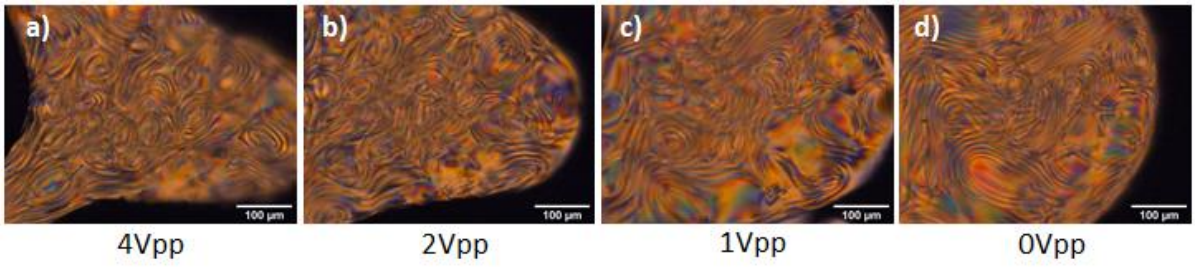

Figure 4.13: texture of the L-Alanine doped DSCG sample observed when decreasing the applied voltage amplitude.

Two hours after the first observation, microspheres with chiral texture appear (Figure 4.14), that in the largest microareas, show the fingerprint texture (Figure 4.14c); the pitch is 19 µm.

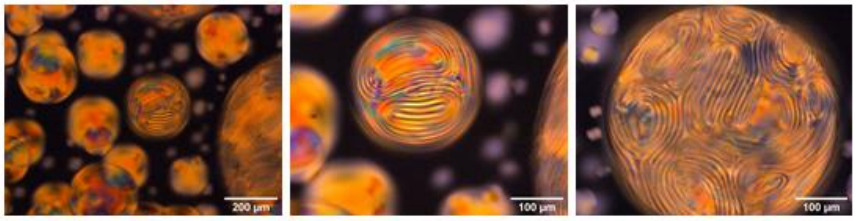

Figure 4.14: chiral DSCG sample textures 2 hours after switching off the electric field.

The effect of the electric field was also evaluated on the mixture of DSCG 13wt% doped with Trans-Hyp 26wt%. Initially, the mixture shows a chiral texture (Figure 4.15a) with a pitch of about 4 μm much smaller with respect to the previous case, since the Trans-Hyp has a higher twisting power with respect to L-Alanine. A pitch decrease was observed until 4Vpp, where the measured pitch is about 3.62 μm (Figure 4.15c). Increasing the signal amplitude, until 6Vpp, there is an increase in the pitch reaching a value of 5.4 μm, after which it starts to decrease to 3.6 μm and then the sample becomes, as in the previous cases, black (Figure 4.15 d-f).

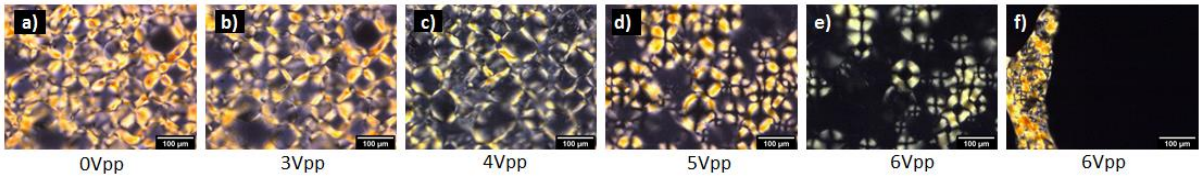

Figure 4.15: texture of the Trans-Hyp doped DSCG sample with: a) no field applied, b) 3Vpp, c) 4Vpp, d)5Vpp and e-f) 6Vpp.

When the field is reversed a small area with chiral texture is formed that gradually expands (Figure 4.16 a-d). The pitch decreases slightly, starting from an amplitude of 4Vpp to 1Vpp. Removing the field, microspheres with a well-defined chiral texture and a pitch varying between 3.6-4.4 μm are visible (Figure 4.16e).

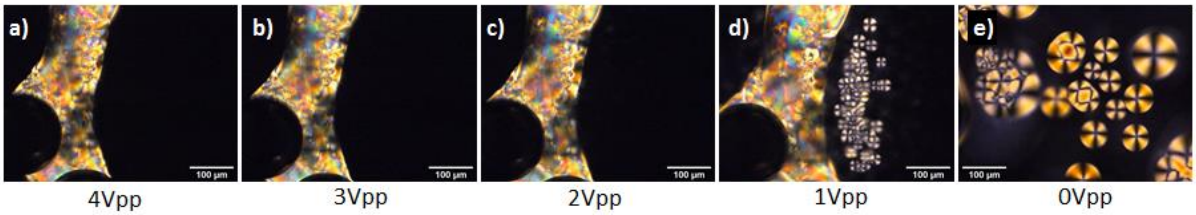

Figure 4.16: texture change in trans-Hyp doped sample decreasing the applied voltage amplitude.

Observing the sample after a few hours, cholesteric microspheres with a small pitch in the range 3/4 μm are present (Figure 4.17).

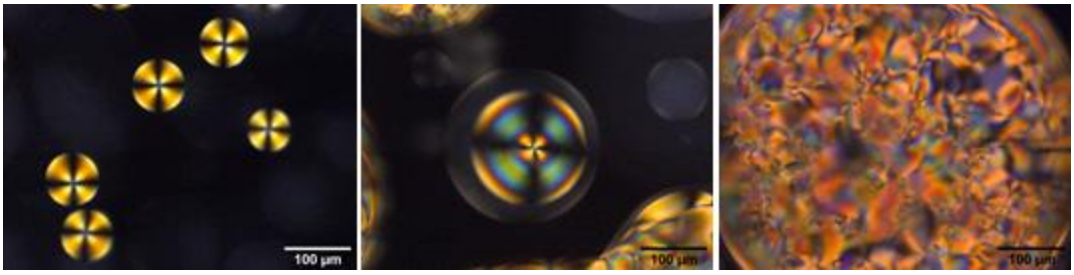

Figure 4.17: observation of the texture after few hours.

The pitch vs. applied voltage is shown in the graphs reported in Figure 4.18.

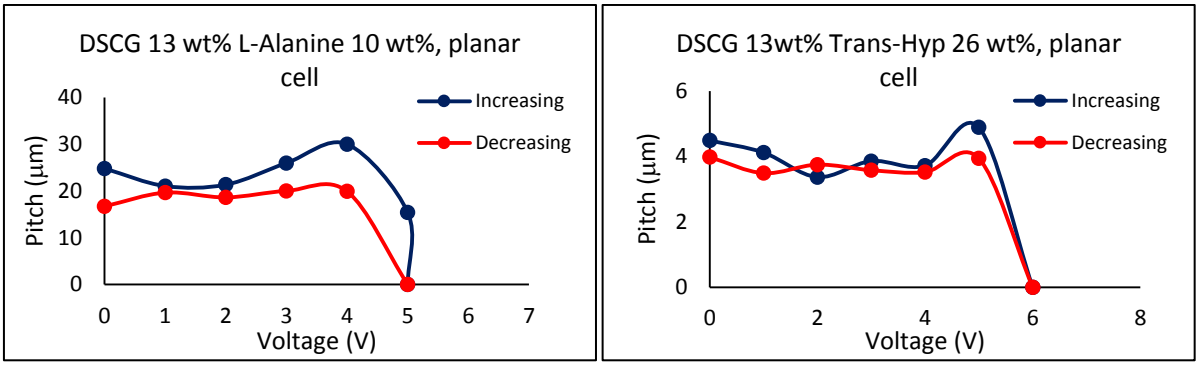

Figure 4.18: Pitch variation as a function of the applied voltage.

These preliminary results show that it is possible to control electrically the chromonic sample in both nematic and cholesteric mesophases. The pitch varies with the field amplitude in a non-monotonic manner and the sample rearranges in microspheres with shorter pitch, after some hours the field has been switched off.

4.2.2 Spherical geometry

The effect of electric field on optical textures was also investigated with chiral DSCG confined in spherical geometry. Emulsions were prepared using two different matrices: PDMS (excellent electrical insulator, electrical conductivity $\simeq 10^{-14}$ Scm^{-1} (71) and paraffin oil whose conductivity depends strongly on material preparation but has a higher value with respect to PDMS (72).

The first experiments were made with DSCG 13wt% doped with 26wt% Trans-Hyp. Analyzing the emulsion produced using PDMS, it is observed that microspheres have a cholesteric texture with a pitch of 4.64±0.06 µm (Figure 4.19a). By application of the field up to an amplitude of 10Vpp, there is no change in texture, the pitch range remains similar, the only effect observed is a slight movement of the microspheres (Figure 4.19b-e).

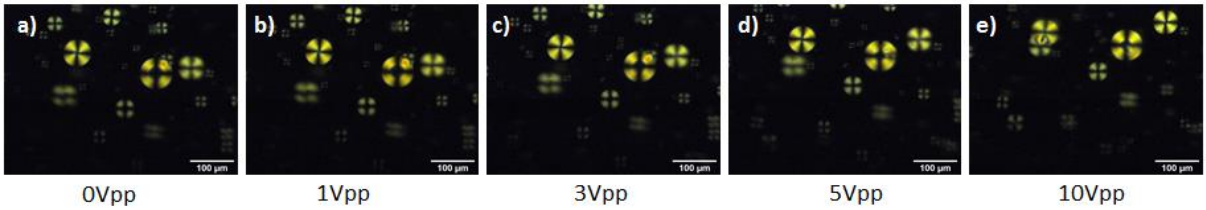

Figure 4.19: DSCG doped with Trans-Hyp microspheres in a PDMS matrix with: a) no field applied, b) 1Vpp, c) 3Vpp, d)5Vpp and e) 10Vpp.

When analyzing the emulsion produced using paraffin oil as a matrix for the emulsion, the results were different.

Initially, microspheres have a disordered texture in which a fingerprint-like structure is recognisable, that exhibits a 5.6 μm cholesteric pitch (Figure 4.20a). By increasing the field microspheres disappear (Figure 4.20b-e). This is a puzzling phenomenon possibly related to the heating of the cell that causes a transition to the isotropic phase.

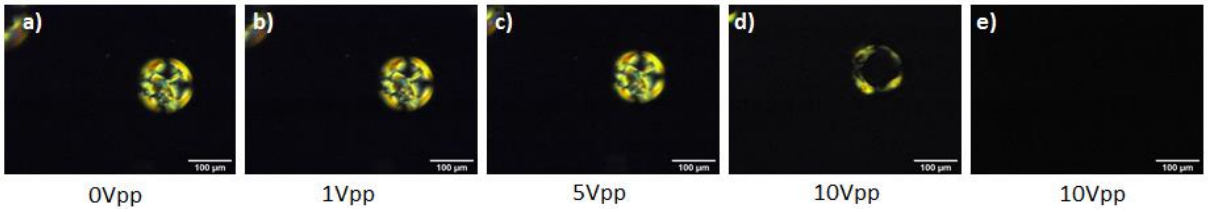

Figure 4.20: DSCG doped with Trans-Hyp microspheres in paraffin oil matrix with:. a) no field applied, b) 1Vpp, c) 5Vpp, d-e)10Vpp.

Observing the sample after 10 minutes, with the electric field switched off, microspheres became visible again with a well-defined cholesteric texture, showing a pitch of 4.8±0.8 μm (Figure 4.21).

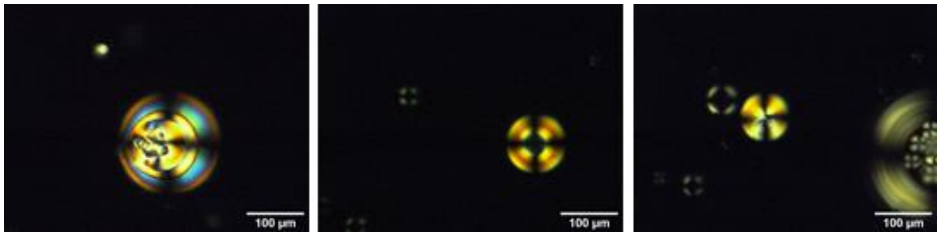

Figure 4.21: observation of the emulsion texture after 10 minutes (20x magnification)

Surprisingly, microspheres maintain a defined cholesteric texture even after 1 month from the first observation, as shown in Figure 4.22. As can be seen from Figure 4.22a, microspheres with cholesteric periodic textures are embedded in macroareas; outside these macroareas there are microspheres showing Maltese cross and twisted Maltese cross (Figure 4.22b-c).

a) 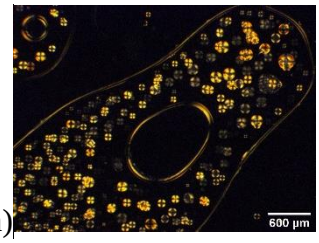

b) 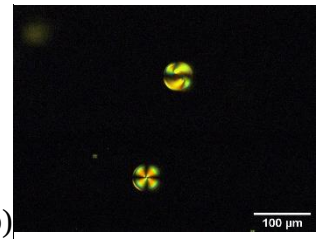

c) 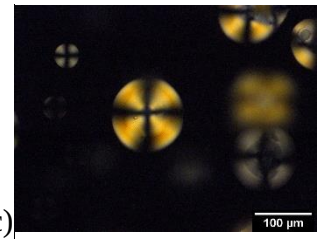

Figure 4.22: observation at different magnifications of the emulsion texture after 1 month: a) 2.5x and b-c) 20x.

The textures remain stable after four months from the preparation (Figure 4.23). We may conclude that paraffin oil is effective in preventing water evaporation from film emulsion.

a) 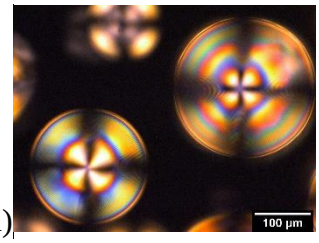

b) 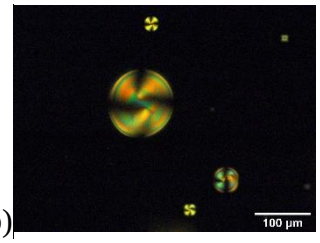

Figure 4.23: observation of the microsphere textures after 3 months: a) microspheres inside macroareas, b) microspheres outside macroareas.

In conclusion, when an electric field is applied to an emulsion of a cholesteric chromonic embedded in a PDMS matrix, no effects are observed: the microspheres have a well-defined cholesteric texture slightly perturbed by the field probably due to the low electrical conductivity of the confining oil. Instead, using the paraffin oil for the emulsions, the initial texture to be a material which of microspheres is not well defined but increasing field amplitude, the microspheres disappears and then recover switching off the field. They show an ordered cholesteric structure in concentric rings. In order to understand the behaviour of the liquid crystal director field inside the microsphere when an electric field is applied further measurement are needed to highlight the role of the anchoring conditions, the helical pitch and the size and type of geometrical confinement.

4.3 Soft colloids in DSCG

In general, not only LCs, but also soft and biological materials have always attracted a lot of attention due to their peculiar self-assembly property. Characteristic that is related, as discussed in previous chapters, to noncovalent interactions that lead to the formation of supramolecular structures that reorganize in response to chemical and mechanical stimuli. In particular, the regulation of mechanical strain is of central importance for the science of living systems (73) (74). Using liquid crystals, several novel responsive materials can be created, exploiting electrical fields and mechanical strain to control their electrooptical properties (75). As an

example, microscopic colloidal particles dispersed in LCs have been used to fabricate tunable self-assembled structures for photonic crystals (76). In these systems, the colloids were "hard" compared with the LC, leading to mechanical straining of the LC but not of the colloids (77). A recent paper has studied the influence of the elasticity of LCs on the shape and physical properties of soft colloids consisting of lipid vesicles (78).

Lipid vesicles in the form of liposomes are multilamellar vesicles (MLVs) obtained by the self-assembly of phospholipids. These latter are amphiphilic molecules organised in a way that those in the most external layer are side by side and expose the polar head (hydrophilic portion of the molecule) towards the aqueous environment surrounding them, while the non-polar tail (hydrophobic portion of the molecule) faces inside, where it intertwines with that of the second lipid layer, which has a specular organisation with respect to the previous one. In the inner phospholipid layer, the polar heads face the aqueous environment contained in the liposome cavity. Multilamellar liposomes reach diameters between 500 and 10000 nm as they are characterised by the presence of several concentric lipid layers (usually more than five), separated from each other by aqueous phases (onion skin structure). Due to this structure, multilamellar vesicles can remain immersed in an aqueous phase while simultaneously containing an aqueous content in which hydrophilic active ingredients or other molecules can be incorporated; they can accommodate hydrophobic compounds in the lipophilic phase.

Lipid vesicles are typically classified according to their multilamellarity and size. Unilamellar liposomes consist of a single phospholipid bilayer enclosing a hydrophilic core. Depending on their size, unilamellar liposomes can be further classified into small unilamellar vesicles (SUVs) whose diameter can range from 20 nm to 100 nm, large unilamellar vesicles (LUVs) whose diameter can range from 100 nm up to 1 μm, and giant unilamellar vesicles (GUVs) whose diameter is larger than 1μm (79).

Mushenheim and co-workers carried out a study of the interaction and mechanical deformation of micrometric sized synthetic GUVs (as a model for soft colloids) when confined in a chromonic phase (78). It was proved that elastic stresses resulting from deformation of the chromonic DSCG would strain the GUVs, resulting in anisometric shapes of the GUVs, expansion of the surface area of the GUV membranes and temporary or permanent breaking of the GUV bilayers. When the chromonic is in its isotropic phase, GUVs have a spherical shape, whereas in the nematic phase they take on a non-spherical shape (an elongated fuse).

Our research aim is to understand if the shape of the soft colloids could be further tuned using chiral DSCG doped with different aminoacids at different concentrations. The study could pave

the way to the design of new reconfigurable soft materials with potential application in sensing and biology.

As first step we have dispersed soft lipid vesicles in aqueous chromonic LC. Specifically, a thin film of dry bilayer-forming lipids of DOPC and sub-micellar content of the polymer-lipid PEG:2000-DPPE has been hydrated with a 15wt% DSCG solution in its isotropic phase at 48°C. Optical observations were then carried out at different temperatures through the I → N phase of the LC. The presence of the polymer-lipid in the DOPC vesicles, by increasing the intralamellar repulsions, favours the formation of large almost unilamellar vesicles.

Figure 4.24 shows vesicles, with an average diameter of 9 μm, that are put in evidence by red circles.

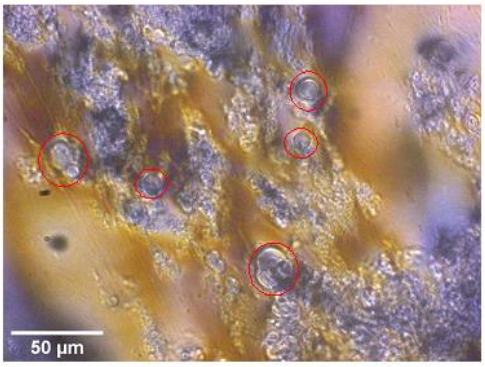

Figure 4.24: Vesicles in a DSCG sample.

An experiment, using polarized light microscopy, was carried out to evaluate the variation of the vesicle shape as a function of temperature. Initially, at a temperature of 35°C (Figure 4.25a), the sample is in the isotropic phase but the presence of bright needles is observed, which are probably small spots where the sample is nematic. The temperature was then gradually lowered, in fact, at 30°C nematic needles become larger (Figure 4.25b), and at 25°C the sample becomes completely nematic (Figure 4.25c). In order to detect the presence of the vesicles, it was necessary to observe them without the use of the analyser; they are small in size, with a diameter of about 4 μm (Figures 4.25d).

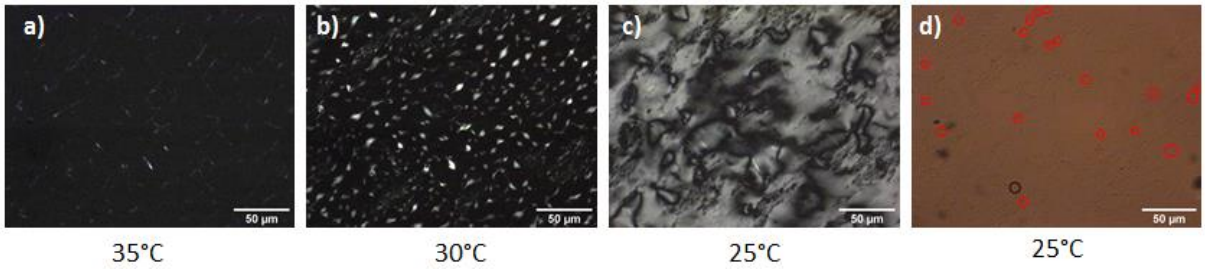

Figure 4.25: variation of the vesicle shape as a function of temperature.

At present, we are working to optimize the soft colloid preparation and composition in order to obtain vesicles of tens of microns by using different lipids and chromonic LC. As future work, the influence of chiral aminoacids on the vesicles' shape will be investigated.

Conclusions

In this thesis work, different types of chromonic liquid crystals confined in microspheres have been studied. Amino acids have been used as dopants to induce chirality in the nematic chromonic phases. Chirality is reflected in the optical textures of microspheres when they are observed using polarized light optical microscopy. The effects of ions due to the presence of salts and small charged molecules on the stability of mesophases and textures have been investigated as well.

Apart optical properties, new insight on the molecular arrangement of chiral dopants with respect to supramolecular aggregates has been achieved using X-Rays diffraction and atomic force microscopy.

The key starting point of this research has been a systematic study carried out on several materials in which to disperse the water based chromonics. This study has allowed to identify few polymers to prepare emulsions encapsulating the chromonics mesophases in microspheres and providing the appropriate anchoring conditions at the interface.

The first investigated chromonics have been DSCG and SSY.

The experiments carried out on DSCG have shown that the typical textures observed in thermotropic liquid crystals can be obtained. In particular, the Frank-Pryce texture, showing a periodic structure made of concentric rings, was observed. This has been an important achievement since this structure has previously been reported only for native chiral lyotropic liquid crystals as cellulose nanocrystals. Also, this is a texture characteristic of a pure material while in our case it has been observed in a water-based solution that contains at maximum a concentration of 13wt% in weight of the chromonic.

The role of ions was also investigated and the experimental results point to their stabilizing effect on the chiral phase. This could probably be attributed to a change in the non-covalent interaction between the chromonic molecules, which influences the packing of supramolecular aggregates. In fact, it was known that the presence of ions in nematic chromonics causes an elongation of the columnar aggregates by electrostatic effect. This fact is reflected in the improved quality of the optical textures even in the curved confinement.

To highlight the role of chiral dopants in the torsion of supramolecular aggregates, X-Rays diffraction experiments were carried out and it was found that the chiral molecules tend to stick

to the outside of the DSCG cylindrical aggregates, favouring their twist. This result was confirmed for two aminoacids: L-Alanine and Trans-Hyp.

The experimental investigations on the other model chromonic, SSY, have allowed to extend our knowledge on the effect of chiral dopants. SSY has demonstrated to be a material whose supramolecular aggregates are difficult to torque and the effect of the chiral dopants are dependent on the type of amino acid used. From optical investigations we have observed for the first time in chiral doped chromonics a variety of optical textures that so far have been observed only in chiral thermotropic materials with homeotropic anchoring conditions at the interface. X-rays diffraction has highlighted the different interaction of two amino acids, L-Lysine and Trans-Hyp, with the supramolecular aggregates. In particular, L-Lysine intercalates in the stacking of SSY, while Trans-Hyp is bound to the outer cylindrical structure. The second interaction mechanism being more efficient in inducing chirality in the system.

Also, for chiral SSY were investigated the effects of the presence of salts, both monovalent and divalent. As opposite to the DSCG case, the ions presence causes a misalignment of the cylinders that, we can infer, is due to the formation of bonding bridges among supramolecular aggregates that increases their disorder.

During the investigations we have noticed that textures are unstable and degrade irreversibly over time probably due to water evaporation from the emulsion. Degradation can be slowed down keeping the samples at 5°C and can be avoided if samples are stored at -18°C. This has suggested the possibility to use these materials as temperature sensors to monitor, for example, the cold food chain. With this purpose in mind, for the first time we have demonstrated the possibility to create a flexible polymeric film in which microspheres can be encapsulated without losing their ordered texture, i.e. the Frank-Pryce texture. This paves the way to the fabrication of new biocompatible time temperature indicators.

Furthermore, in the frame of this research work, other topics are still under investigation.

In particular, at present we have successfully identified a protocol to produce nematic and chiral SSY microspheres of controlled size and topology. This is a relevant result considering that in literature only a couple of papers on microfluidic production of chromonic nematic SSY microspheres is present and no works are available for chiral SSY microspheres. The possible implications of this achievement are important since it allows the possibility to add dopants to both the immiscible matrix and the chromonic mixture in a controlled way to easily study their

effect on topology. Furthermore, it provides a massive production of microspheres, monodisperse in size, useful to obtain a much-improved statistics.

Also, a study on a newly synthesised chromonic, an Ag(I) complex, was carried out. We have successfully amplified chirality also in this material that shows the same optical features of SSY. This suggests that the self-assembly and twisting mechanism for the Ag(I) complex is similar to that of SSY. For both materials, the induction of chirality is less efficient than when DSCG is doped with the same amino acid. One of the main difference between DSCG and SSY is in their molecular flexibility that could be the key parameter for the design of new materials in which chirality can be easily amplified. This point needs to be further investigated.

Bibliography

1. E. B. Priestley, P. J. Wojtowicz, P. Sheng. Introduction to liquid Crystals. s.l. : Plenum Press, 1976.

2. Tone, C. M. Properties of biomolecules at the interfaces: studies and characterization of chromonic mesogens. tesi di dottorato . Unversità della Calabria, Dipartimento di Fisica : s.n., 2013.

3. Collings, P. J. Liquid Crystals: Nature's Delicate Phase of Matter. s.l. : Princeton University Press, 2001.

4. Salinas, A. M. F. Neto e S. R. A. The Physics of Lyotropic Liquid Crystals: Phase Transitions and Structural Properties. s.l. : Oxford University Press, 2005.

5. Chromone: A Valid Scaffold in Medicinal Chemistry. A. Gaspar, M. J. Matos, J. Garrido, E. Uriarte e F. Borges. s.l. : Chemical Reviews, 2014, Vol. 114, p. 4960−4992.

6. Chromonic liquid crystalline phases. Lydon, J. s.l. : Liquid Crystals, 2011, Vol. 38, pp. 1663-1681.

7. Chromonics: Reviewing a High-performance Self-assembling Structure. Mohanty, Sanat. s.l. : Taylor & Francis, 2011, Vol. 53, pp. 84-94.

8. The Nature of π-π Interactions. C. A. Hunter, J. K. M. Sanders. s.l. : J. Am. Chem. Soc., 1990, Vol. 112, pp. 5525-5534.

9. Peter J. Collings, Michael Hird. Introduction to liquid crystals chemistry and physics. s.l. : Taylor & Francis, 1998.

10. Amphiphiles Self-Assembly: Basic Concepts and Future Perspectives of Supramolecular Approaches. Domenico Lombardo, Mikhail A. Kiselev, Salvatore Magazù, Pietro Calandra. 2015, s.l. : Hindawi, Vol. 2015. 151683.

11. Influence of Proton and Salt Concentration on the Chromonic Liquid Crystal Phase Diagram of Disodium Cromoglycate Solutions: Prospects and Limitations of a Host for DNA Nanostructures. Kitzerow, Bingru Zhang and Heinz-S. s.l. : J. Phys. Chem. B, 2016, Vol. 120, pp. 3250-3256.

12. Liquid crystals in micron-scale droplets, shells and fibers. al, M. Urbanski e. s.l. : J. Phys.: Condens. Matter, 2017, Vol. 29. 133003.

13. Dierking, Ingo. Textures of Liquid Crystals. s.l. : WILEY-VCH, 2003.

14. Drops and shells of liquid crystals. Lopez-Leon T., Fernandez-Nieves A. s.l. : Colloid and Polymer Science, 2011, Vol. 289, pp. 345-359.

15. Orientational structures in cholesteric droplets with homeotropic surface anchoring. Mikhail N. Krakhalev, Vladimir Yu. Rudyak, Oxana O. Prishchepa, Anna P. Gardymova, Alexander V. Emelyanenko, Jui-Hsiang Liu, and Victor Ya. Zyryanov. s.l. : Soft Matter, 2019, Vol. 15, pp. 5554-5561.

16. Bipolar configuration with twisted loop defect in chiral nematic droplets under homeotropic surface anchoring. Mikhail N. Krakhalev, Anna P. Gardymova, Oxana O.

Prishchepa, Vladimir Yu. Rudyak, Alexander V. Emelyanenko, Jui-Hsiang Liu & Victor Ya. Zyryanov. s.l. : scientific reports, 2017, Vol. 7. 14582.

17. Untwisting of the Helical Structure of Cholesteric Droplets with Homeotropic Surface Anchoring. M. N. Krakhalev, A. P. Gardymova, A. V. Emel'yanenko, Jui-Hsiang Liu, and V. Ya. Zyryanov. 1, s.l. : JETP LETTERS, 2017, Vol. 105, pp. 51-54.

18. Chiral symmetry breaking and surface faceting in chromonic liquid crystal droplets with giant elastic anisotropy. Joonwoo Jeong, Zoey S. Davidson, Peter J. Collings, Tom C. Lubensky, and A. G. Yodh. s.l. : PNAS, 2014, Vol. 111, pp. 1742-1747.

19. Colloidal cholesteric liquid crystal in spherical confinement. Yunfeng Li, Jeffrey Jun-Yan Suen, Elisabeth Prince, Egor M. Larin, Anna Klinkova, Heloise Therien-Aubin, Shoujun Zhu, Bai Yang, Amr S. Helmy, Oleg D. Lavrentovich & Eugenia Kumacheva. s.l. : Nature communication, 2016, Vol. 7. 12520.

20. Interfacial Tension between Isotropic and Anisotropic Phases of a Suspension of Rodlike Particles. Gray, Weiliang Chen and Derek G. s.l. : Langmuir, 2002, Vol. 18, pp. 633-637.

21. Retrieving the saddle-splay elastic constant K24 of nematic liquid crystals from an algebraic approach. Sebastien Fumeron, Fernando Moraes, and Erms Pereira. s.l. : Eur. Phis. J. E., 2016, Vol. 39. 83.

22. Deformations Induced by d.c. Electric Field in Cholesteric Liquid Crystals. R. Bartolino, A. Ruffolo, F. Simoni, N. Scaramuzza. 5, s.l. : Il nuovo cimento, 1982, Vol. 1, pp. 607-614.

23. Solid-state Chemistry of Cromolyn Sodium (Disodium Cromoglycate). J. S. G. COX, G. D. WOODARD, and W. C. McCRONE. 10, s.l. : Journal of Pharmaceutical Sciences, 1971, Vol. 60, pp. 1458-65.

24. Elasticity, viscosity, and orientational fluctuations of a lyotropic chromonic nematic liquid crystal disodium cromoglycate. Shuang Zhou, Krishna Neupane, Yuriy A. Nastishin, Alan R. Baldwin, Sergij V. Shiyanovskii, Oleg D. Lavrentovich and Samuel Sprunt. s.l. : the royal society of chemistry, 2014, Vol. 10, pp. 6571-6581.

25. Self-Assembly of Lyotropic Chromonic Liquid Crystal Mixtures. Yamaguchi, Akihiro. 2015.

26. Chromonic Liquid Crystal Formation by Edicol Sunset Yellow. D. J. Edwards, | J. W. Jones, O. Lozman, A. P. Ormerod, M. Sintyureva, and G. J. T. Tiddy. s.l. : J. Phis. Chem, 2008, Vol. 112, pp. 14628-14636.

27. Low viscosity lyotropic cholesteric liquid crystal composition. US4460492 1984.

28. Chiral lyotropic chromonic liquid crystals composed of disodium cromoglycate doped with water-soluble chiral additives. Tatsuya Shirai, Min Shuai, Keita Nakamura, Akihiro Yamaguchi, Yumiko Naka, Takeo Sasaki, Noel A. Clark and Khoa V. Le. s.l. : Soft Matter, 2018, Vol. 14, pp. 1511-1516.

29. Helical Twisting Power of Amino Acids in a Nematic Lyophase. H. Lee, M. M. Labes. s.l. : Mol. Cryst. Liq, 1984, Vol. 108, pp. 125-132.

30. Homeotropic Alignment of Lyotropic Chromonic Liquid Crystals Using Noncovalent Interactions. Joonwoo Jeong, Ganghee Han, A. T. Charlie Johnson, Peter J. Collings, Tom C. Lubensky, Arjun G. Yodh. s.l. : Langmuir, 2014, Vol. 30, pp. 2914-2920.

31. Aligning lyotropic liquid crystals with unconventional organic layers. Eva Otón, Morten A. Geday, Caterina M. Tone, José M. Otón, Xabier Quintana. s.l. : PHOTONICS LETTERS OF POLAND, 2017, Vol. 9, pp. 8-10.

32. Spherical Confinement of Chromonics: Effects of a Chiral Aminoacid. Lorenza Spina, Federica Ciuchi, Caterina Maria Tone, Riccardo Barberi, and Maria Penelope De Santo. s.l. : Nanomaterials, 2022, Vol. 12. 619.

33. Topological Transition in Spontaneously Formed Cellulosic Liquid-Crystalline Microspheres in a w/o Emulsion. Arindam Chakrabarty, Kazuma Miyagi, Monali Maiti, Yoshikuni Teramoto. s.l. : Biomacromolecules, 2018, Vol. 19, pp. 4650-4657.

34. Confinement-Induced Liquid Crystalline Transitions in Amyloid Fibril Cholesteric Tactoids. Gustav Nyström, Mario Arcari, Raffaele Mezzenga. s.l. : Nat Nanotechnol., 2018, Vol. 13, pp. 330-336.

35. Water-Vapor Permeability Control of PDMS by the Dispersion of Collagen Powder. Yuhua Zhang, Masatoshi Ishida, Yutaka Kazoe, Yohei Sato, Norihisa Miki. s.l. : IEEJ Trans, 2009, Vol. 4, pp. 442-449.

36. Stability of cellulose lyotropic liquid crystal emulsions. T. Tixier, M. Heppenstall-Butler, and E.M. Terentjev. s.l. : Eur. Phys. J. E, 2005, Vol. 18, pp. 417-423.

37. Salt Effects on the Phase Behavior, Structure, and Rheology of Chromonic Liquid Crystals. Andrei F. Kostko, Bani H. Cipriano, Olga A. Pinchuk, Lior Ziserman, Mikhail A. Anisimov, Dganit Danino, and Srinivasa R. Raghavan. s.l. : J. Phys. Chem. B, 2005, Vol. 109, pp. 19126-19133.

38. Crystallization of L-Alanine in the presence of additives on a circular PMMA platform designed for metal-assisted and microwave-accelerated evaporative crystallization. Anginelle M. Alabanza, Muzaffer Mohammed and Kadir Aslan. s.l. : CrystEngComm, 2012, Vol. 14, pp. 8424-8431.

39. Columnar molecular aggregation in the aqueous solutions of disodium cromoglycate. Dena M. Agra-Kooijman, Gautam Singh, Alexander Lorenz, Peter J. Collings, Heinz-S. Kitzerow, and Satyendra Kumar. s.l. : PHYSICAL REVIEW, 2014, Vol. 89. 062504.

40. Induced Chiral Chromonics Confined in Micrometric Droplets. Chiara Pellegrino, Maria Penelope De Santo, Lorenza Spina, and Federica Ciuchi. s.l. : Adv. Funct. Mater., 2020, Vol. 31. 2010394.

41. Planar anchoring strength and pitch measurements in achiral and chiral chromonic liquid crystals using 90-degree twist cells. Christine K. McGinn, Laura I. Laderman, Natalie Zimmermann, Heinz-S. Kitzerow, and Peter J. Collings. s.l. : PHYSICAL REVIEW, 2013, Vol. 88. 062513.

42. Dynamical homeotropic and planar alignments of chromonic liquid crystals. Caterina Maria Tone, Maria Penelope De Santo, Maria Giovanna Buonomenna, Giovanni Golemme, Federica Ciuchi. s.l. : Soft Matter, 2012, Vol. 8, pp. 8478-8482.

43. Growth, structural, physical and computational perspectives of trans-4-hydroxy-l-proline: a promising organic nonlinear optical material with large laser-induced damage threshold. Ramaiah Thirumurugan, Kandasamy Anitha. s.l. : Mater. Res. Express, 2017, Vol. 4. 056202.

44. Chromonic liquid crystals: Properties and applications as functional materials. Tam-Chang, S.-W. and Huang, L. s.l. : Chem. Commun., 2008, Vol. 17, pp. 1957–1967.

45. Alignment of Chromonic Liquid Crystals: A Difficult Task. Tone, C.M., De Santo, M.P. and Ciuchi, F. s.l. : Mol. Cryst. Liq. Cryst, 2013, Vol. 576, pp. 2-7.

46. Lyotropic Chromonic Liquid Crystals for Biological Sensing Applications. Shiyanovskii, S.V., et al. s.l. : Mol. Cryst. Liq. Cryst., 2005, Vol. 434, pp. 259-587.

47. Humidity sensing with printable films of lyotropic. Glushchenko, A., et al. s.l. : Appl. Phys. Lett., 2020, Vol. 117. 071902.

48. Research progress of packaging indicating materials for real-time monitoring of food. Liu, D., et al. s.l. : Mater. Express, 2019, Vol. 9, pp. 377–396.

49. Intercalation or external binding: How to torque chromonic Sunset Yellow. Lorenza Spina, Maria Penelope De Santo, Caterina Maria Tone, Michela Pisani, Francesco Vita, Riccardo Barberi, Federica Ciuchi. s.l. : Journal of Molecular Liquids, 2022, Vol. 359. 119265.

50. Topological defects due to twist-bend nematic drops mimicking colloidal particles in a nematic medium. Kanakapura S. Krishnamurthy, D. S. Shankar Rao, Madhu B. Kanakala, Channabasaveshwar V. Yelamaggad, and Maurice Kleman. s.l. : Soft Matter, 2020, Vol. 16, pp. 7479-7491.

51. Self-Assembly of Lyotropic Chromonic Liquid Crystal Sunset Yellow and Effects of Ionic Additives. Heung-Shik Park, Shin-Woong Kang, Luana Tortora, Yuriy Nastishin, Daniele Finotello, Satyendra Kumar, and Oleg D. Lavrentovich. s.l. : J. Phys. Chem. B,, 2008, Vol. 112, pp. 16307-19.

52. Concentration, temperature, and pH dependence of sunset-yellow aggregates in aqueous solutions: An x-ray investigation. Leela Joshi, Shin-Woong Kang, Dena Mae Agra-Kooijman, and Satyendra Kumar. s.l. : PHYSICAL REVIEW E, 2009, Vol. 80. 041703.

53. Lyotropic Chromonic Liquid Crystal and Their Impurities Reveal the Importance of the Position of Functional Groups in the Self-Assembly. Jonghee Eun, Jiyong Cheon, Sung-Jo Kim, Tae Joo Shin, and Joonwoo Jeong. s.l. : J. Phys. Chem. B, 2020, Vol. 124, pp. 9246-9254.

54. Isotropic, nematic, and columnar ordering in systems of persistent flexible hard rods. Reinhard Hentschke, Judith Herzfeld. 2, 1991, Vol. 44, pp. 1148-1155.

55. The effects of shape on the interaction of colloidal particles. Onsager, Lars. s.l. : Molecular Interaction, 1949, Vol. 51, pp. 627-659.

56. Structural Correspondence of Solution, Liquid Crystal, and Crystalline Phases of the Chromonic Mesogen Sunset Yellow. Wenchang Xiao, Chunhua Hu, Damien John Carter, Shane M Nichols, Michael D. Ward, Paolo Raiteri, Andrew L. Rohl, and Bart Kahr. s.l. : Cryst. Growth Des., 2014, Vol. 14, pp. 4166-4176.

57. From Intercalation to Groove Binding: Switching the DNA-Binding Mode of Isostructural Transition-Metal Complexes. Haslina Ahmad, Ashley Wragg, Will Cullen, Claire Wombwell, Anthony J. H. M. Meijer, and Jim A. Thomas. s.l. : Chem. Eur. J., 2014, Vol. 20, pp. 3089-3096.

58. Nematic textures in microfluidics environment. Segupta, A., Tkalec, U., Bahr, C. A. s.l. : Soft Matter, 2011, Vol. 7, pp. 6542-6549.

59. Sculpting stable structures in pure liquids. Emeršiˇc, T., et al. s.l. : Sci. Adv., 2019, Vol. 5. eaav4283.

60. Colloidal cholesteric liquid crystal in spherical confinement. Li, Y., Suen, et al. s.l. : Nature communication, 2016, Vol. 7. 12520.

61. Compound droplets derived from a cholesteric suspension of cellulose nanocrystals. Suzuki, T., Li,Y., Gevorkiana,A. and Kumacheva,E. s.l. : Soft Matter, 2018, Vol. 14, pp. 9713-9719.

62. Stable and Metastable Patterns in Chromonic Nematic Liquid Crystal Droplets Forced with Static and Dynamic Magnetic Fields. Jordi Ignés-Mullol, Marc Mora, Berta Martínez-Prat, Ignasi Vélez-Cerón, R. Santiago Herrera, Francesc Sagués. s.l. : Crystals, 2020, Vol. 10. 138.

63. Droplet microfluidics. Teh, S-Y, et al. s.l. : Lab on a Chip, 2008, Vol. 2, pp. 198-220.

64. Topological zoo of free-standing knots in confined chiral nematic fluids. David Sec, Simon Copar & Slobodan Zumer. s.l. : Nature communications, 2013, Vol. 5. 3057.

65. Phosphorescent nematic hydrogels and chromonic mesophases driven by intra- and intermolecular interactions of bridged dinuclear cyclometalated platinum(II) complexes. Xin-Shan Xiao, Wei Lu,Chi-Ming Che. s.l. : Chem. Sci., 2014, Vol. 5, pp. 2482-2488.

66. Chromonic-Like Physical Luminescent Gels Formed by Ionic Octahedral Iridium(III) Complexes in Diluted Water Solutions. Yogesh Jivajirao Yadav, Benoît Heinrich, Giuseppina De Luca , Anna Maria Talarico, Teresa Fina Mastropietro, Mauro Ghedini, Bertrand Donnio, Elisabeta Ildyko Szerb. s.l. : Adv. Optical Mater., 2013, Vol. 11, pp. 844-854.

67. Supramolecular Polymers and Chromonic Mesophases Self-Organized from Phosphorescent Cationic Organoplatinum(II) Complexes in Water. Wei Lu, Yong Chen, V. A. L. Roy, Stephen Sin-Yin Chui, Chi-Ming Che. s.l. : Angew. Chem. Int. Ed., 2009, Vol. 48, pp. 7621-5.

68. Unconventionally shaped chromonic liquid crystals formed by novel silver(I) complexes. Daniela Pucci, Barbara Sanz Mendiguchia, Caterina Maria Tone, Elisabeta Ildyko Szerb, Federica Ciuchi, Min Gao, Mauro Ghedini, Alessandra Crispini. s.l. : J. Mater. Chem. C, 2014, Vol. 2, pp. 8780-8788.

69. Electric Field-Driven Control of Cholesteric Cellulose Nanocrystal Orientation and Morphology. Dan Qu, Eyal Zussman. 2101659, s.l. : Adv. Optical Mater., 2022, Vol. 10.

70. Electro-optical properties of nematic lyotropic chromonic liquid crystals. Gu-Yuan Li, Jia-Jia Yu, Dong-Ming Mo, Maitiniyazi Bake, Ling-Feng Chen, You-Rong Li. s.l. : Journal of Molecular Liquids, 2022, Vol. 348. 118442.

71. High electrical conductivity in polydimethylsiloxane composite with tailored graphene foam architecture. Bo Han, Hongyun Chen, Te Hu, Huijian Ye, Lixin Xu. s.l. : Journal of Molecular Structure, 2019, Vol. 1203. 12741.

72. Studies of different types of insulating oils and their mixtures as an alternative to mineral oil for cooling power transformers. Jilani Rouabeh, Lotfi M'barki, Amor Hammami, Ibrahim Jallouli, and Ameni Driss. s.l. : Elsevier, 2019, Vol. 5. e01159.

73. Cardiolipin microdomains localize to negatively curved regions of Escherichia coli membranes. Renner L. D., Weibel D. B. s.l. : Proc Natl Acad Sci USA, 2011, Vol. 108, pp. 6264-9.

74. Mechanotransduction across the cell surface and through the cytoskeleton. Wang N., Butler J. P., Ingber D. E. s.l. : Science, 1993, Vol. 260, pp. 1124-7.

75. Photoalignment of liquid-crystal systems. K., Ichimura. s.l. : Chem Rev, 2000, Vol. 100, pp. 1847-1874.

76. Two-dimensional nematic colloidal crystals self-assembled by topological defects. Musevic I., Skarabot M., Tkalec U., Ravnik M., Zumer S. s.l. : Science, 2006, Vol. 313, pp. 954-8.

77. Physics of colloidal dispersions in nematic liquid crystals. H., Stark. s.l. : Phys Rep, 2001, Vol. 351, pp. 387-474.

78. Straining soft colloids in aqueous nematic liquid crystals. Peter C. Mushenheim, Joel S. Pendery, Douglas B. Weibel, Saverio E. Spagnolie, and Nicholas L. Abbott. s.l. : PNAS, 2016, Vol. 113, pp. 5564-9.

79. Giant Vesicles: A Biomimetic Tool for Membrane Characterization. Dimova, Rumiana. s.l. : Advances in Planar Lipid Bilayers and Liposomes, 2012, Vol. 16, pp. 1-50.

Publications

Chiara Pellegrino, Maria Penelope De Santo, Lorenza Spina, Federica Ciuchi *"Induced Chiral Chromonics Confined in Micrometric Droplets"* Adv. Funct. Mater. 2020, 2010394. DOI: 10.1002/adfm.202010394

L. Spina, F. Ciuchi, C. M. Tone, R. Barberi and M. P. De Santo "*Spherical Confinement of Chromonics: Effects of a Chiral Aminoacid*" Nanomaterials 2022, 12, 619. DOI: 10.3390/nano12040619

Lorenza Spina, Maria Penelope De Santo, Caterina Maria Tone, Michela Pisani, Francesco Vita, Riccardo Barberi, Federica Ciuchi *"Intercalation or External Binding How to Torque Chromonic Sunset Yellow", Journal of Molecular Liquids 359 (2022) 119265. DOI: 10.1016/j.molliq.2022.119265*

In preparation

Caterina Maria Tone, Alessandra Zizzari, Lorenza Spina, Monica Bianco, Maria P De Santo, Valentina Arima, Riccardo C Barberi and Federica Ciuchi *"Sunset Yellow confined in curved geometry: a microfluidic approach"*
submitted to ACS Applied Materials & Interfaces

Lorenza Spina, Maria Penelope De Santo, Nicholas Godbert, Iolinda Aiello, Eugenia Giorno and Federica Ciuchi *"A comparison among chromonic materials: a commercial and a laboratory synthesized material"*
in preparation

Carmen Cretu, Massimo La Deda, Giuseppe Di Maio, Adèl Len, Zoltan Dudas, Lorenza Spina, Federica Ciuchi, Oana-Alina Cadar, Liliana Cseh, Alessandra Crispini and Elisabeta I. Szerb *"Chromonic-like lyotropic liquid crystals with non-conventional Rh(III) coordination complexes"*
in preparation

Acknowledgements

Un sentito grazie a tutte le persone che mi hanno permesso di arrivare fin qui e di portare a termine questo lavoro.

Ringrazio, i miei supervisor Maria Penelope De Santo, Federica Ciuchi e Rosa Bartucci per la continua disponibilità sia sul piano scientifico che umano. In questi anni di lavoro, con immensa pazienza, hanno saputo guidarmi nelle ricerche e nella stesura dell'elaborato trasmettendomi fondamentali conoscenze.

Ringrazio il Dr N.Godbert e la Prof.ssa I.Aiello del Dipartimento di Chimica dell'Unical che hanno fornito il complesso di nuova sintesi investigato.

Ringrazio la dott.ssa Valentina Arima e la dott.ssa Alessandra Zizzari del CNR-Nanotec (Istituto di Nanotecnologie) di Lecce con cui è stato sviluppato un protocollo per produrre microgocce cromoniche.

Ringrazio i progetti: INCOMARC (Innovative coating materials for arc resistant electric contacts), DEMETRA (Sviluppo di tecnologie di materiali e di tracciabilità per la sicurezza e a qualità dei cibi) e SI.F.I.PA.CRO.DE (Sviluppo e industrializzazione farmaci innovativi per terapia molecolare personalizzata PA.CRO.DE.), che mi hanno finanziata durante questo percorso.

Ringrazio i miei genitori e mia sorella Giorgia. Non sarei mai potuta arrivare fin qui senza il loro supporto morale. Grazie per esserci sempre stati soprattutto nei momenti di sconforto.

Ringrazio il mio fidanzato Mario per avermi trasmesso la sua immensa forza e il suo coraggio. Grazie per tutto il tempo che mi hai dedicato. Grazie perché ci sei sempre stato.

Infine, vorrei dedicare questo traguardo a me stessa, per tutto il duro lavoro che ho fatto e per non aver mai mollato. Che possa essere l'inizio di una lunga e brillante carriera professionale.